AD-A101 226 NAVAL RESEARCH LAB WASHINGTON DC F/G 20/9
NON-LTE RADIATION FROM AN ARGON SEEDED MICROBALLOON IMPLOSION.(U)
JUL 81 P C KEPPLE, K G WHITNEY
UNCLASSIFIED NRL-MR NL

END
DATE FILMED
8-81
DTIC

SECURITY CLASSIFICATION OF THIS PAGE (When Data Entered)

REPORT DOCUMENTATION PAGE	READ INSTRUCTIONS BEFORE COMPLETING FORM
1. REPORT NUMBER (14) NRL-MR-4565 / NRL Memorandum Report 4565	2. GOVT ACCESSION NO. AD-A107 326 / 3. RECIPIENT'S CATALOG NUMBER
4. TITLE (and Subtitle) NON-LTE RADIATION FROM AN ARGON SEEDED MICROBALLOON IMPLOSION	5. TYPE OF REPORT & PERIOD COVERED Final report, (9)
	6. PERFORMING ORG. REPORT NUMBER
7. AUTHOR(s) (10) P.C. Kepple and K.G. Whitney / 11 18 11	8. CONTRACT OR GRANT NUMBER(s)
9. PERFORMING ORGANIZATION NAME AND ADDRESS Naval Research Laboratory Washington, D.C. 20375 / 1 91	10. PROGRAM ELEMENT, PROJECT, TASK AREA & WORK UNIT NUMBERS Report Control Symbol 79 299 47-0858-01
11. CONTROLLING OFFICE NAME AND ADDRESS Los Alamos National Laboratory Los Alamos, New Mexico	12. REPORT DATE July 13, 1981
	13. NUMBER OF PAGES 90
14. MONITORING AGENCY NAME & ADDRESS(if different from Controlling Office)	15. SECURITY CLASS. (of this report) UNCLASSIFIED
	15a. DECLASSIFICATION/DOWNGRADING SCHEDULE

16. DISTRIBUTION STATEMENT (of this Report)

Approved for public release; distribution unlimited.

17. DISTRIBUTION STATEMENT (of the abstract entered in Block 20, if different from Report)

18. SUPPLEMENTARY NOTES

This work was funded by the Los Alamos National Laboratory.

19. KEY WORDS (Continue on reverse side if necessary and identify by block number)

Stark broadening
Non-LTE radiation
Microballoon implosions

20. ABSTRACT (Continue on reverse side if necessary and identify by block number)

The K-shell radiation emitted by the argon seeded in the DT fuel of a CO_2 Laser driven microballoon implosion is modeled by post processing the results of a hydrodynamic (LANL) calculation. The entire K-shell spectrum is self-consistently calculated including: transport of both lines and continua, collisional-radiative equilibrium (CRE) number densities, Stark profiles for the first four resonance lines of Ar XVII and XVIII, and Voigt profiles for the remaining lines.

(Continues)

DD FORM 1 JAN 73 1473 EDITION OF 1 NOV 65 IS OBSOLETE
S/N 0102-014-6601

SECURITY CLASSIFICATION OF THIS PAGE (When Data Entered)

251950

20. ABSTRACT (Continued)

The CRE ionic number densities are presented and compared to the corresponding Average Atom quantities calculated by LASNEX.

CONTENTS

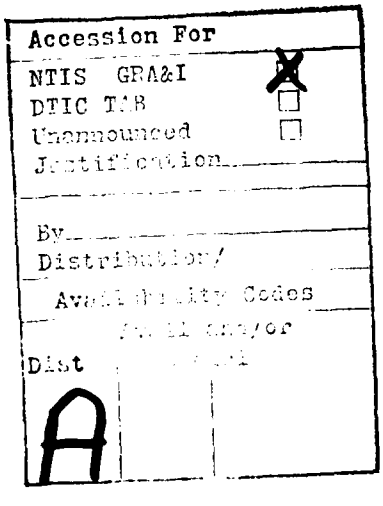

Non-LTE Radiation From an Argon Seeded Microballoon Implosion

I. INTRODUCTION

In this report, we will describe some results of calculations of K-shell emission from argon, seeded in the DT fuel of a microballoon that is imploded by high intensity irradiation from a CO_2 laser. The argon is added to the DT in order to diagnose the extent of DT compression that is obtained by ablation of the outside microballoon materials (in the case described here, plastic-coated glass). One can then determine the compressed density by analyzing the emission profiles of the argon K-series lines for Stark effects caused by the mixing of states within the principal quantum number multiplets at high densities by electron collisions and ion electric microfields. The success of this analysis depends on a number of theoretical considerations: how well (1) the microfield distributions and the Stark profiles, (2) the combined effects of electron impact excitation and ionization and of optical pumping on the ionization state of the argon, and (3) opacity corrections to the line emission profiles can be calculated. Moreover, one is also interested in how well the hydrodynamic implosion of the microballoon can be described and whether or not a post-processing of the predicted hydrodynamic behavior of the microballoon for the time integrated argon emission spectrum will agree with experimental observations. All of these issues are under investigation in this joint NRL/LANL program, and this final report will provide a status of achievements to date.

Efforts during the last year concentrated on several important tasks: (1) the calculation of Stark profiles for L_α, L_β, L_γ, and L_δ lines in hydrogen-like and helium-like argon (Ar XVIII and Ar XVII respectively), (2) the coupling of these profiles to a calculation of the collisional-radiative ionization equilibrium state of argon, and (3) the use of diagnostic procedures that allowed comparison of the results of these calculations both to experimentally obtained argon K-series spectra and to the ionization state of argon as theoretically predicted by average ion models. The Stark profiles used in the emission spectrum calculations included both the effects of electron collisions and ion microfields as well as Doppler convolutions. The ionization calculations contained an extensive level structure and an

Manuscript submitted May 20, 1981.

extensive set of collisional and radiative couplings. Finally, the diagnostic procedures consisted of cell-by-cell monitoring of all ground and excited state populations densities and the calculation of time integrated emission spectra that included the additional effects of instrumental broadening.

A hydrodynamics LASNEX[#] calculation carried out at LANL provided the description of the argon/DT implosion. Time histories of the central radii of the spherical shells, r(i,t), the total electron densities, $N_e(i,t)$, the electron and ion temperatures, $T_e(i,t)$, $T_i(i,t)$, and the total average charge states $\bar{Z}(i,t)$ (for each of the 11 cells describing the argon/DT core region of the microballoon, i = 1, ..., 11) were obtained from this calculation and used as input to the radiation-ionization calculations described in this report. Let α denote the (molecular) ratio of DT to Ar, which was 50 in these calculations. Since $\bar{Z}$ is related to the total ion density, N_i, of D, T, and Ar ions by $N_e = \bar{Z}\, N_i$ and since N_i is related to the density of argon ions N_{Ar} by $N_i = (2\,\alpha + 1)\, N_{Ar}$, the argon density was calculated from N_e and $\bar{Z}$ by

$$N_{Ar}(i,t) = N_e(i,t) \,/\, \left[(2\,\alpha + 1)\,\bar{Z}\ (i,t)\right] \tag{1}$$

Argon emission spectra were computed for each time by approximately calculating the collisional-radiative equilibrium by solving the coupled, nonlinear set of equations[1,2]:

$$\sum_{\ell} W_{m\ell}\,(N_\ell,\, U_\upsilon)\, N_\ell\,(i,t) = 0 \qquad m = 1,\ \ldots.,\ M \tag{2}$$

$$\sum_{\ell} N_\ell\,(i,t) = N_{Ar}\,(i,t) \tag{3}$$

$$N_e^{CRE}\,(i,t) = \sum_{\ell} N_\ell(i,t)\ \ (Z_\ell + 2\,\alpha)\ ^{*} \tag{4}$$

[#] The LASNEX calculations invoked the XSNQ Non-LTE subroutine. See Ref. 25 for a description of XSNQ.

* The electron density, N_e^{CRE}, is not necessarily equal to the quantity calculated by LASNEX, the latter is used only to obtain the argon number density (Eq. 1).

$$\left\{ \mu \frac{\partial}{\partial r} + \frac{1-\mu^2}{r^2} \frac{\partial}{\partial \mu} \right\} I_\nu(i,\mu,t) =$$

$$k(\nu,i,t) \left\{ S(\nu,i,t) - I_\nu(i,\mu,t) \right\} \tag{5}$$

$$U_\nu(i,t) = \frac{2\pi}{c} \int_{-1}^{1} d\mu \, I_\nu(i,\mu,t) \tag{6}$$

for the argon population densities $\{N_\ell\}$ and for the radiation energy densities $U_\nu(i,t)$ that couple to these populations. The emission spectrum $P_\nu(t)$ was also obtained from I_ν evaluated at the surface of the core region (i.e. no attenuation of this emission on passage through the glass or plastic was computed):

$$P_\nu(t) = 2\pi \int_{-1}^{1} d\mu \, \mu \, I_\nu \, (i = 12,\mu,t) \tag{7}$$

In these equations, μ is the cosine of the angle between the radius vector and the ray of specific intensity I_ν, Z_ℓ is the charge of the ionization state ℓ, k and S are the absorption coefficient and source function respectively, and $\{W_{m\ell}\}$ is the collection of rate coefficients describing the collisional and radiative couplings between the various states of the ionized argon.

An important part of the physics of Equations (2) - (6) is contained in the frequency dependence of the absorption coefficient and source function for the Lyman-series lines. For the H-L_α, H-L_β, H-L_γ, H-L_δ, He-L_α, He-L_β, He-L_γ, and He-L_δ lines, these frequency dependences were calculated as the convolution of Doppler and Stark line profile functions. All higher members of the Lyman-series were assigned Voigt line profiles, with Stark width estimates. The Stark profiles that were used in these calculations are described extensively in the Appendix.

There are several ways to evaluate the self-consistency of these calculations. One is to note how closely the given electron density N_e agrees

with the inferred electron density N_e^{CRE}. Another more detailed approach, which is presented in this report, is to compare the argon population densities that are obtained from the hydrodynamics calculations, which used average atom theory, to these densities as obtained from the CRE calculation. Finally, of course, one can compare calculated emission spectra to time integrated (or resolved) argon Lyman-series spectra that are measured in CO_2-microballoon compression experiments. Several examples of calculated time integrated emission spectra, showing the spectral detail that is possible, will be shown later in this report.

II. ATOMIC DATA

The spectra produced by the model is sensitive to the atomic data used, and the level structure and rates can be extended and improved as the need arises. Those used for the present calculations are as follows.

The atomic model contains all 19 ground states plus those excited states shown in Fig. 1 minus the five doubly-excited states which lie above the first ionization limit. Transitions from these doubly-excited states to their respective ground state produce the satellite lines to the resonance line of the next higher series. Since we were not focusing on these satellite lines in this calculation, the doubly excited states were, in fact, not used in the present calculation. These satellite structures can be incorporated into these calculations, as mentioned above as the need arises. Note also that many of the higher states are actually multiplets (or supermultiplets), the assumption being that collisions are fast enough to equilibrate the individual levels that have been included in the multiplet. The energy levels were obtained from the tables of Bashkin and Stoner[3], Kelly and Palumbo[4] and from scaling laws, for those high-lying states that are not tabulated. The ground and excited states of the ion of charge Z are coupled to the ground state of the Z + 1 ion by collisional ionization (calculated by the exchange-classical impact parameter method[5]), photo-ionization (hydrogenic cross-section[6] with Karzas-Latter free-bound Gaunt factors[7]), and the collisional and radiative recombination rates obtained by detail-balancing the above. Adjacent ground states can be coupled by dielectronic recombination[8] (although they were not, due to the omission of satellite lines from the present model). Each excited state of the ion Z is coupled by electron impact to the ground

state and other excited states of the ion Z. The excitation rates for transitions with principal quantum number $n < 6$ were calculated by the method of distorted waves[9,10]. The levels with $n \geq 6$ the rates were calculated by the semi-classical impact method.[11] The collisional de-excitation rates were calculated by detail-balancing the corresponding excitation rates. Spontaneous decay rates were collected from a number of sources[12-16].

The broadband radiative coupling theory that is employed in this model has been described in detail elsewhere[1,17]. It includes a self-consistent treatment of the overlap of line and continuum absorption and emission processes, under the assumption that these processes detail balance in the sense that line emission and absorption profiles are identical. The number of radiative couplings used in the present argon model is more extensive than those employed earlier for aluminum[1]. They include principal Lyman series couplings in Ar XVII and XVIII from n = 2 to n = 10. With the inclusion of the intercombination line, $1s^2\ ^1S - 1s2p\ ^3P$, there are 19 line couplings in all in this model and no more. In addition, there are 8 continuum couplings: Z→H(n=1), Z→H(n=2), H→He($1s^2\ ^1S$), H→He($1s2s\ ^3S$), H→He($1s2p\ ^3P$), H→He($1s2s\ ^1S$), H→He($1s2p\ ^1P$), and He→Li where Z, H, He, and Li denote Ar XIX, Ar XVIII (n=1), Ar XVII ($1s^2\ ^1S$) and Ar XVI ($1s^2 2p$) respectively.

The initial conditions of the hydrodynamics calculation are shown in Figure 2. Six kilojoules of CO_2 laser energy with a pulse risetime of 392 psec. are used to drive the 350 μm diameter microballoon. The plastic coating is intended to shield the fuel region from electron preheat. This region, containing DT and argon, is initially 247 μm in diameter. It implodes to a minimum diameter of 32 μm at ∿ 1160 psec. (roughly an eight-fold decrease in size). During this compression, peak temperatures are reached at approximately 1070 psec, and Argon K-shell emission substantially ends at around 1300 psec.

III. RESULTS: ATOMIC STATE NUMBER DENSITIES AND ORBITAL OCCUPATION NUMBERS

In Figs. 3-25 more of the details of the hydrodynamics calculations are shown; the solid line refers to quantities in cell No. 1 (the inner center cell), the dash-dot line, to quantities in cell No. 6 (the middle cell) and the dashed line to quantities in cell No. 11, (the outer cell). In Fig. 3 we show the radial distances to the center of each of these three cells as functions of time. Figure 4 shows the corresponding electron temperatures

while Fig. 5 contains the corresponding argon number densities (see equation 1). Notice as noted above that peak temperature precedes peak density by 0.1 ns. It is also worth noting that while the peak temperature occurs at the center (cell No. 1) the peak in density occurs at the outside (cell No. 11).

From these plasma conditions, we have computed the following ionization behavior for argon. The fractions of ions that are fully stripped is plotted in Fig. 6. Not surprisingly, these plots peak at the same time as the electron temperature. Next, Figures 7-10 are plots of the fraction of the argon atoms that are stripped down to one electron. In Fig. 7 the remaining electron is in the ground state, while it is in the state with n = 2,3 and 4 in Figs. 8-10. These plots again peak at the time of peak electron temperature. Finally, the fractions of the argon atoms with two bound electrons are plotted in Figs. 11-17. Since the temperature to remove the last L-shell electron (ionize Ar XVI) is much lower than the peak temperature achieved (1 keV), ground state Ar XVII is abundant during the early part of the calculation and is drastically reduced near peak temperatures, (See Fig. 11). On the other hand the temperature necessary to excite an n = 1 electron is of the order of a keV so the excited states of Ar XVII do not become prevalent until the time of peak temperature, at this point the density is increasing and the excited states thus track the density profiles rather than the temperature (see Figs. 12-17). As stated above the energy to ionize Ar XVI is quite low, thus its abundance is low throughout much of the calculation but does build up a bit during the reexpansion of the plasma, (See Figs. 18-21).

A simpler "Average Atom" model of the atomic structure was used in the hydrodynamics calculation. In such models one does not distinguish to which nucleus a given electron is bound, or, more precisely, whether other electrons are or are not bound to the same nucleus. One only determines a distribution of quantum numbers of the bound electrons. Thus one calculates the number of "2p orbitals" (per nucleus) that are occupied. Or if one is satisfied with even less detail, one calculates the number of "n = 2 orbitals" (per nucleus) that are occupied.

The orbital occupation numbers, ϕ_k can be calculated from our fractional population numbers as follows: Denote by f_{ij}, the fractional population of the ion with i bound electrons in the j-th excited state. The excited states are ordered by excitation energy and j = 0 is the ground state.

$$\phi_{1s} = f_{1,0} + 2 \sum_{i=2}^{18} f_{i,0} + \sum_{j=1}^{13} f_{2,j} + 2 \sum_{j=1}^{7} f_{3,j} + f_{3,8}$$

$$\phi_{2s} = f_{3,0} + 2 \sum_{i=4}^{18} f_{i,o} + 1/4\ f_{1,1} + f_{2,1} + f_{2,3} + f_{2,14} + f_{2,16}$$

$$\phi_{2p} = \sum_{i=5}^{18} \min\ (6, i-4)\ f_{i,o} + 3/4\ f_{1,1} + f_{2,2} + f_{2,4} + f_{2,14} + f_{2,15}$$

$$+ f_{2,16} + 2 f_{2,17} + f_{3,1} + 2 f_{3,8}$$

$$\phi_{3s} = f_{11,o} + 2 \sum_{i=12}^{18} f_{i,o} + 1/9 \left[f_{1,2} + f_{2,5} + f_{2,6} \right] + f_{3,2}$$

$$\phi_{3p} = \sum_{i=13}^{18} \min\ (6, i-12)\ f_{i,o} + 3/9 \left[f_{1,2} + f_{2,5} + f_{2,6} \right] + f_{3,3}$$

$$\phi_{3d} = 5/9 \left[f_{1,2} + f_{2,5} + f_{2,6} \right] + f_{3,4}$$

$$\phi_{n=1} = \phi_{1s}$$

$$\phi_{n=2} = \phi_{2s} + \phi_{2p}$$

$$\phi_{n=3} = \phi_{3s} + \phi_{3p} + \phi_{3d}$$

$$\phi_{n=4} = f_{1,3} + f_{2,7} + f_{3,5}$$

where $\sum_{i,j} f_{ij} = 1$, $\phi_{n=1} \leq 2$, $\phi_{n-2} \leq 8$, $\phi_{n=3} \leq 18$, etc.

The orbital occupation numbers are plotted in Figs. 22-25. Again, the solid line corresponds to the inner cell (#1), the dot dashed line to cell #6 and the dashed line to the outer cell (#11). On Fig. 22 we show the n = 1 orbital occupation; we have also plotted a few points calculated for cell #1 by LASNEX in the Average Atom approximation. The difference is of the order of 30%. This indicates discrepancies in these two ionization equilibrium calculations of the order of 30%!

In Fig. 23 the n = 2 orbital occupation data is plotted along with some LASNEX results for cell #1. The LASNEX and CRE differences in n = 2 orbitals are even larger! Since the x-ray emission calculations depend critically on the strength of emission and self-absorption as determined by the state occupation numbers, these discrepancies will have a marked influence on the use of the CRE or average atom calculations to carry out diagnostics. An interesting question as to the effect of these occupation number differences on x-ray energetics during compression remains to be investigated.

IV. RESULTS: SPECTRA

Time integrated spectra are presented for several times. In Fig. 26 we show the spectra integrated for t = .8 ns to 1.06 ns. The spectral region shown, 3.0 to 4.1 keV, contains all the strong K-shell lines that are measured and distinct at these densities. As stated in the introduction we do not as yet include the doubly excited states that would produce the satellites to the Ar XVIII Lα and the Ar XVII Lα-like resonance line. All the lines in Fig. 26 except the Ar XVII intercombination line and $1s6p \rightarrow 1s^2$ were calculated using the convolution of Doppler and Stark profiles. In addition approximate corrections have been included for the effects of ion-dynamics and microfields due to the fluctuations of the electrons in the screening cloud (see the Appendix for more details). The fine structure splitting of Lα is larger than the Stark width at the electron density of these calculations. Since the fine structure splitting is of the order of the instrumental plus source broadening, so that the splitting cannot be resolved by this type of experiment, we convolved Lα with an additional Gaussian whose width is the fine structure splitting. For this reason Lα appears relatively too wide on Fig. 26. In Fig. 27 the whole of the spectra has been convolved with a Gaussian profile whose width is equal to 7 m Å, the combined instrumental plus source broadening. In Fig. 27 Lα appears with a relative width much closer to those observed. In addition the apparent intensity of the intercombination line is reduced to normally seen levels, and some of the detailed features of the Stark profiles (central dips) are washed out.

In Figs. 28 and 29 these same spectra as obtained from time integrations from .8 to 1.18 ns are plotted. By comparing the intensities on Fig. 26(27) to those on Fig. 28(29) we note that Lα and L_β have increased more than the other lines, from which we conclude that the Ar ions have spent a (relatively) larger part of the time as Ar XVIII during the time between 1.06 to 1.18 ns (a fact that is confirmed by Fig. 7 and 11). Finally, in Fig. 30, we show the emission spectrum, fully formed, integrated out to 1.3 ns. Unfortunately an experimental spectrum for this 18 atm. fill case is not available for comparison at this time. A calculation for 30 atm. fill for which there are experimental spectra will be made in the near future, as soon as the LASNEX calculation is made available to us.

V. SUMMARY

We have described two sets of efforts that were successfully carried out this last year. One, which was brought to a fairly mature state, involves the calculation of emission profiles that are convolutions of Doppler and Stark profile functions for both one and two electron systems (Ar XVII and XVIII) from Lyman-α all the way to the Lyman-δ lines including both electron and ion contributions. The other effort to merge these Stark profile calculations with calculations of the implosion dynamics and argon x-ray emission behavior, on the other hand, has only recently been inaugurated. Hence, they are much less mature, yet they contain considerable potential. Nevertheless, in this latter effort, we have successfully demonstrated (1) that the fully developed theories and calculations of Stark broadening can be merged self-consistently with equally developed and detailed calculations of the collisional-radiative equilibrium state of the argon K-shell, (2) that in turn this full set of calculations can be utilized to post-process and analyze a partial set of LASNEX hydrodynamics data containing spatial gradients, and finally (3) that the result of these analyses can comprise a fairly complete set of predictions of both the emission spectrum and ionization state to compare against experimental observations and average atom theories.

Although the analysis described in this report dealt with a case for which no experimental data is presently available, it did provide some initial comparisons with the average atom predictions of LASNEX. CRE number densities were selfconsistently (to reasonable approximation) calculated along with the radiative emission. By forming the appropriate combinations of the fractional populations of the atomic states, we were able to calculate what would appear to be equivalent orbital occupation numbers. When these numbers were compared to the average atom quantities calculated directly by LASNEX it was found in this one case that a discrepancy exists. For the $n = 1$ orbital LASNEX and the CRE calculation differed by $\approx$ 30% while for the $n = 2$ orbital, the difference was a factor of $\sim$ 2-3. Because the orbital occupation numbers are different it follows that the ionization/excitation level is also different, (i.e. the apparent differences in the conception of the two models lead to differences in consequences in this case).

The success of our efforts to date raises important questions that need to be addressed in the future. For example, the calculations described in this report were carried out with a minimum of time steps, using substantially the time steps required in the hydrodynamics calculations, which do not necessarily guarantee good CRE solutions nor accurate time integrations of the emission spectrum. A similar problem may exist because of the spatial gradients in temperature and density. More or better placed cells may be required in order to obtain an adequate resolution to these gradients for integration of the radiative transport equations. The atomic structure of our model is no doubt adequate, however, some of the important radiative couplings (eg. Balmer line couplings) may have been excluded from the model, as well as some of the important doubly excited state couplings. The present calculations also neglect the effects of the glass either to radiate and photoexcite the argon or to absorb and modify its K-shell emissions.

In future work the atomic model will be further enriched, in particular we will begin to work in the L-shell to investigate L-shell energetics. The K-shell Stark profiles will be improved with the addition of quantum mechanical strong collision terms, and the correction for the finite duration of collisions will be incorporated into the two electron code. Finally, we look forward to direct comparisons of the time intergrated K-shell spectrum to experimental spectra (as soon as the appropriate LASNEX simulation data is made available to us), and to much more detailed analyses of the differences in energetics and diagnostics between CRE and average atom theories than was given in the one comparison made in this report.

APPENDIX

VI. STARK PROFILES

The stark profiles used in the radiation transfer calculations were computed based on a theory which treats the electron collisions by an impact approximation that allows for the level splittings caused by the ion fields, the finite duration of the collisions,* and the screening of the electric fields. The ion effects are calculated in a quasi-static, linear Stark effect approximation, using the electric microfield distribution functions of Hooper and Tighe[18] which accounts for both correlation and shielding effects.

The profiles for Ar XVII and XVIII have already been discussed[19]. The modifications of the one electron calculation that were necessary to treat the He-Like profiles were also discussed[19]. The Ar XVIII profiles we use are the same as those in Ref. 19; however, it has subsequently been found, at least for argon, that L-S coupling is not an adequate approximation to determine level splittings. Instead, it was necessary to express the D, F, G, etc states as combinations of singlets and triplets. These energy levels and their mixing coefficients were obtained from the work of R. Cowan[20] and are summarized in tables 1 - 3. The effect of these mixed states on the profiles is shown in Figs. 31-34 (the solid line is the "mixed state" result, the dashed line is from the "singlet only" approximation).

The electron collision operator for a system of more than one bound electron is complex and one would like to look for ways of simplifying it. In Figs. 31-34 we show the effect of neglecting the imaginary (shift) part of the operator (points marked by circles). If in addition to this approximation a simplification that is often used in the evaluation of the real

* The correction for the finite duration of collisions has not yet been implemented into the two electron code. (It will increase the expense of the calculations and the implementation has been delayed pending the inclusion of the correct quantum mechanical strong collision term.) The effect of the neglect of the finite collision time is only important for frequency deviations from line center larger than the plasma frequency. (For 1s5p-1s(2) the plasma frequency is near the half intensity point, so the wings of this line suffer larger errors than the rest of the profiles).

part of the operator[21] is used, one obtains the points marked by crosses. As can be seen, the imaginary part has a negligible effect and we subsequently ignore it. The simplification of the real part does not lead to a large error, but we retain the more correct form in anticipation of a larger correction once the quantum mechanical correction for the strong collisions has been extended to the two electron system.

A theory has been developed by Griem for the correction to line profiles due to the motion of the ions and to the fluctuations in the electric microfield caused by electrons in the Debye screening cloud. These effects have been evaluated for Lyman alpha[22] and Lyman beta[23] lines, an approximate correction for these effects is to convolve the Stark profiles with a Gaussian whose width was discussed by Griem et al.[24] Table 4 contains the appropriate Gaussian widths for the argon XVII and XVIII profiles.

In summary, the Stark profiles that were used in the calculations and described in the text are shown in Figs. 35-50 and Table 5-20.

ACKNOWLEDGMENTS

We would like to thank Allen Hauer and Eldon Linnebur for providing the LASNEX simulation data which was analyzed in this report. We would also like to acknowledge many profitable discussions with Hans Griem on the subject of Stark broadening. Last, but certainly not least, we would acknowledge the extensive contributions of J. Davis and Dwight Duston to the collisional model.

This work was supported by the Los Alamos National Laboratory.

REFERENCES

1. K.G. Whitney, J. Davis and J.P. Apruzese, Phys. Rev. A 22 2196 (1980).

2. D. Duston and J. Davis, Phys. Rev. A 21 932 (1980).

3. S. Bashkin and J.O. Stoner, Jr., Atomic Energy Levels and Grotrain Diagrams (North-Holland, Amsterdam, 1978) Vol. II.

4. R.L. Kelly and L.J. Palumbo, NRL Report No. 7599 (1973).

5. A. Burgess, H.P. Summers, D.M. Cochrane, and R.W.P. McWhirter, Mon. Not. R. Astro. Soc. 179, 275 (1977).

6. V.L. Jacobs, J. Davis, P.C. Kepple, and M. Blaha, Astrophys. J. 211, 604 (1977).

7. W.J. Karzas and R. Latter, Astrophys. J. Suppl. Sec. 6, 167 (1961).

8. V.L. Jacobs and J. Davis, Phys. Rev. A18, 697 (1978).

9. J. Davis, P.C. Kepple, and M. Blaha, JQSRT 16, 1043 (1976).

10. A.L. Merts, J.B. Mann, W.D. Robb, and N.H. Magee, Jr., LASL Report No. 8267 (1980).

11. E. Oran and J. Davis, J. Appl. Phys. 45, 2480 (1974).

12. A. Lindgard and S.E. Nielsen, Atomic Data and Nucl. Data Tables 19, 533 (1977).

13. B.C. Fawcett, At. Data and Nucl. Data Tables 22, 473 (1978).

14. C.D. Lin, W.R. Johnson, and A. Dalgarno, Phys. Rev. A 15, 154 (1977).

15. C. Laughlin, J. Phys. B. 11, L391 (1978).

16. W. Wiese, M. Smith, and B. Miles, Atomic Transition Probabilities (U.S. GPO, Wash. D.C., 1969), Vol. II.

17. K.G. Whitney and P.C. Kepple, talk given at the conference on "Radiative Properties of Hot Dense Matter", Monterey, Cal., Nov. 17-20, 1980, (to be published (JQSRT)).

18. Private communication.

19. P.C. Kepple and J.E. Rogerson, NRL Memorandum Rpt. 4216 (1980).

20. Private communications.

21. See pg. 66 of "Spectral Line Broadening," by H.R. Griem, Academic Press (New York, 1979).

22. H.R. Griem, Phys. Rev. A 20, 606 (1979).

23. H.R. Griem, Submitted for publication.

24. H.R. Griem, M. Blaha and P.C. Kepple, Phys. Rev. A 19, 2421 (1979).

25. W.A. Lokke and W.H. Grasberger, "XSNQ-U a Non-LTE Emission and Absorption Coefficient Subroutine," UCRL-52276, June 1977.

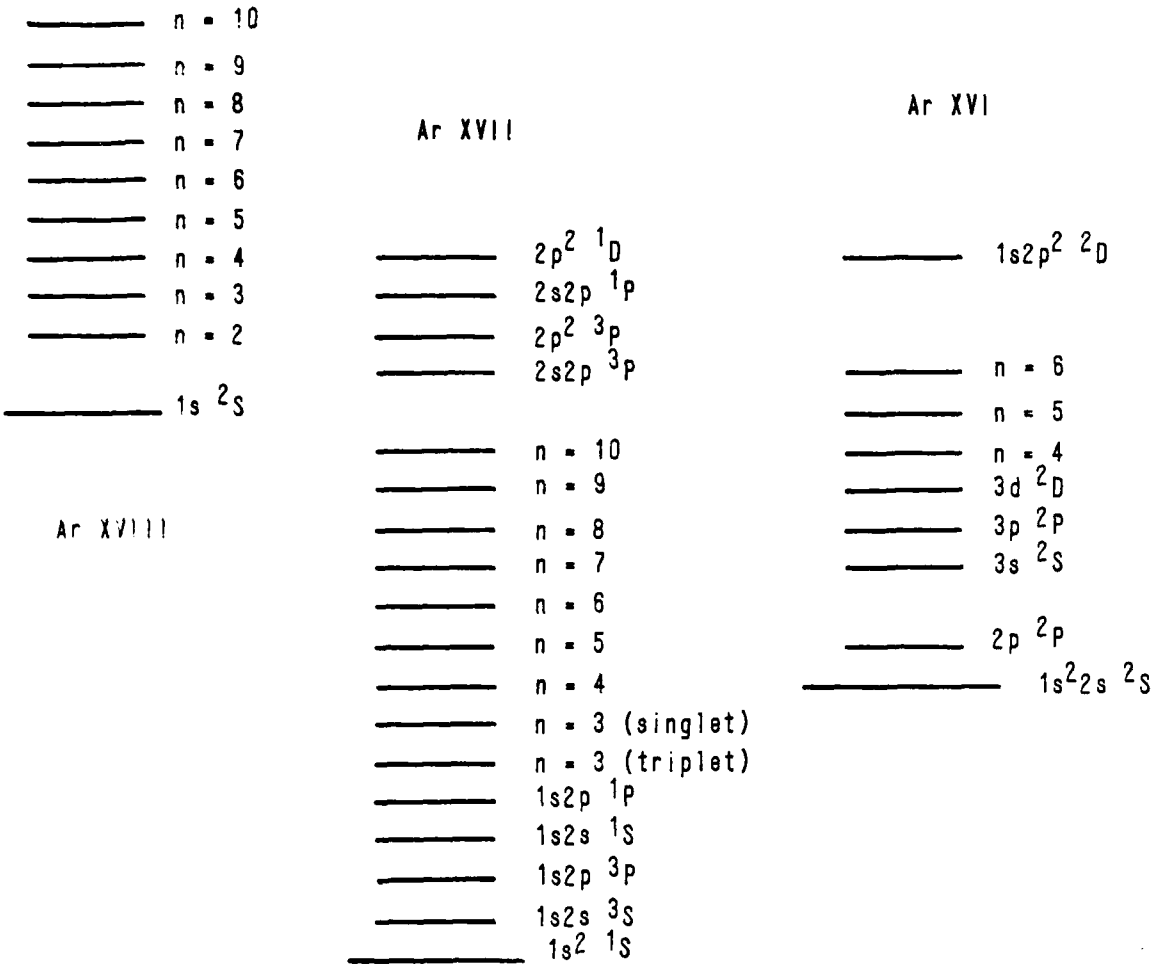

Fig. 1 — Energy level diagram for those levels included in the model

PELLET CONDITIONS

DT/ARGON PELLET: PARTICLE RATIO OF

DT-TO-ARGON: 50 to 1

FUEL RADIUS: 123.5 MICRONS

LASER: ENERGY =6 KJ

RISETIME = 392 PS

ELECTRON TEMPERATURE: LASNEX

ELECTRON DENSITIES: LASNEX

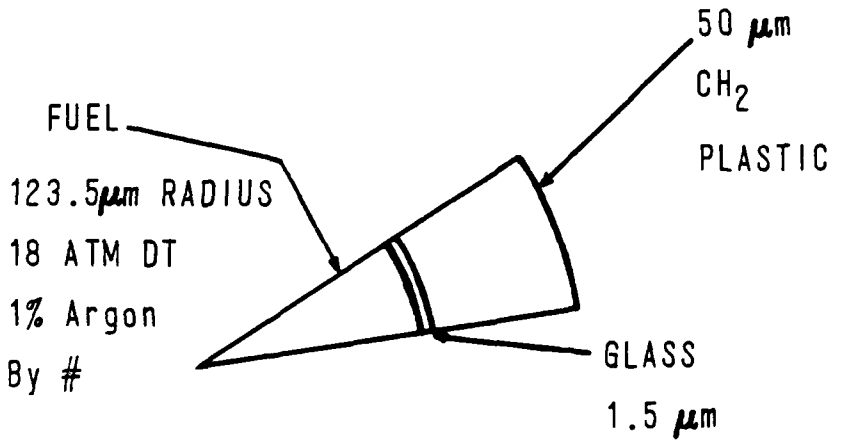

Fig. 2 — Pellet and laser conditions for the microballoon implosion modeled

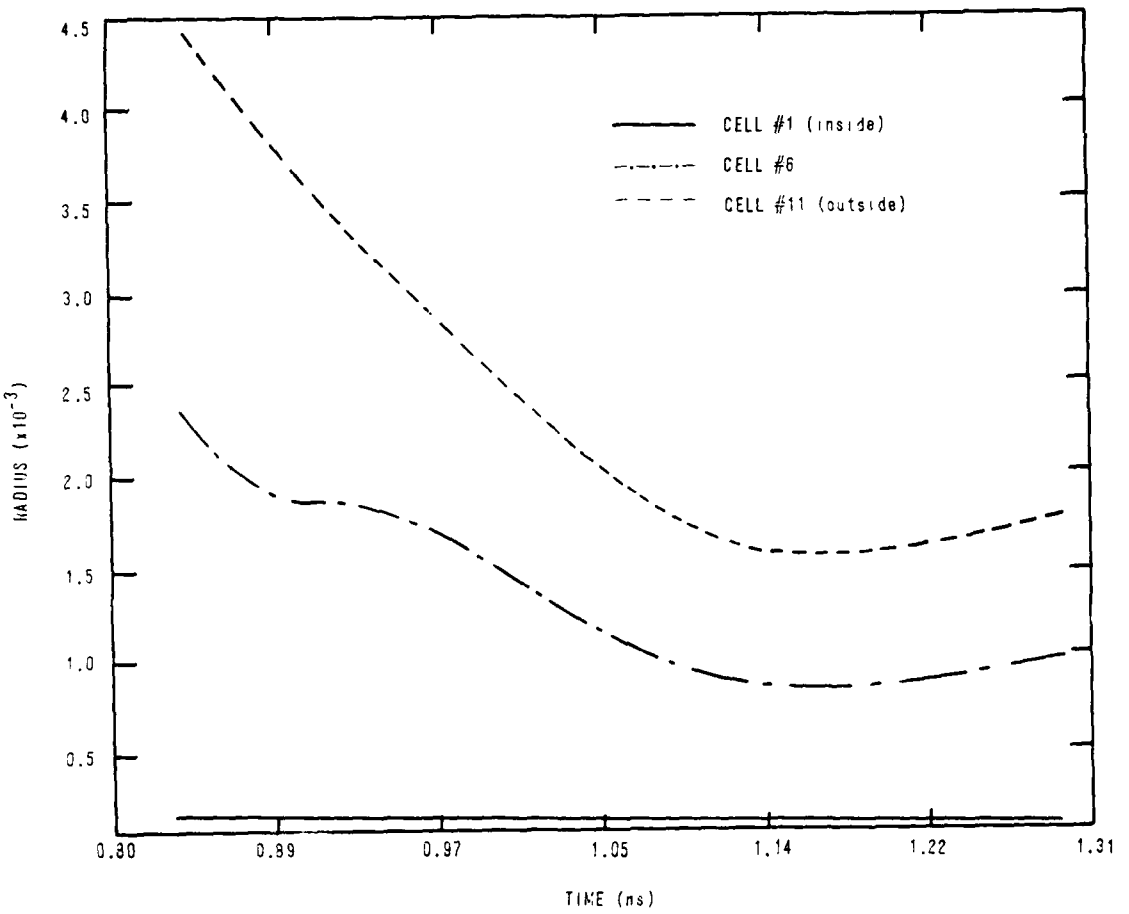

Fig. 3 — Radius of cell center vs time

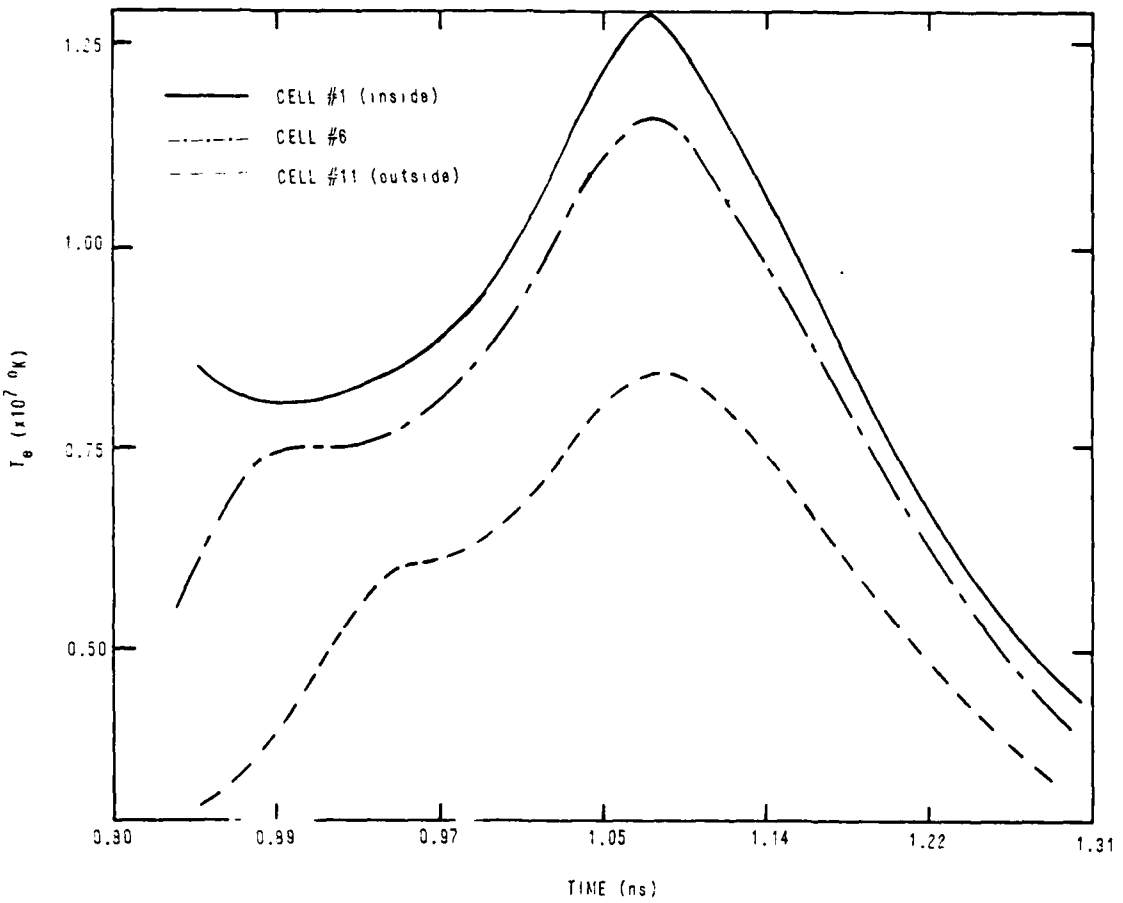

Fig. 4 — Electron temperature vs time

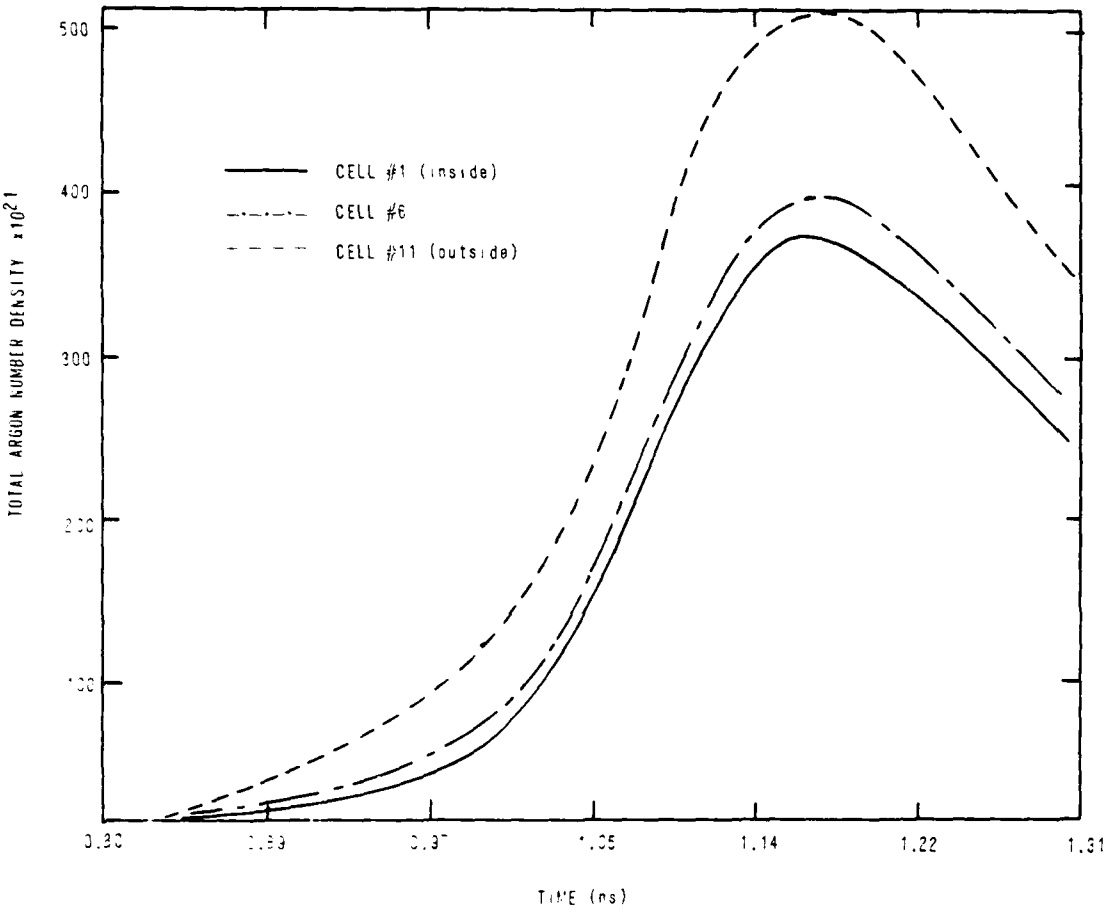

Fig. 5 — Total argon number density vs time

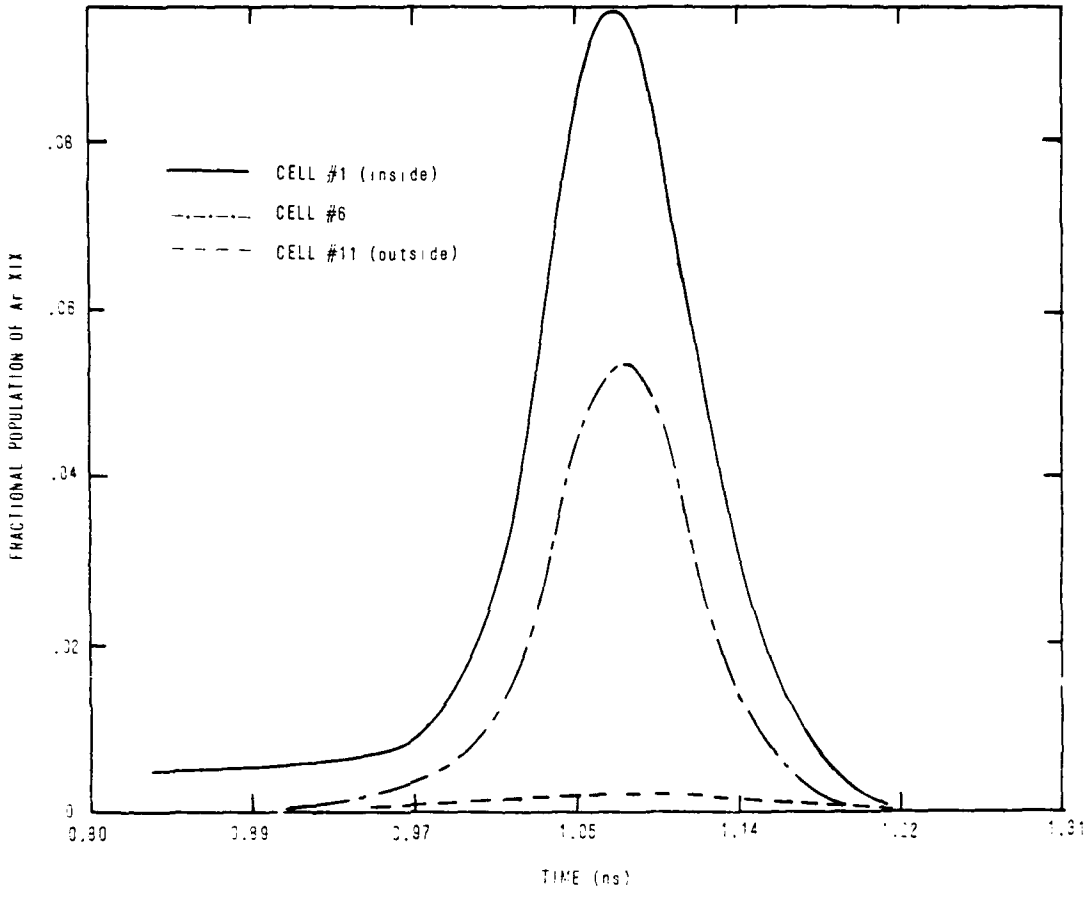

Fig. 6 — Fractional population of Ar XIX vs time

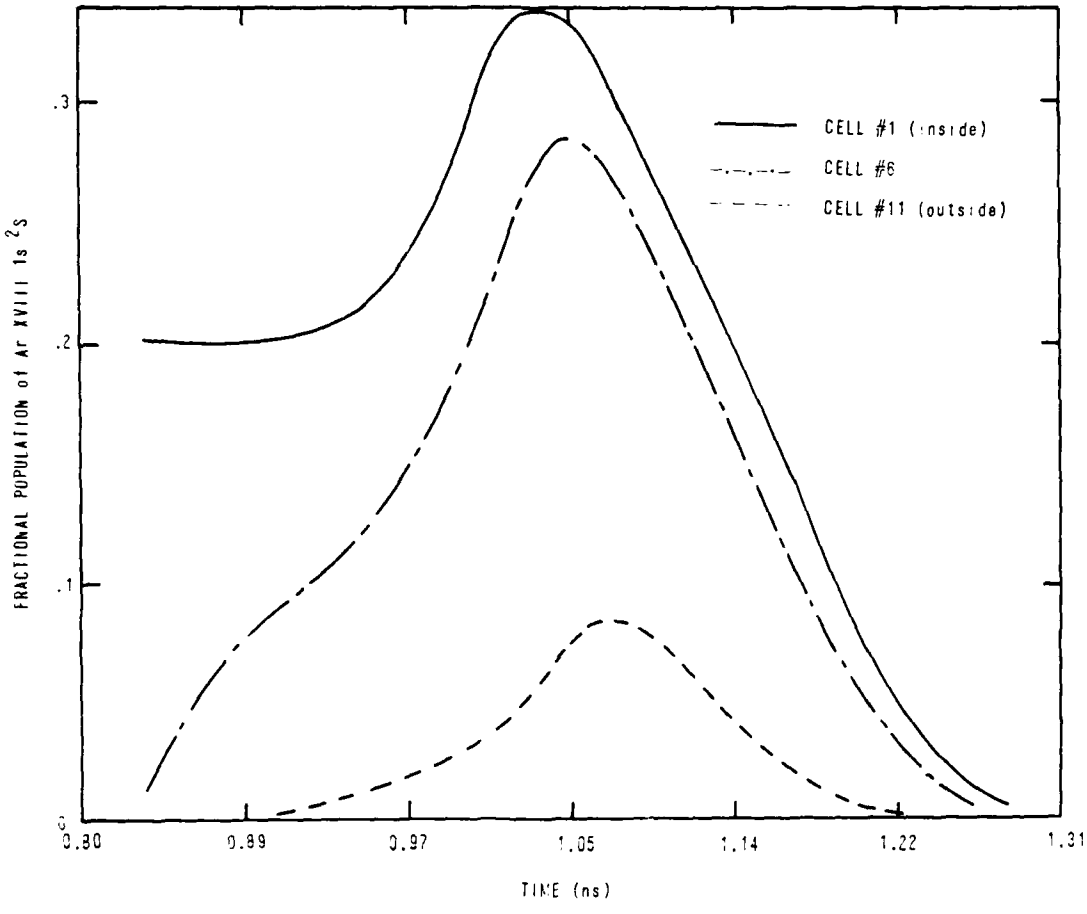

Fig. 7 — Fractional population of Ar XVIII $1s^2S$ vs time

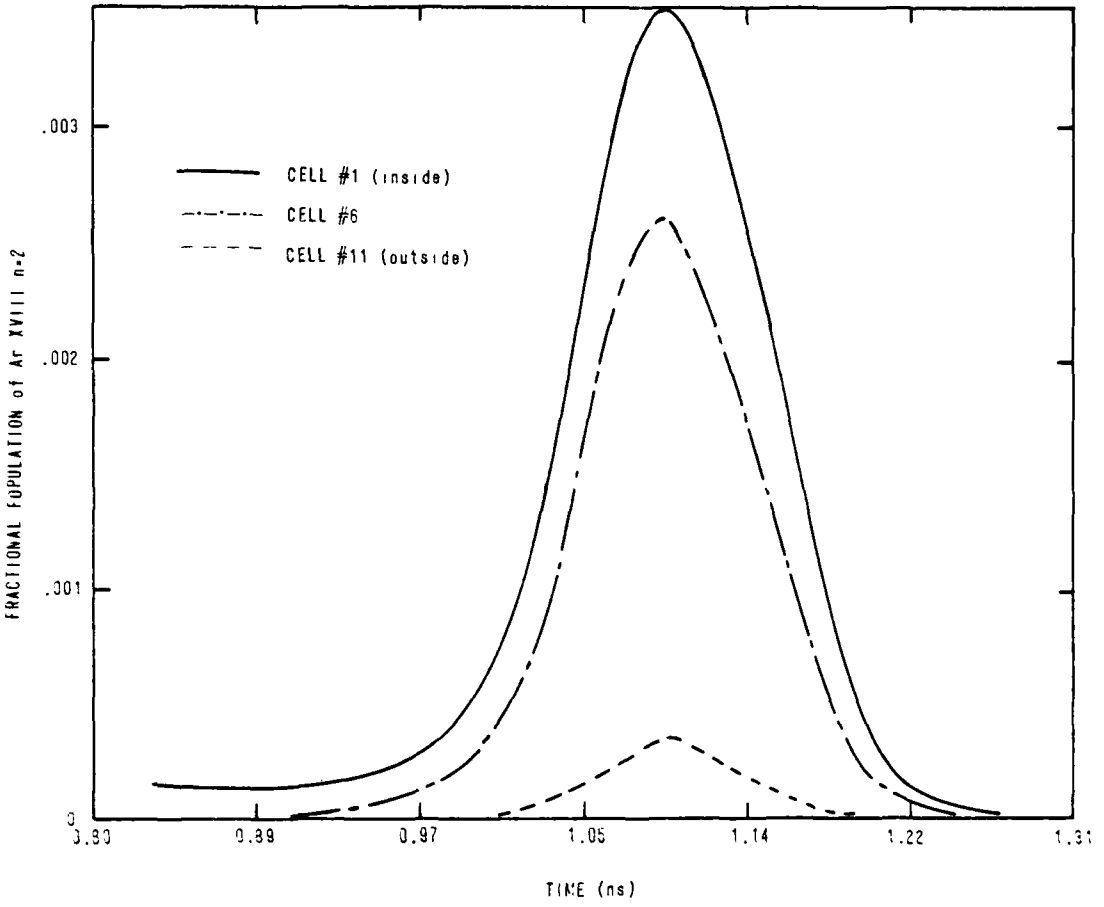

Fig. 8 — Fractional population of Ar XVIII n=2 vs time

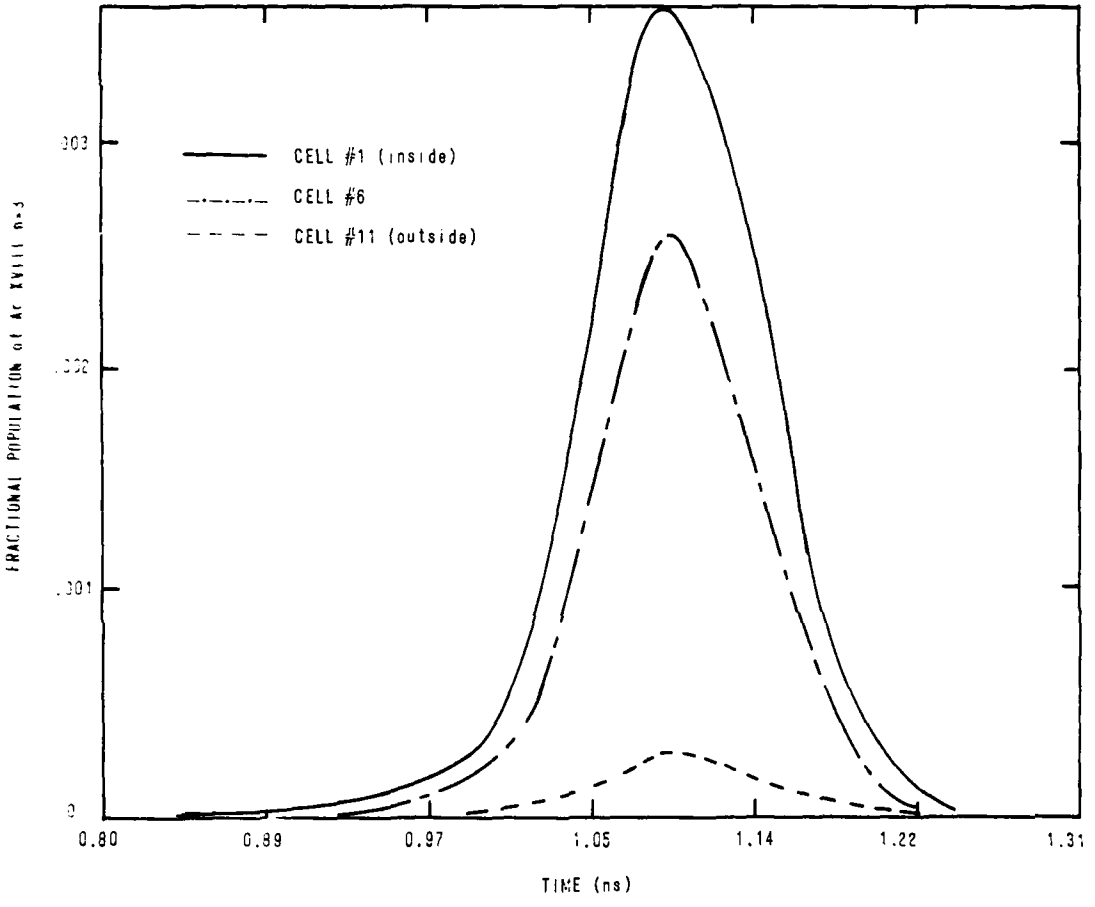

Fig. 9 — Fractional population of Ar XVIII n=3 vs time

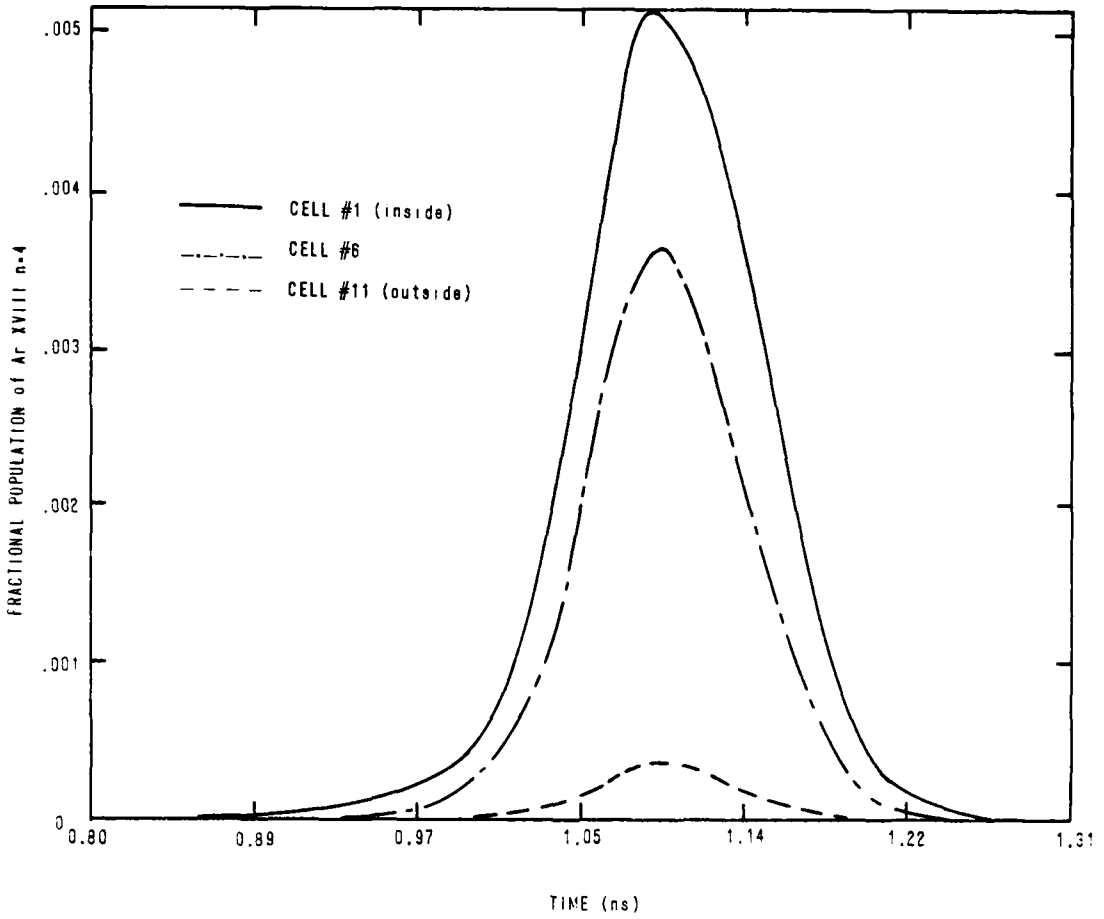

Fig. 10 — Fractional population of Ar XVIII n=4 vs time

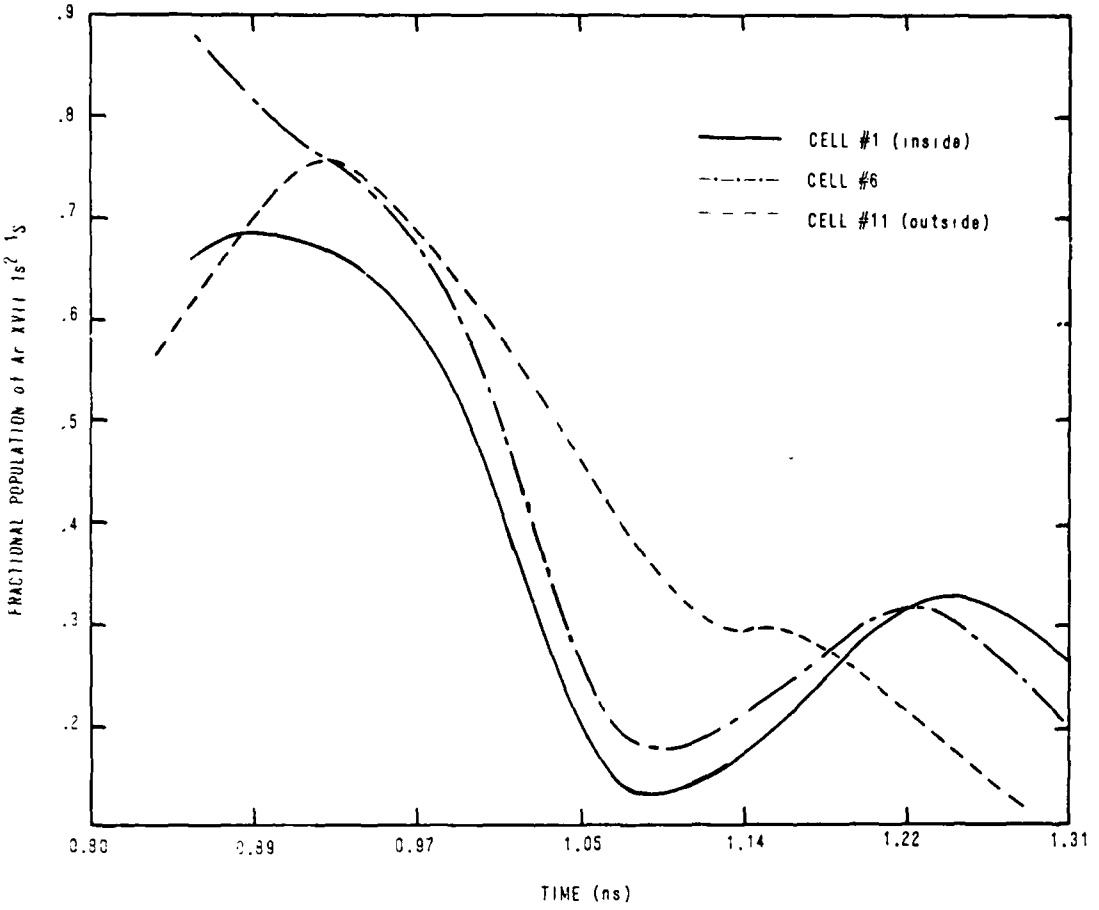

Fig. 11 — Fractional population of Ar XVII $1s^2\ ^1S$ vs time

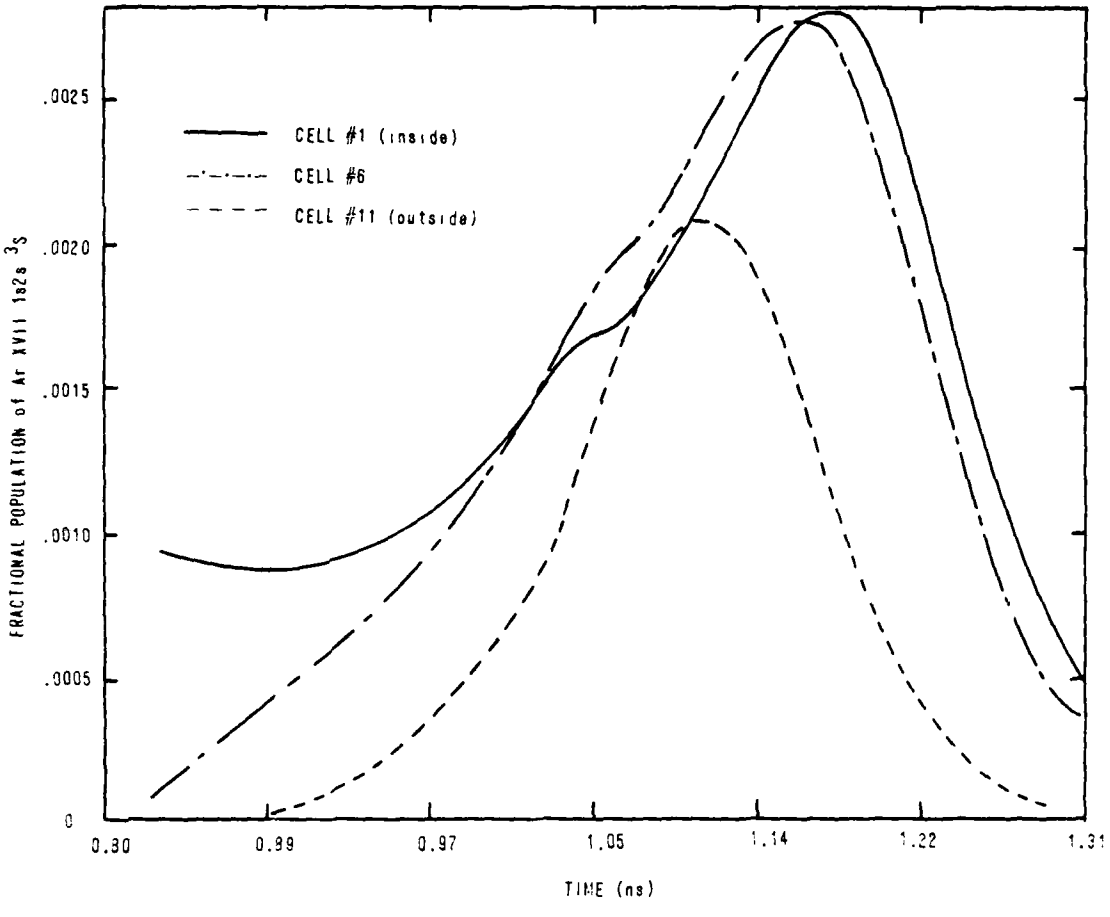

Fig. 12 — Fractional population of Ar XVII 1s2s ^{3}S vs time

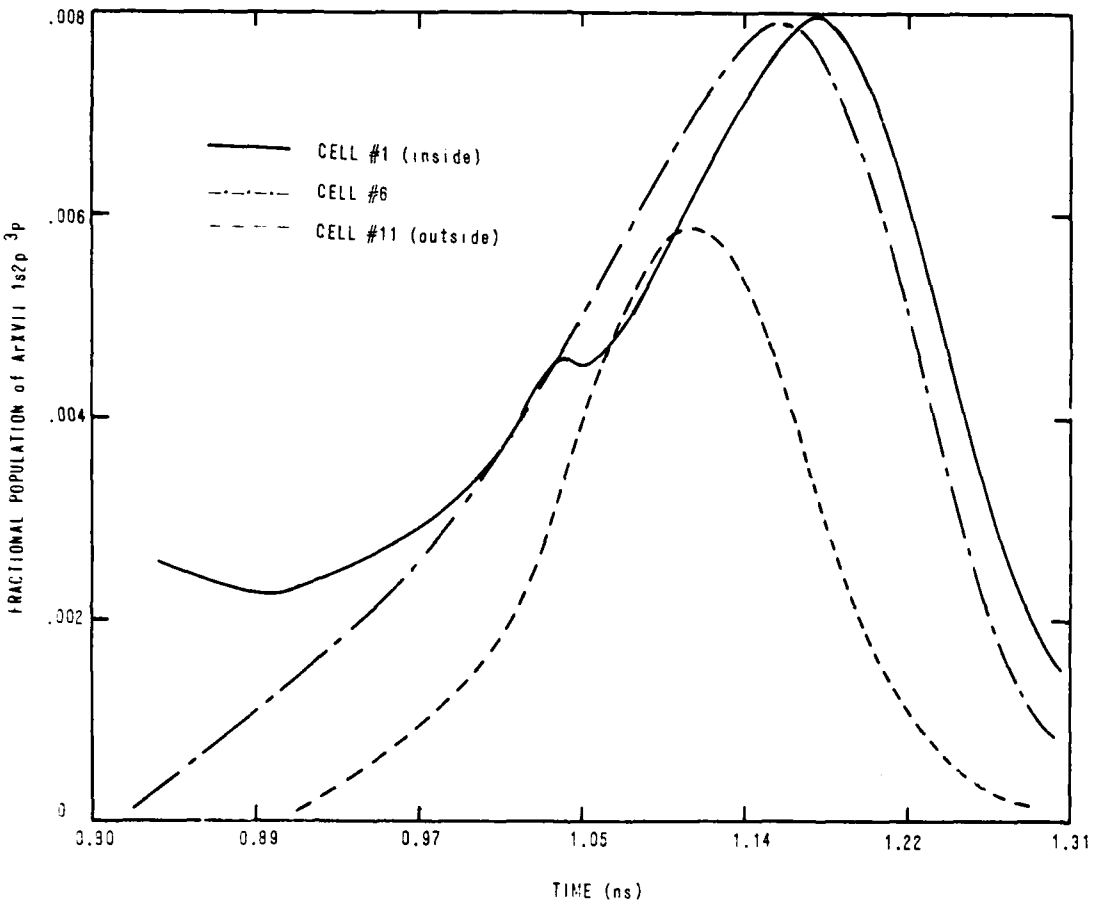

Fig. 13 — Fractional population of Ar XVII 1s2p ^{3}P vs time

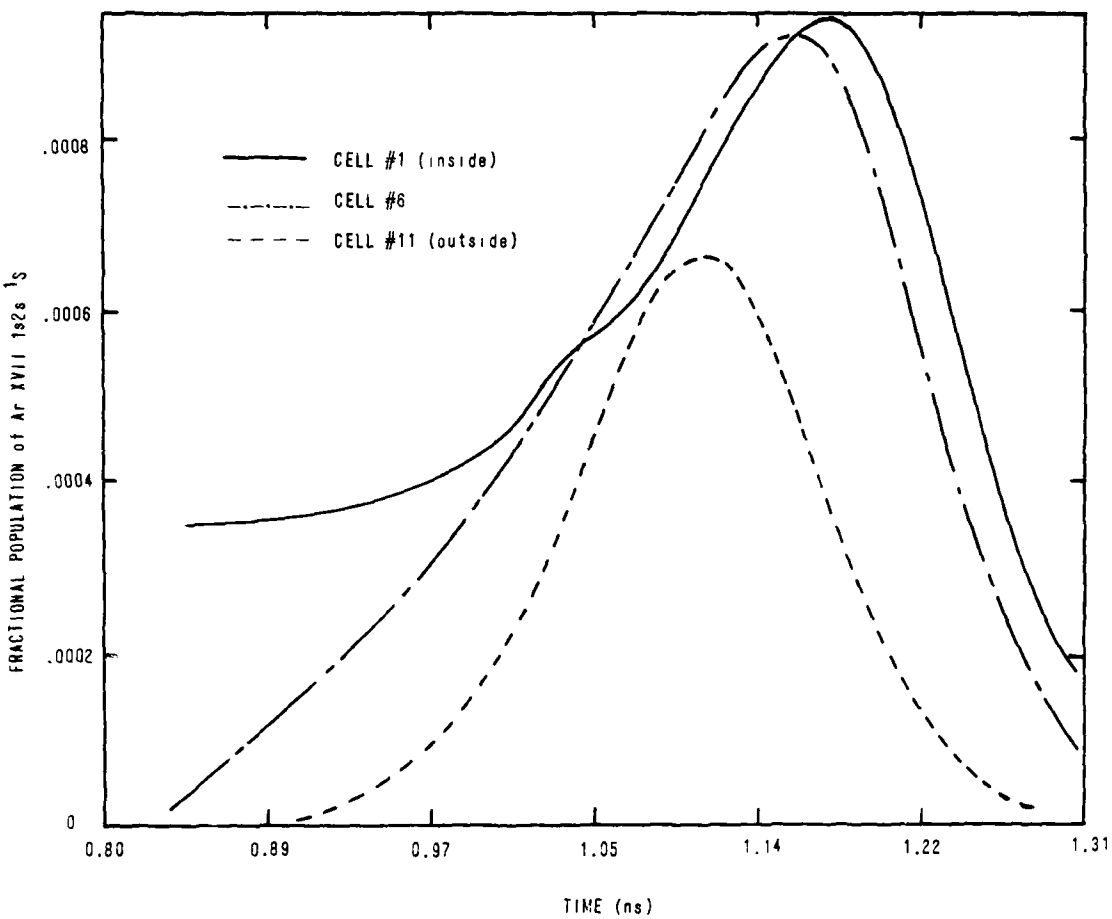

Fig. 14 — Fractional population of A^{+} XVII 1s2s ^{1}S vs time

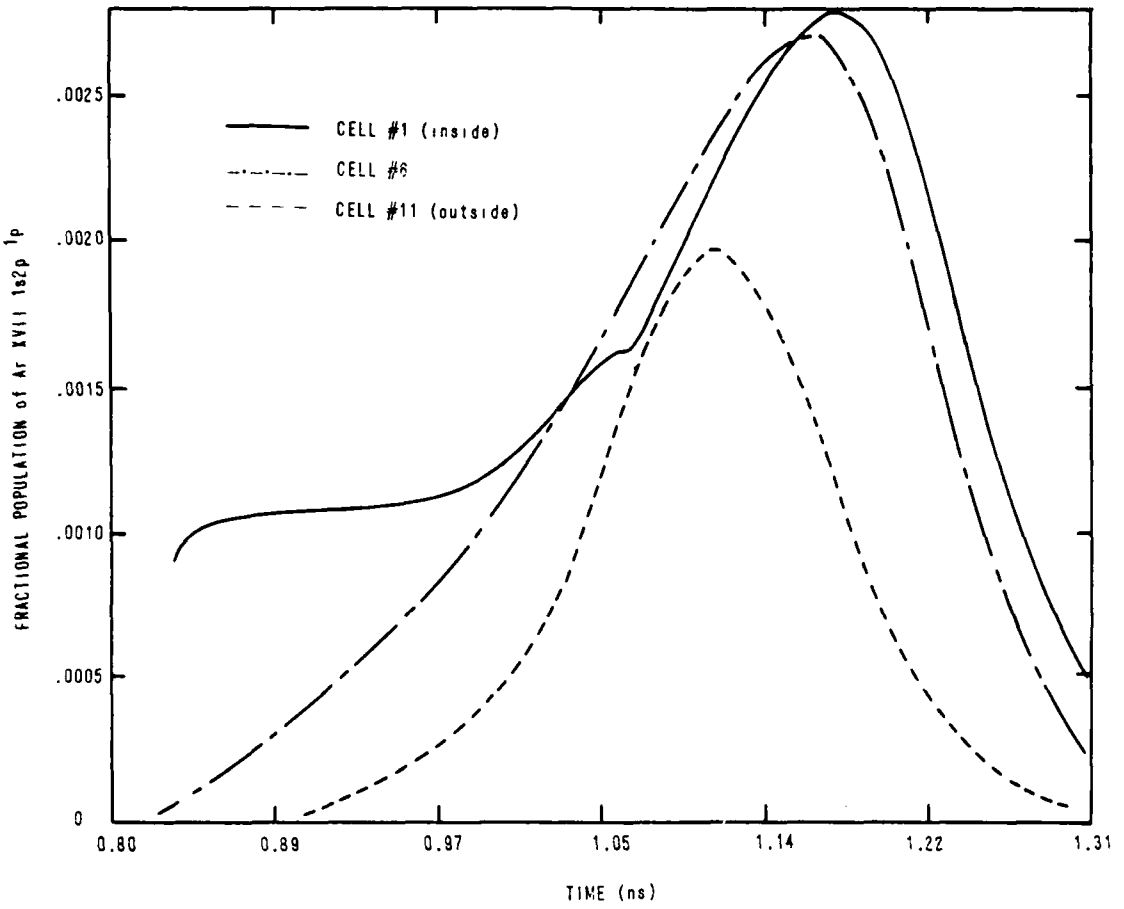

Fig. 15 — Fractional population of Ar XVII 1s2p ^{1}P vs time

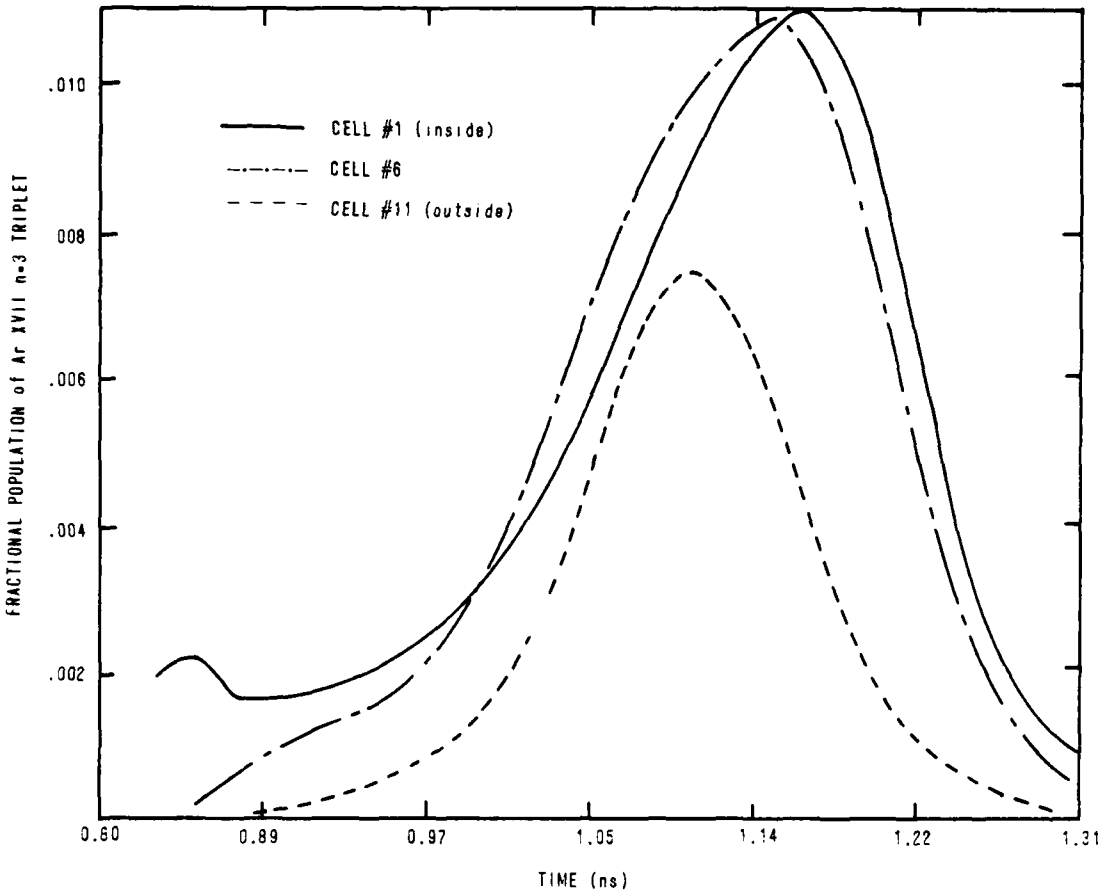

Fig. 16 — Fractional population of Ar XVII n=3 triplet vs time

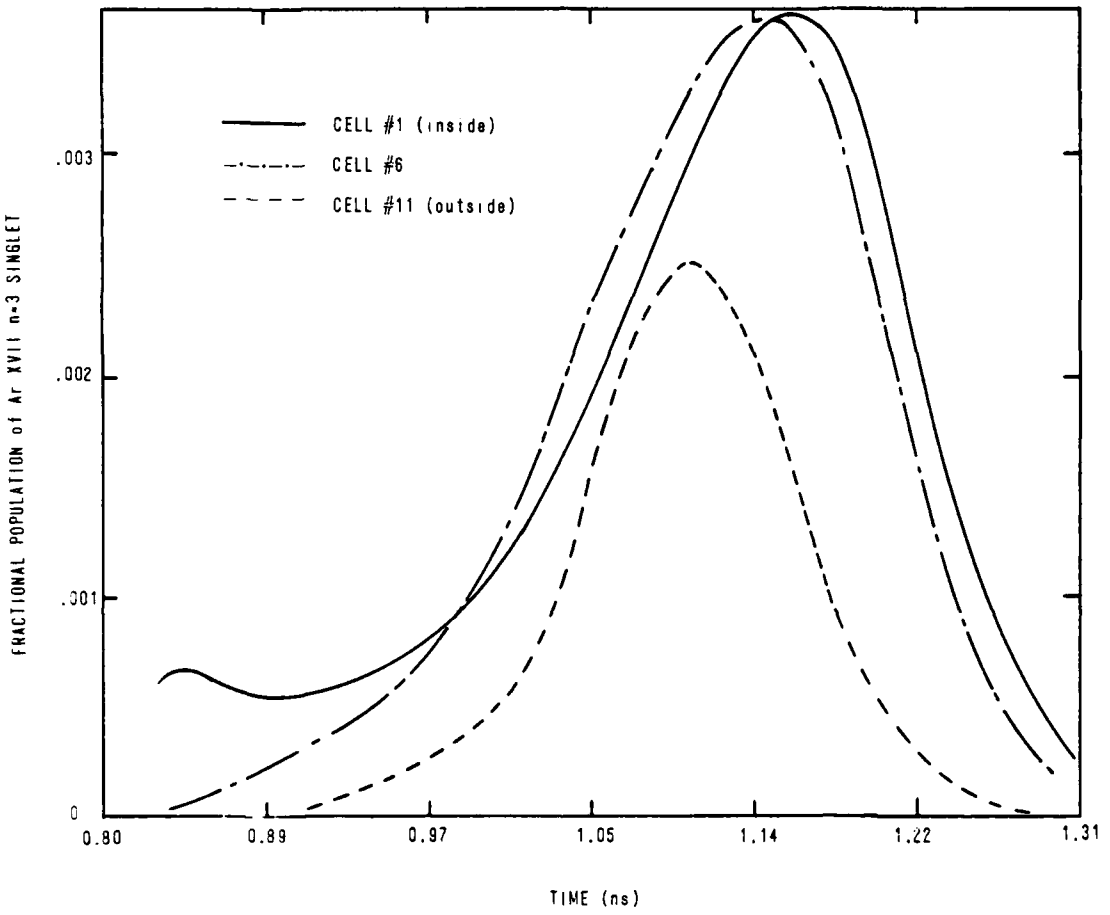

Fig. 17 — Fractional population of Ar XVII n=3 singlet vs time

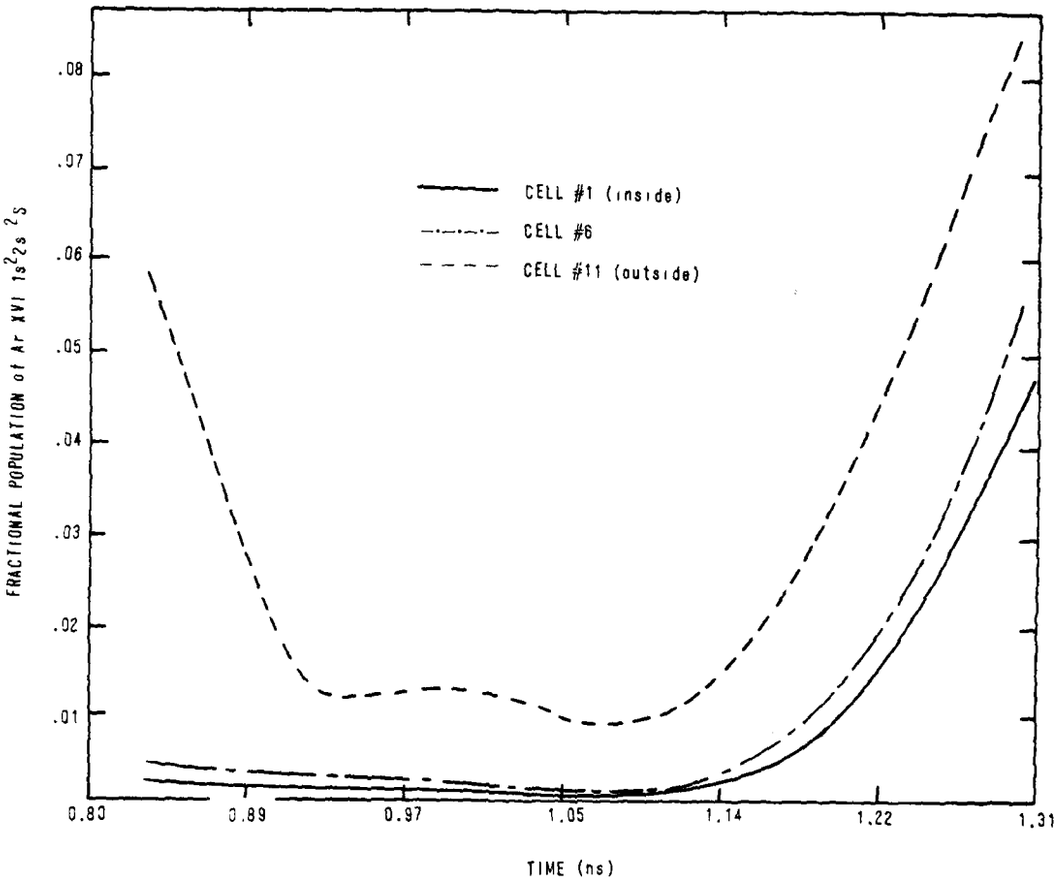

Fig. 18 — Fractional population of Ar XVI $1s^2 2s\ ^2S$ vs time

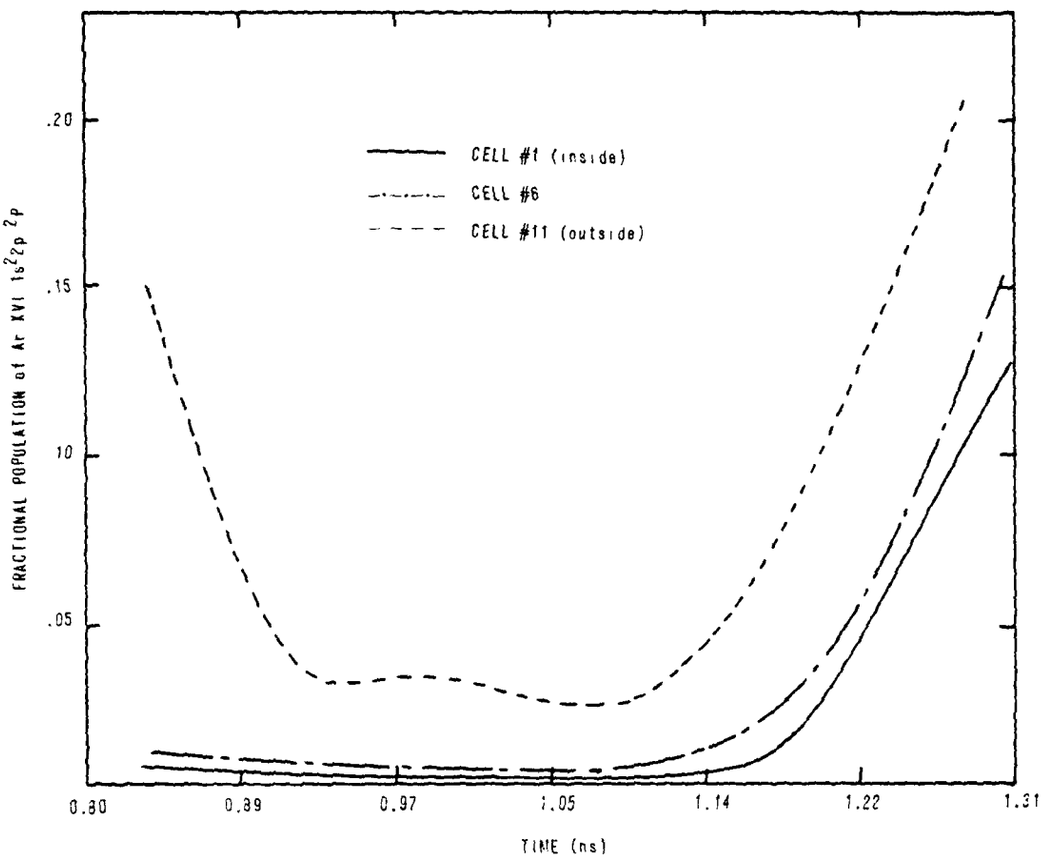

Fig. 19 — Fractional population of Ar XVI $1s^2 2p\ ^2P$ vs time

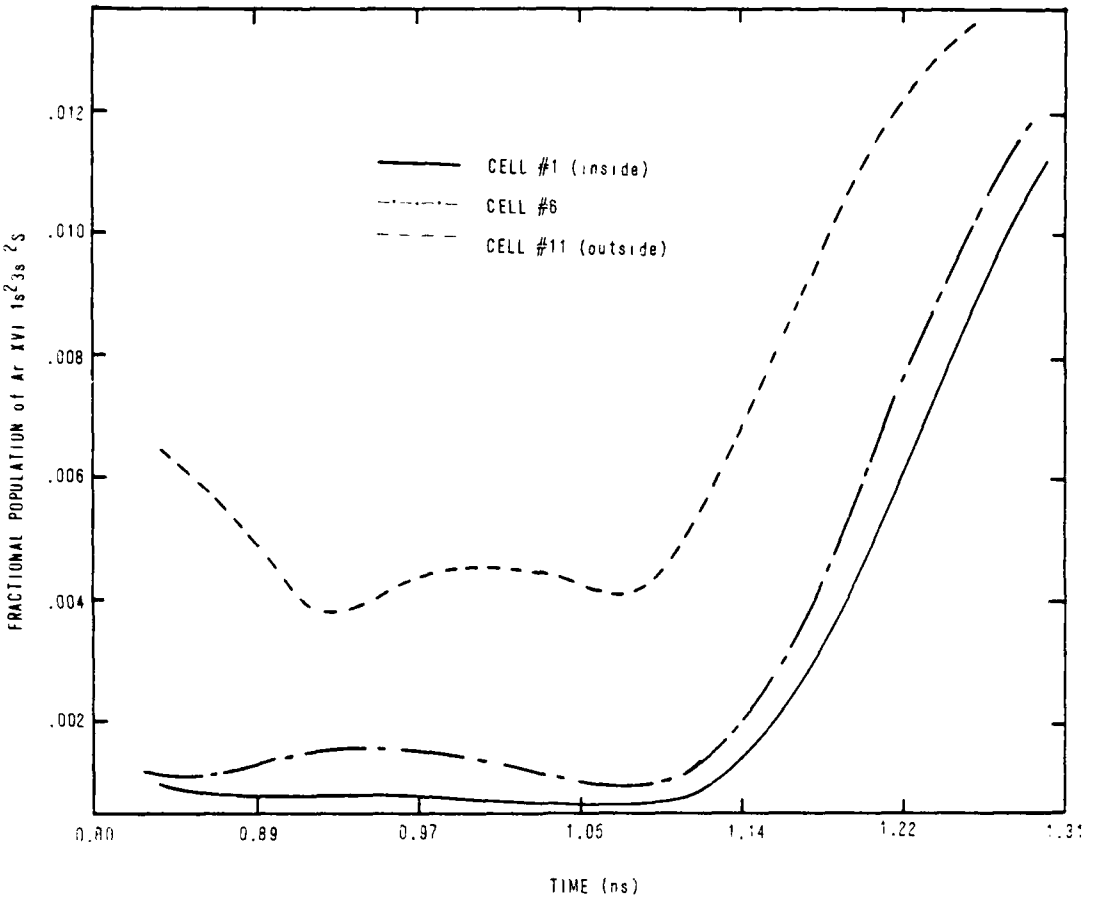

Fig. 20 — Fractional population of Ar XVI $1s^2 3s\ ^2S$ vs time

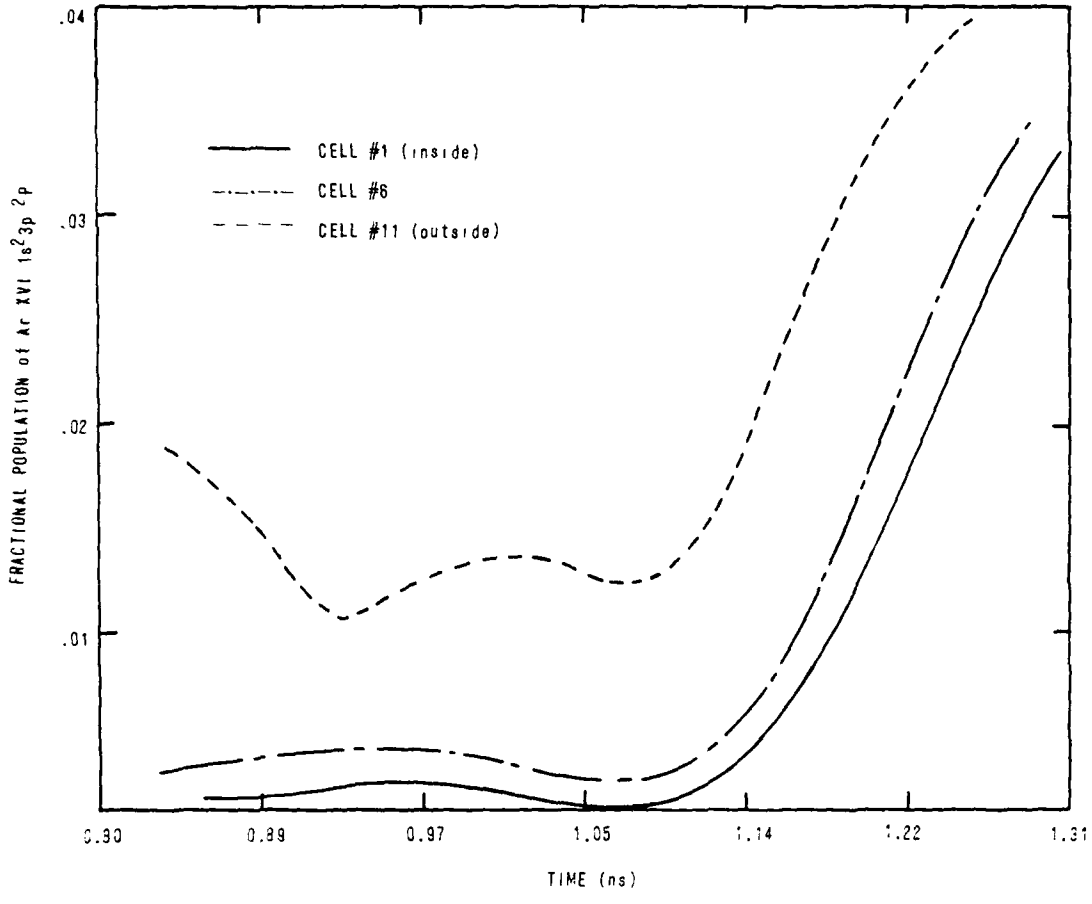

Fig. 21 — Fractional population of Ar XVI $1s^2 3p\ ^2P$ vs time

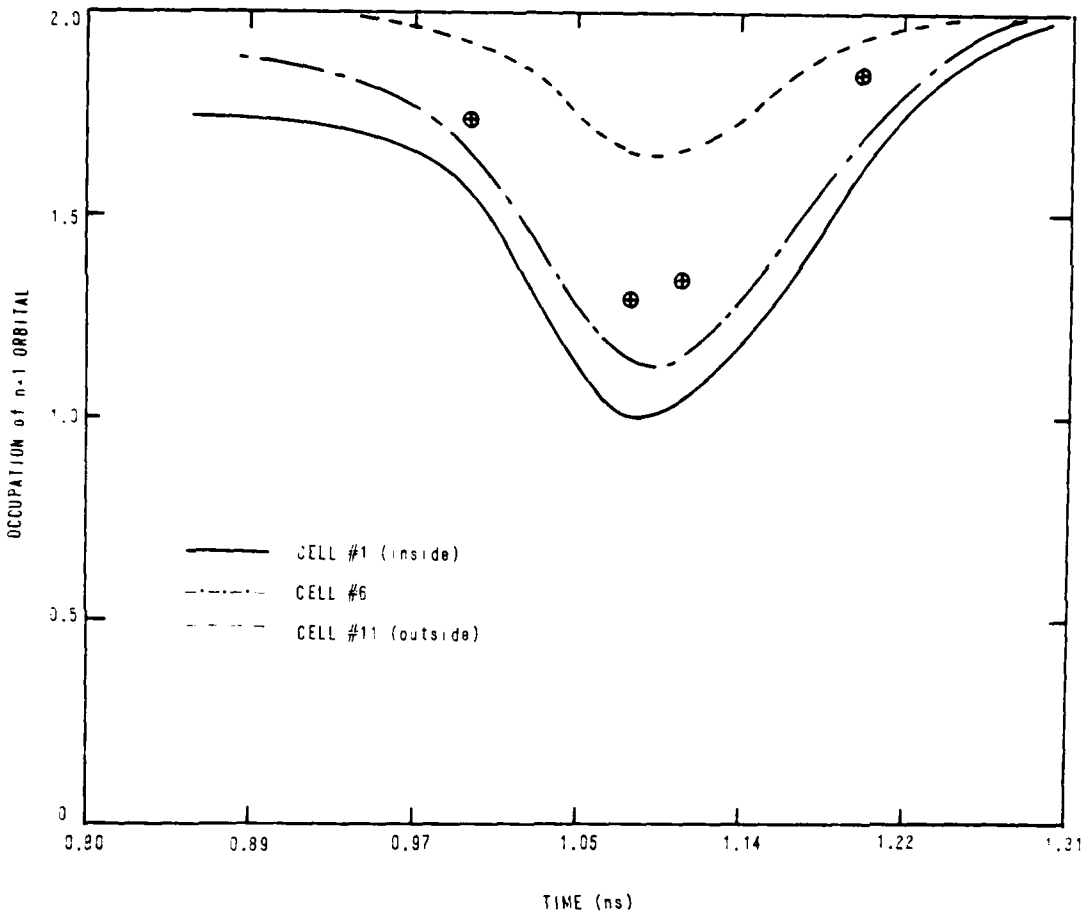

Fig. 22 — Occupation of the n=1 orbital vs time. The points marked ⊕ were calculated by LASNEX for the inner cell (no. 1).

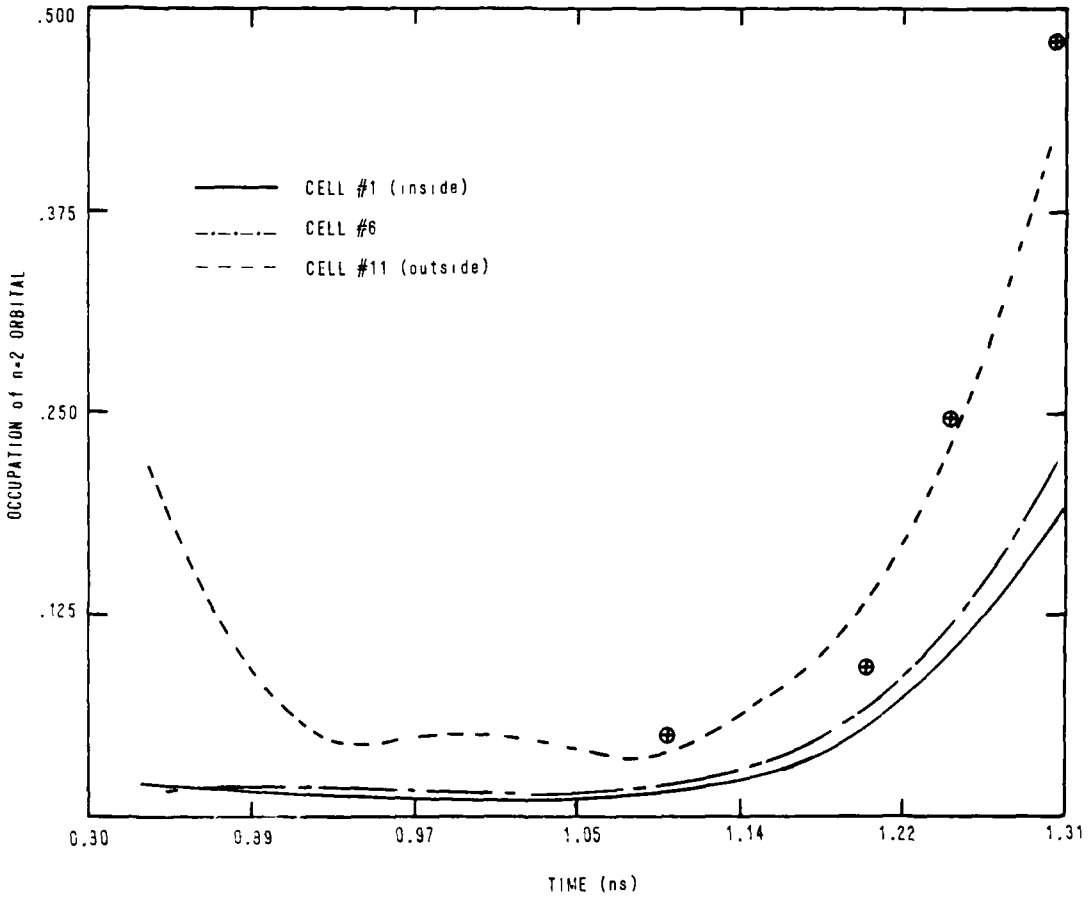

Fig. 23 — Occupation of the n=2 orbital vs time. The points marked ⊕ were calculated by LASNEX for the inner cell (no. 1).

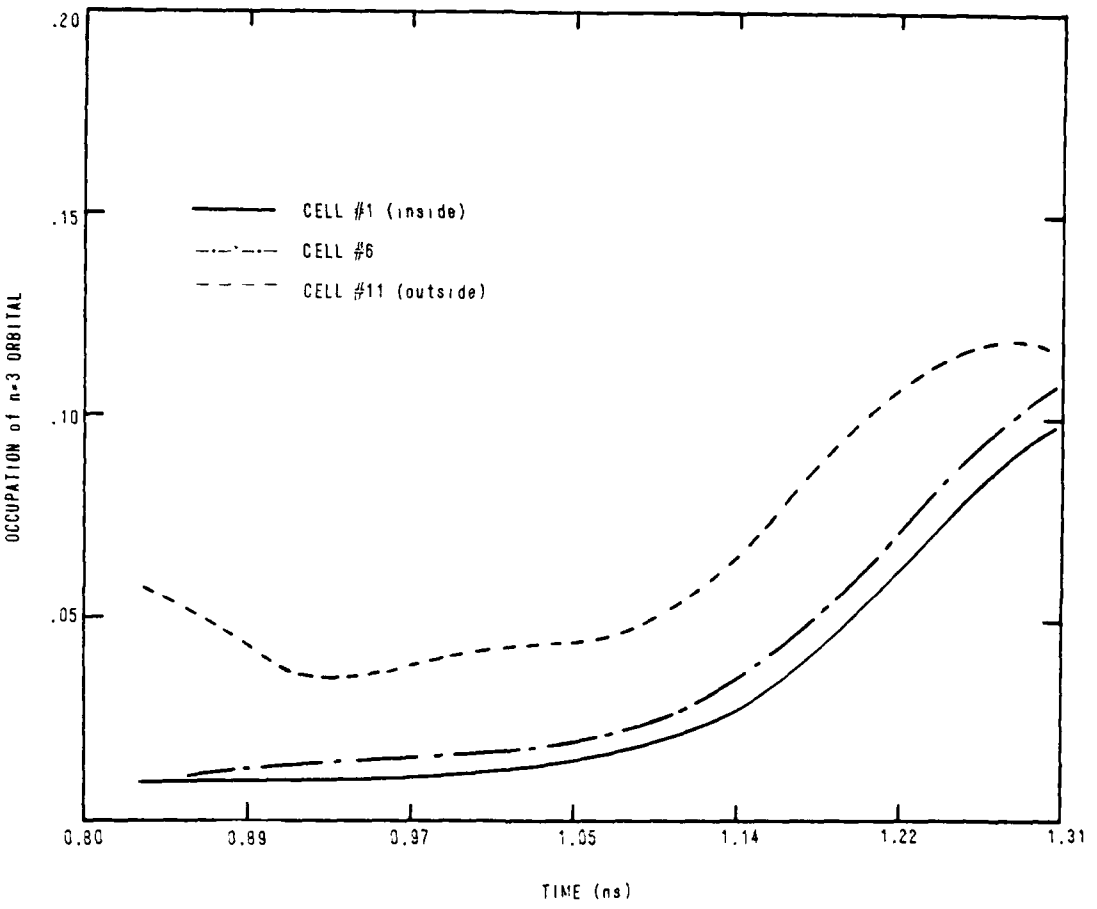

Fig. 24 — Occupation of the n=3 orbital vs time

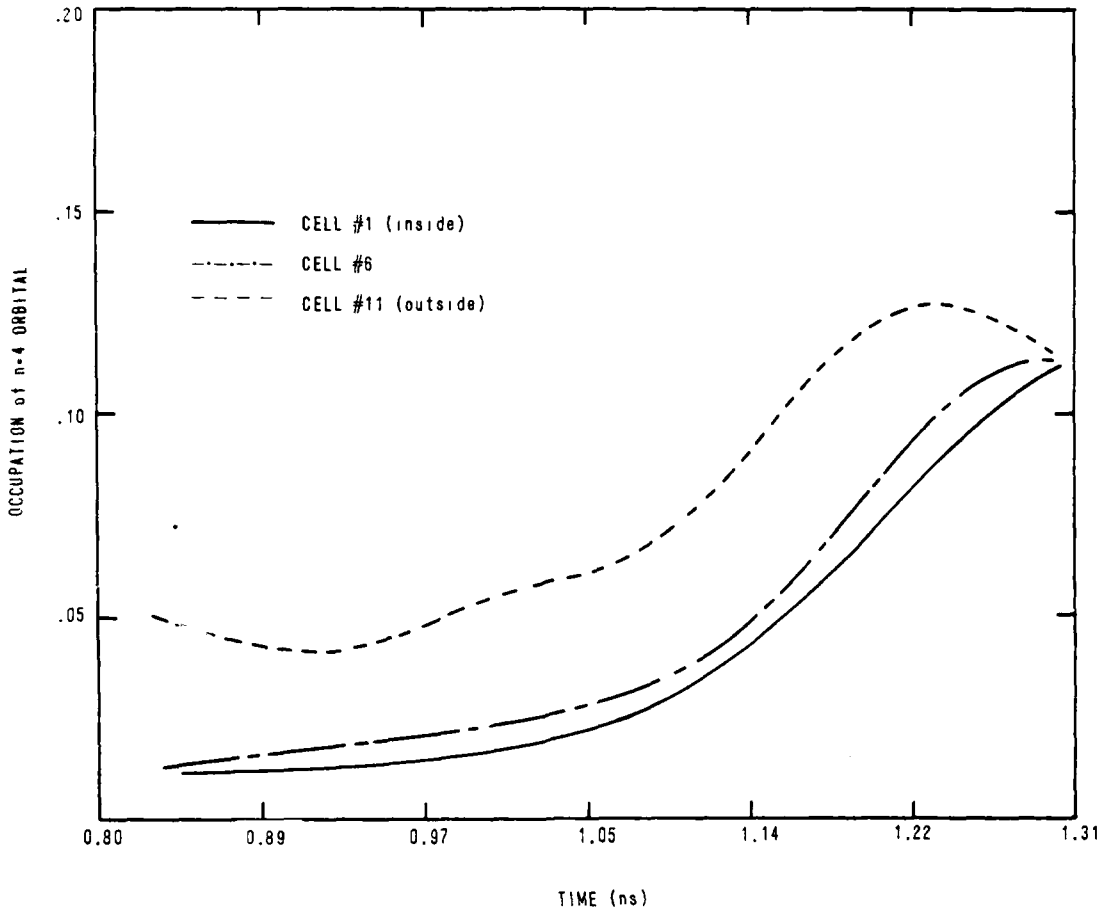

Fig. 25 — Occupation of the n=4 orbital vs time

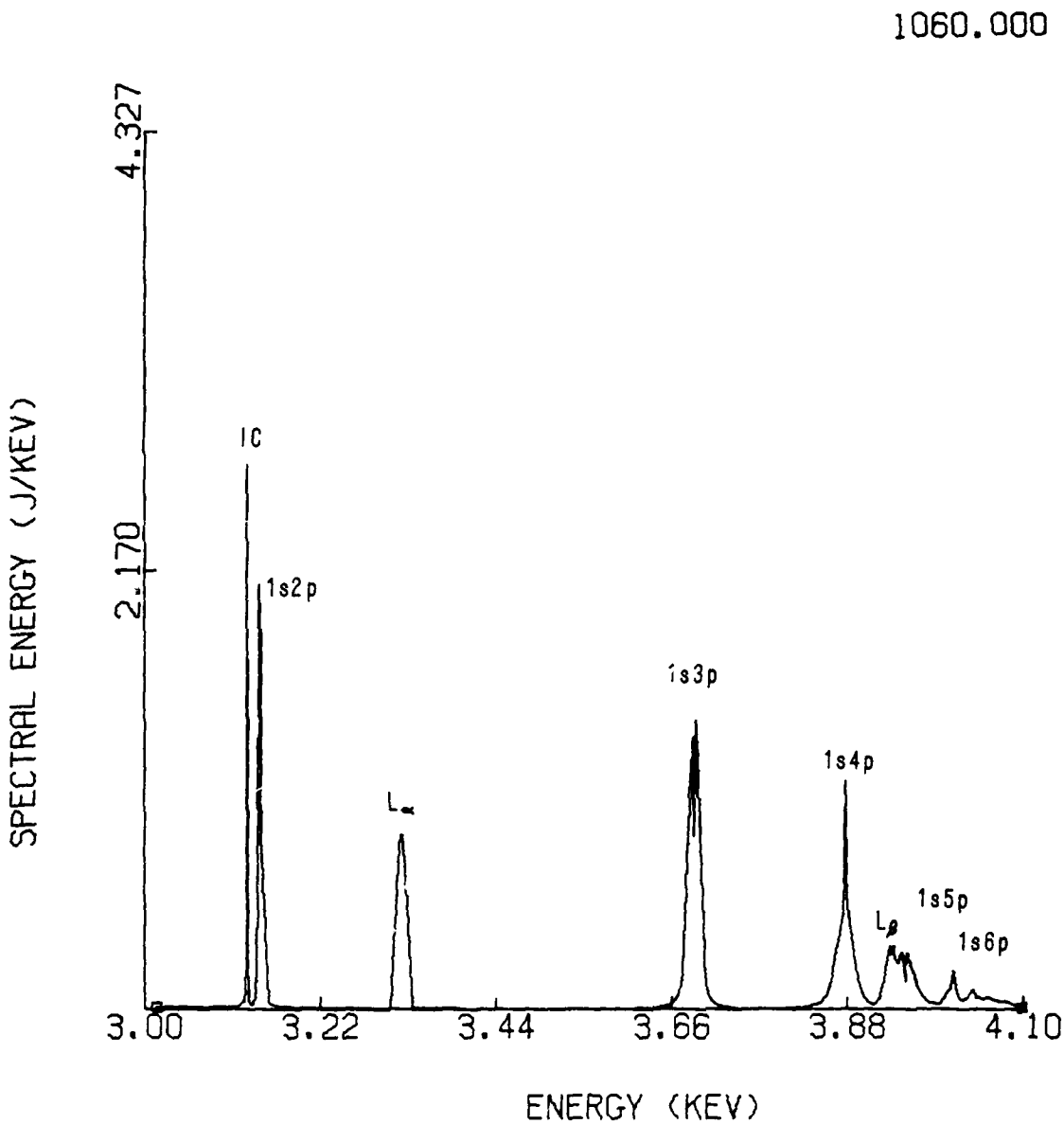

Fig. 26 — Spectrum integrated from 0.8 to 1.06 ns

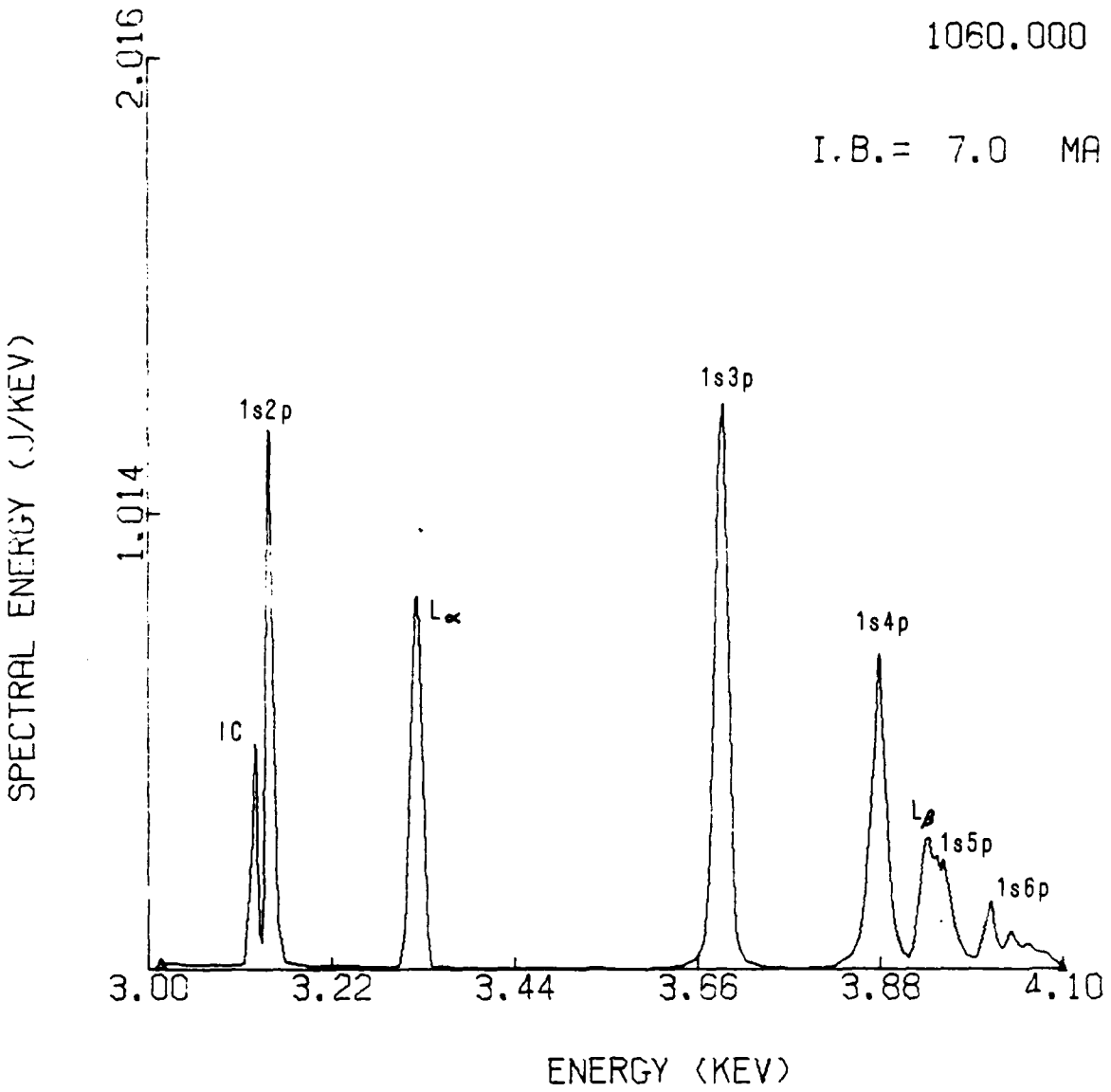

Fig. 27 — Spectrum integrated from 0.8 to 1.06 ns. (Corrected for source and instrumental broadening.)

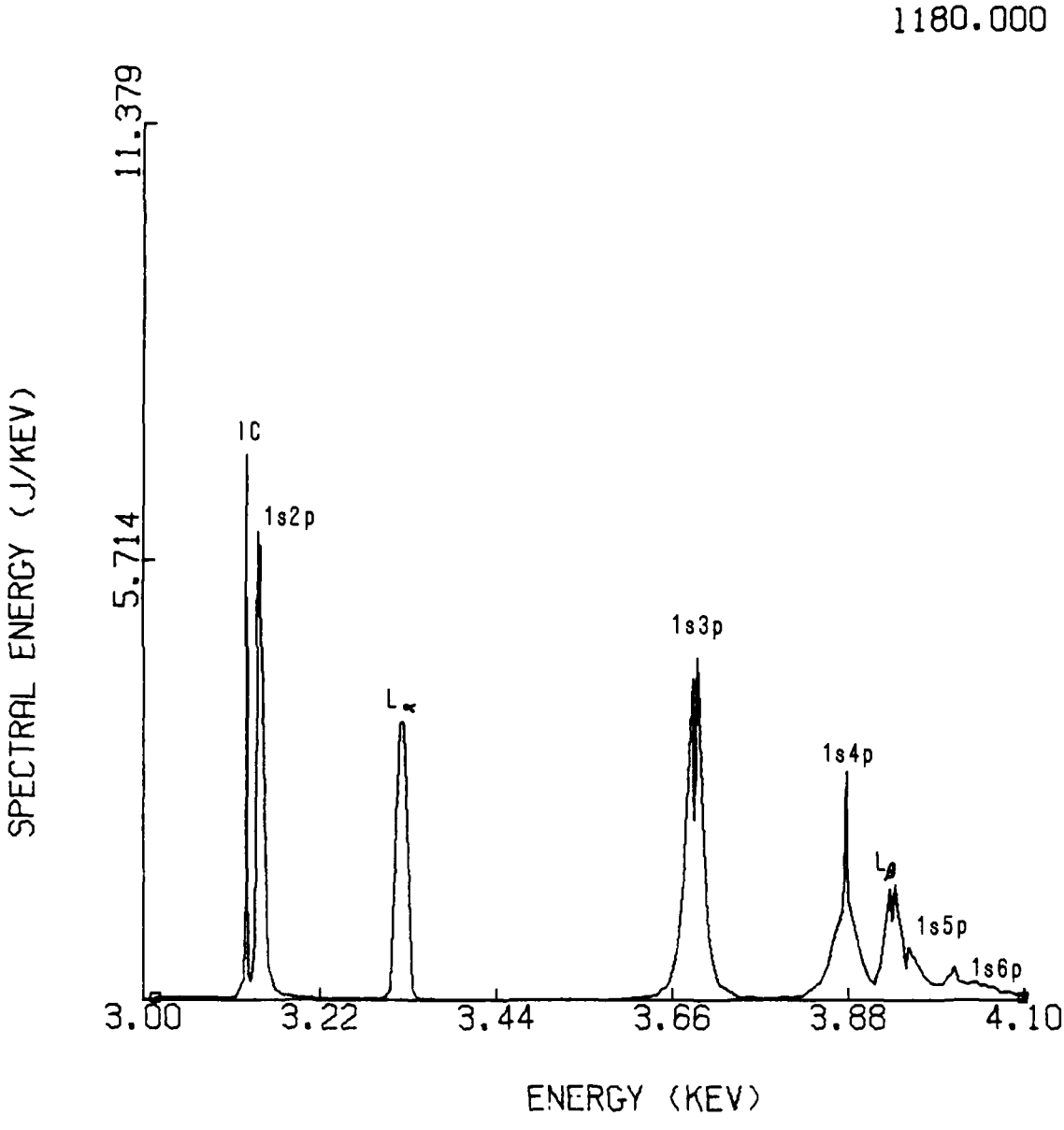

Fig. 28 — Spectrum integrated from 0.8 to 1.18 ns

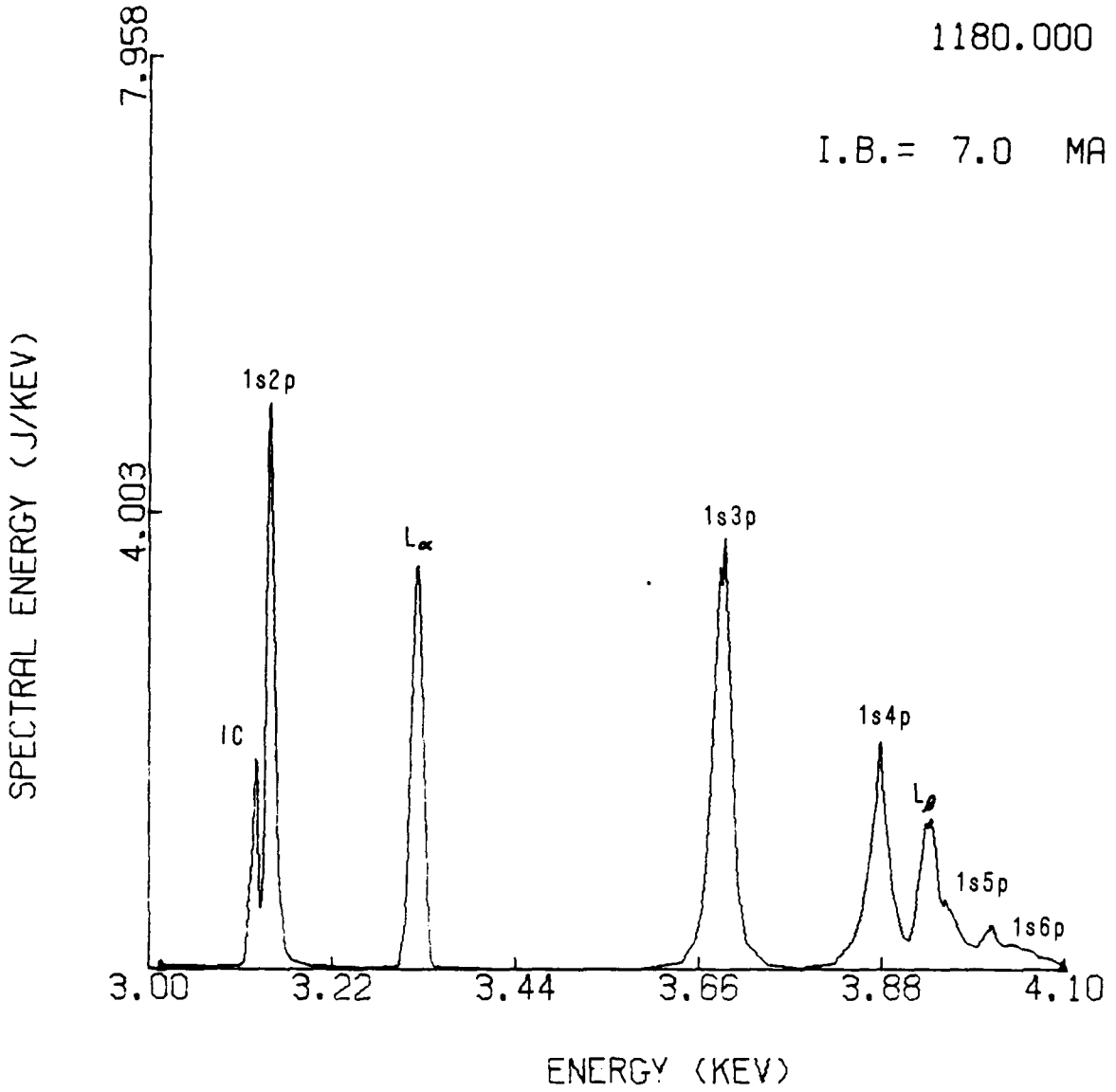

Fig. 29 — Spectrum integrated from 0.8 to 1.18 ns. (Corrected for source and instrumental broadening.)

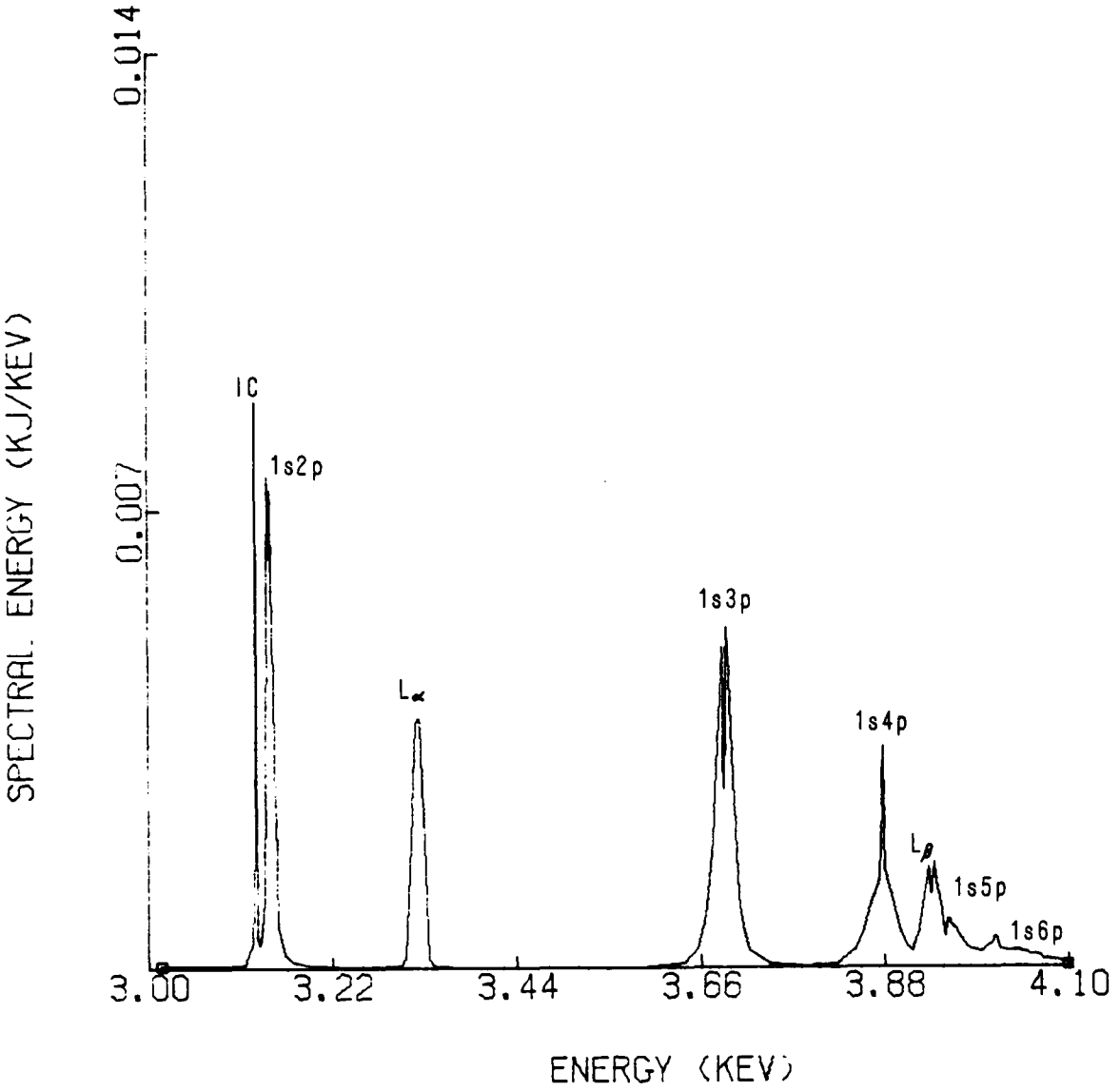

Fig. 30 — Spectrum integrated from 0.8 to 1.3 ns

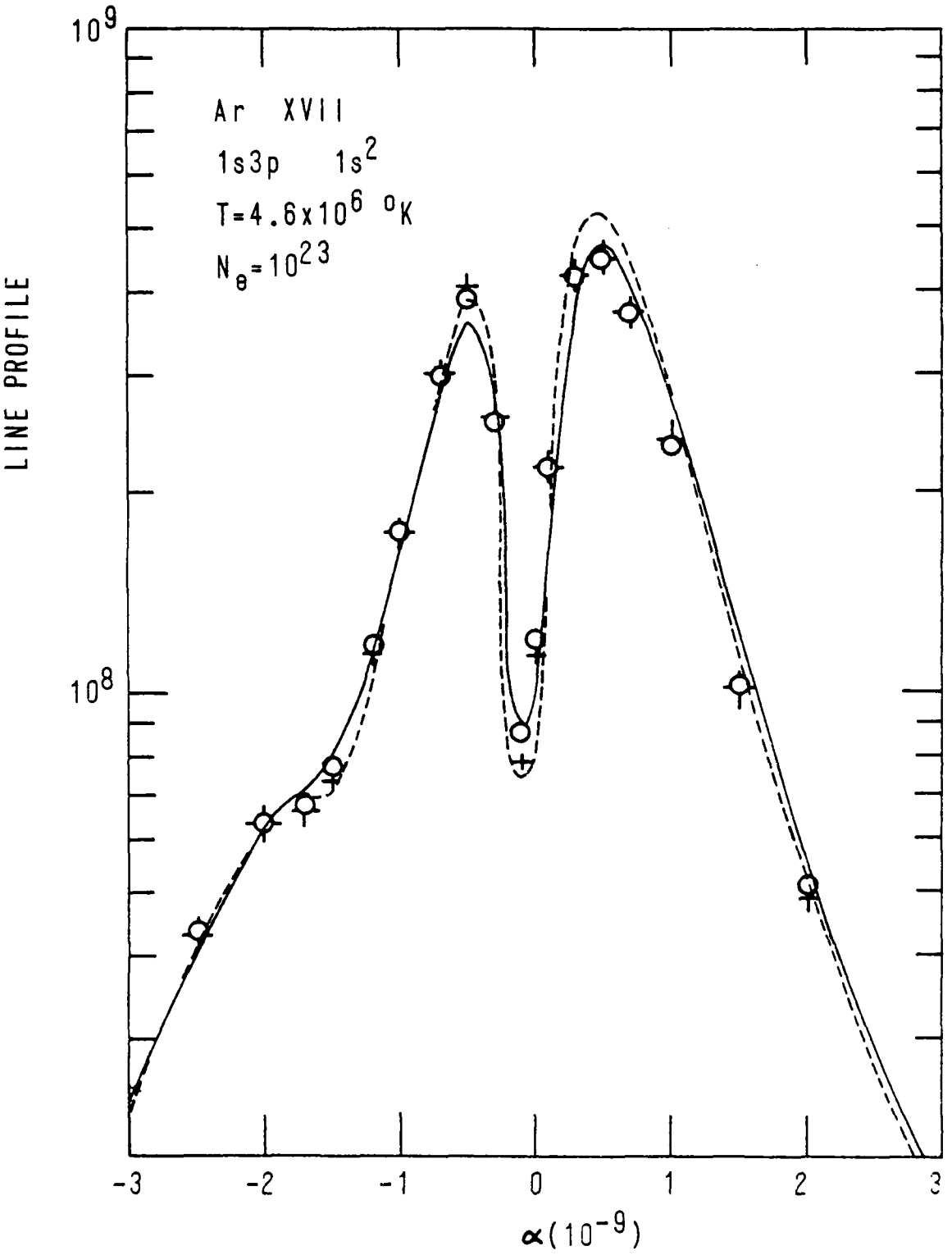

Fig. 31 — Stark profile of Ar XVII 1s3p—1s^2. The dashed line corresponds to calculations which include the singlet states only. The solid line to calculations which include mixing of singlet and triplet states. The points marked O and + were calculated neglecting the imaginary (shift) part of the electron operator. The points marked + were calculated using an approximation in the real part of the electron broadening.

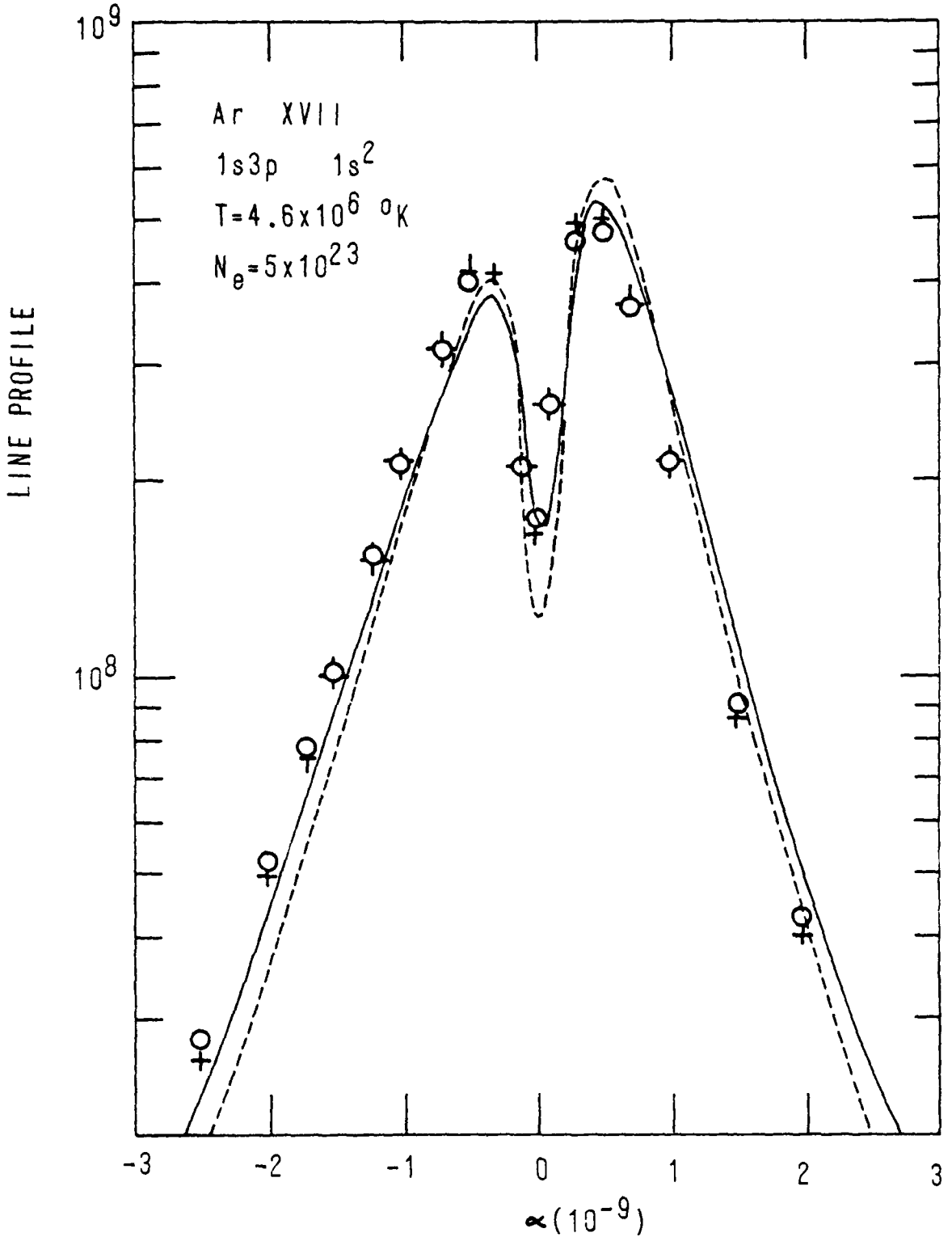

Fig. 32 — Stark profile of Ar XVII $1s3p-1s^2$. The dashed line corresponds to calculations which include the singlet states only. The solid line to calculations which include mixing of singlet and triplet states. The points marked O and + were calculated neglecting the imaginary (shift) part of the electron operator. The points marked + were calculated using an approximation in the real part of the electron broadening.

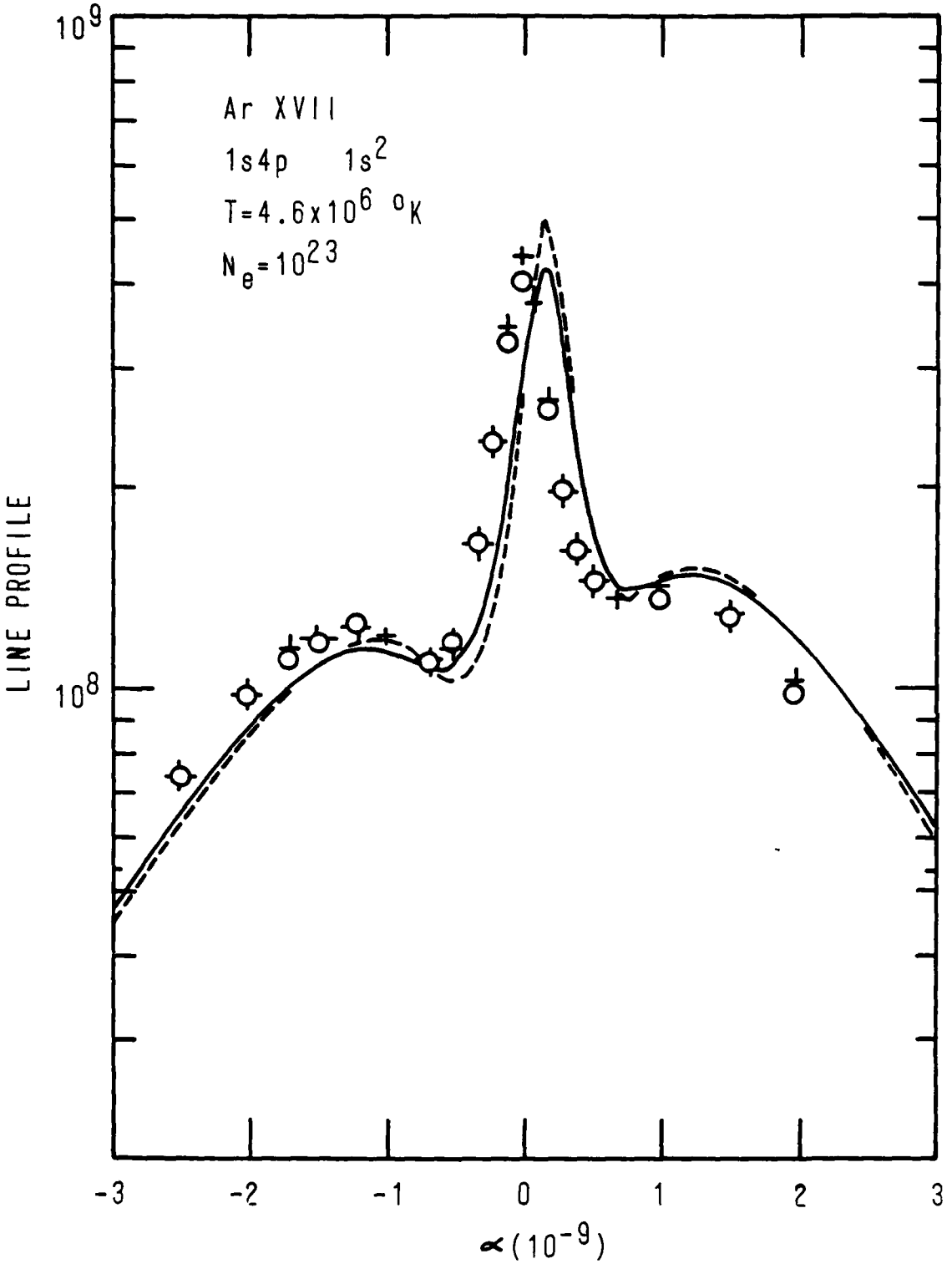

Fig. 33 — Stark profile of Ar XVII 1s4p—1s^2. The dashed line corresponds to calculations which include the singlet states only. The solid line to calculations which include mixing of singlet and triplet states. The points marked O and + were calculated neglecting the imaginary (shift) part of the electron operator. The points marked + were calculated using an approximation in the real part of the electron broadening.

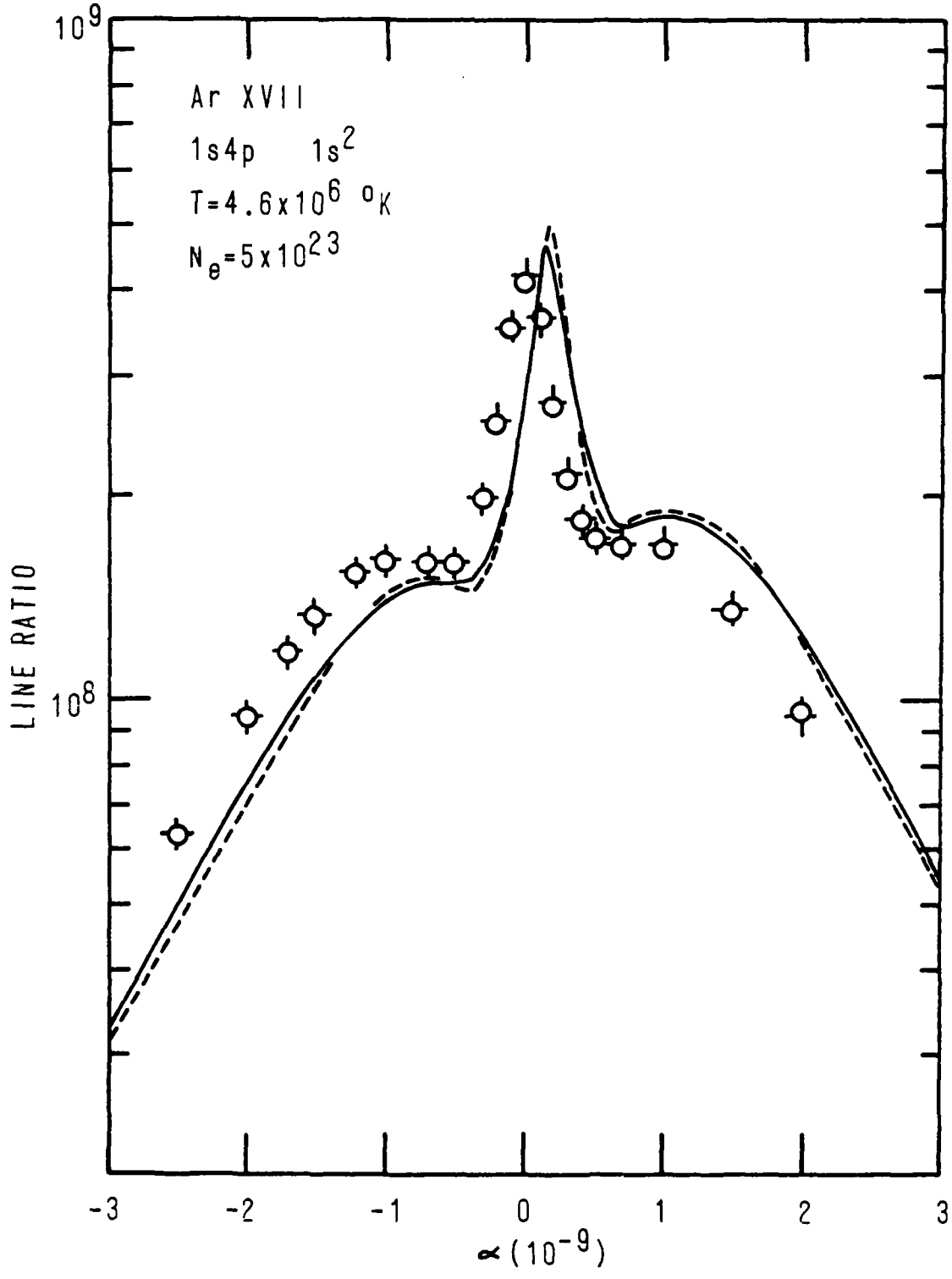

Fig. 34 — Stark profile of Ar XVII 1s4p—1s^2. The dashed line corresponds to calculations which include the singlet states only. The solid line to calculations which include mixing of singlet and triplet states. The points marked O and + were calculated neglecting the imaginary (shift) part of the electron operator. The points marked + were calculated using an approximation in the real part of the electron broadening.

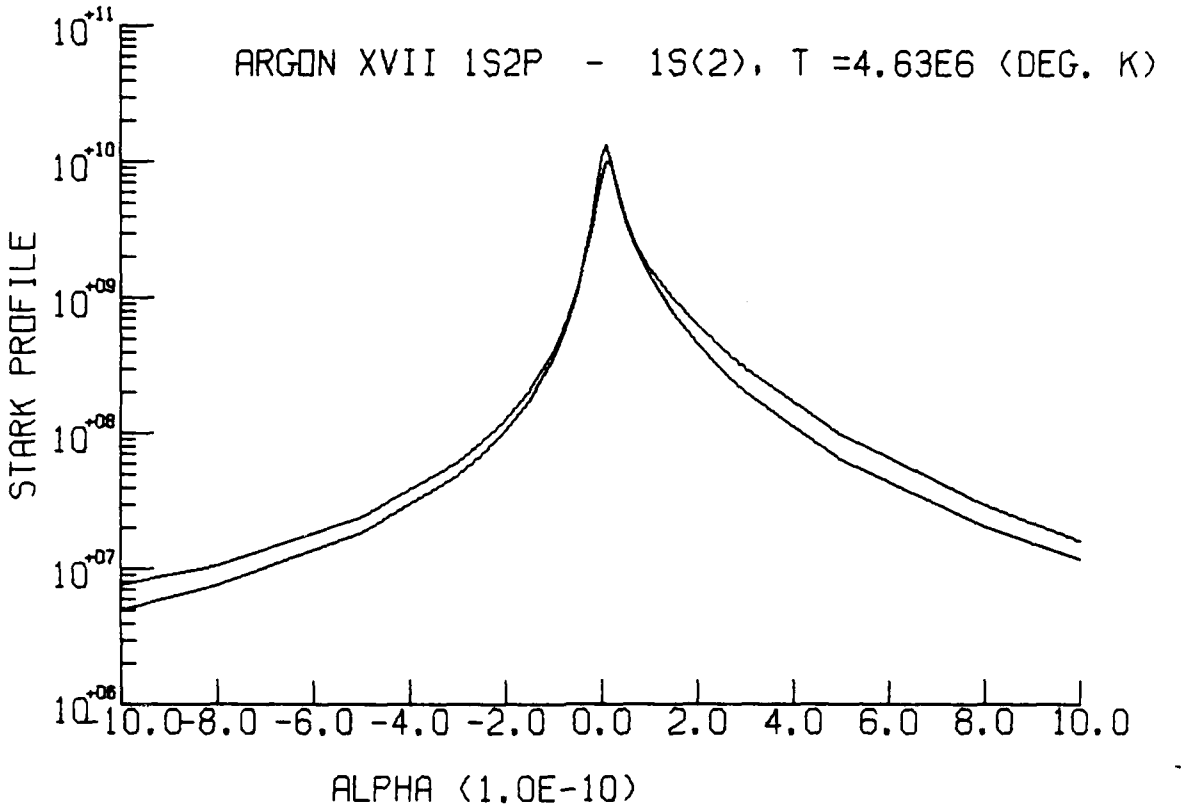

Fig. 35 — Stark profile of Ar XVII $1s2p—1s^2$

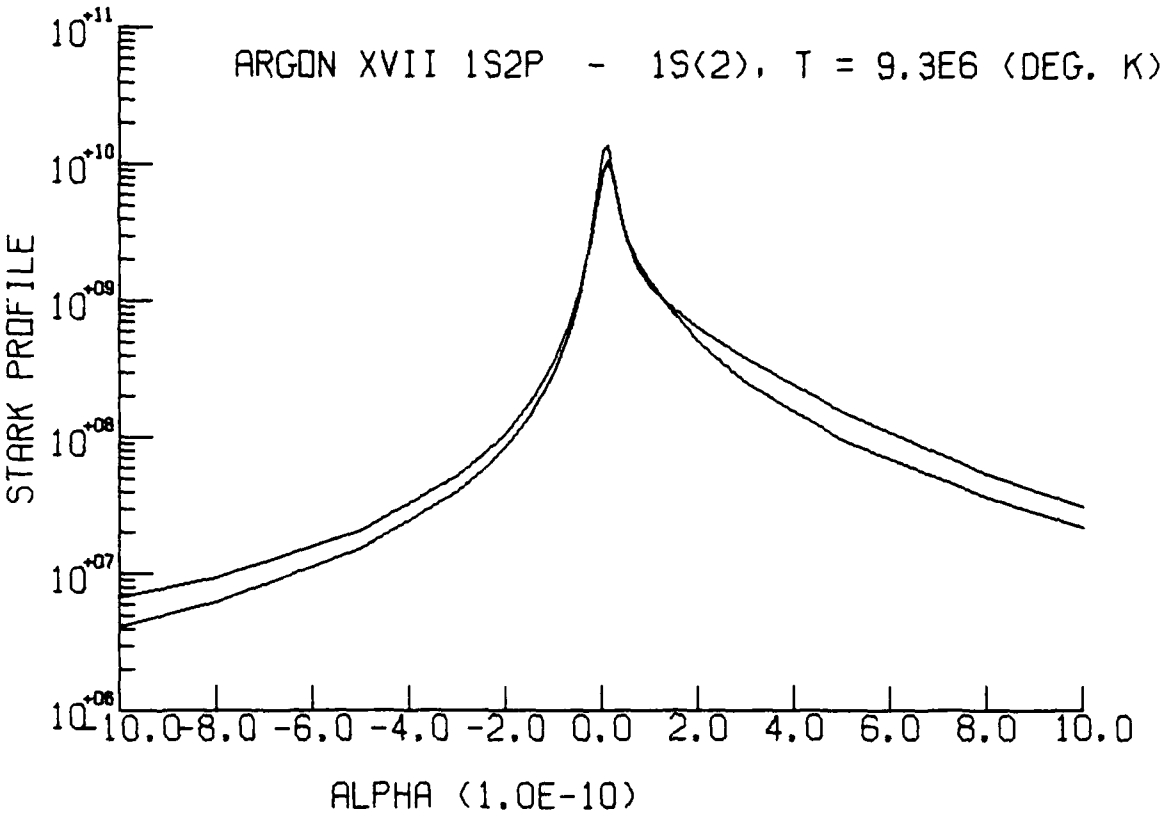

Fig. 36 — Stark profile of Ar XVII 1s2p—1s^2

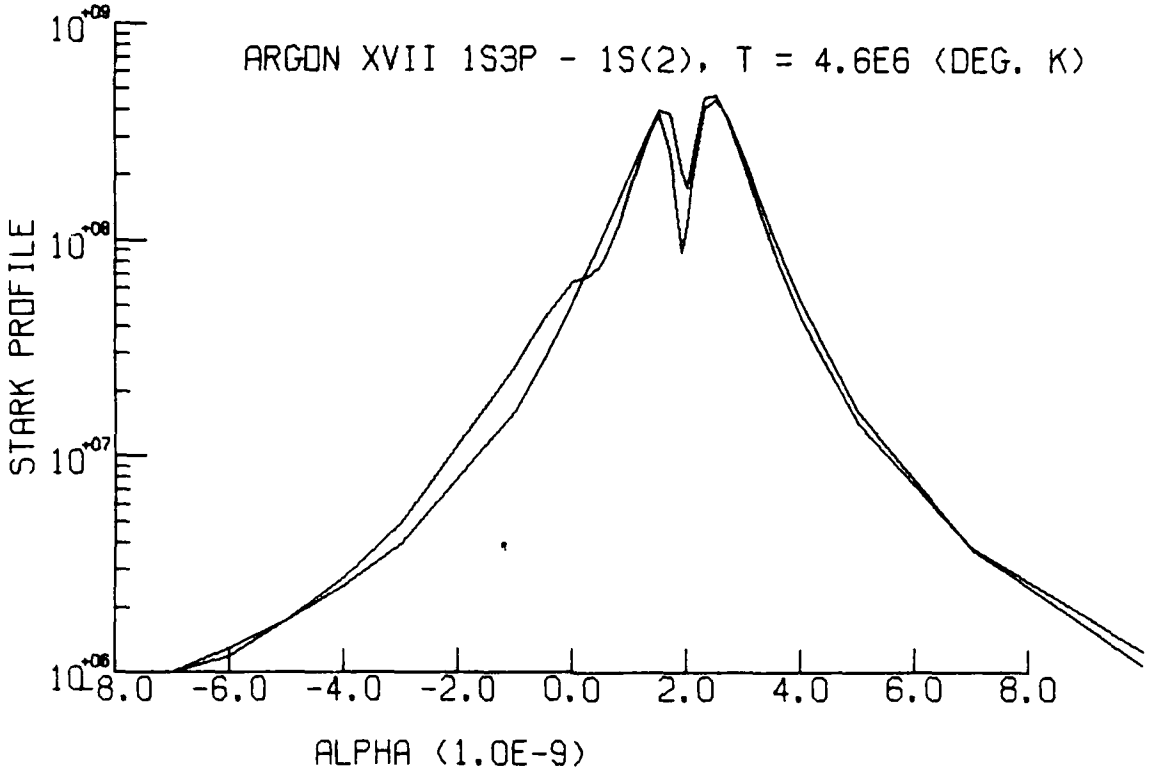

Fig. 37 — Stark profile of Ar XVII 1s3p—1s^2

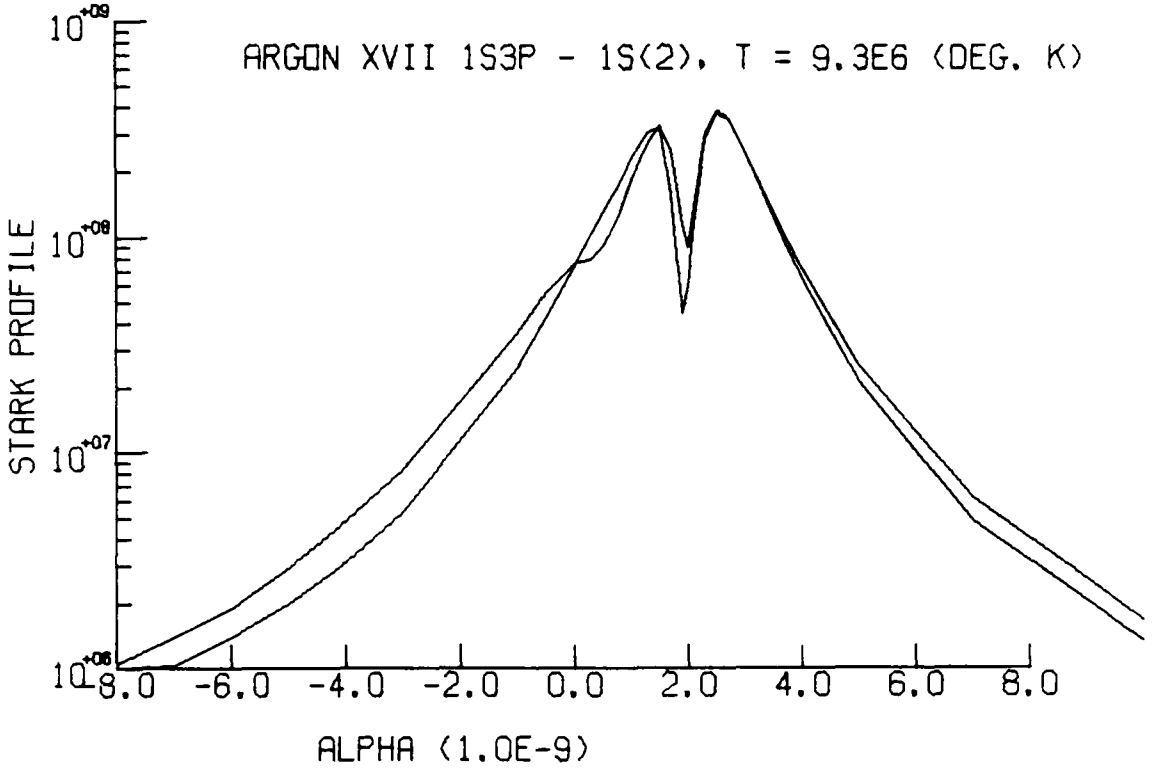

Fig. 38 — Stark profile of Ar XVII 1s3p—1s^2

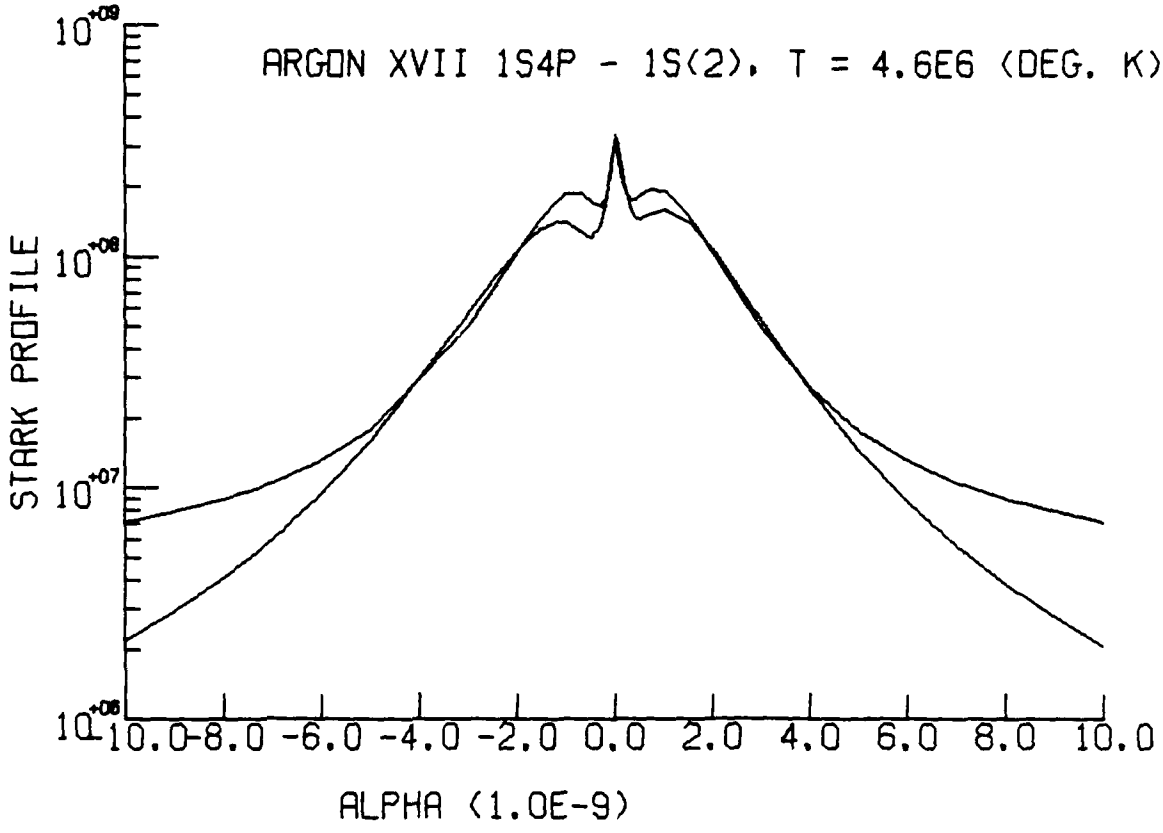

Fig. 39 — Stark profile of Ar XVII 1s4p—1s^2

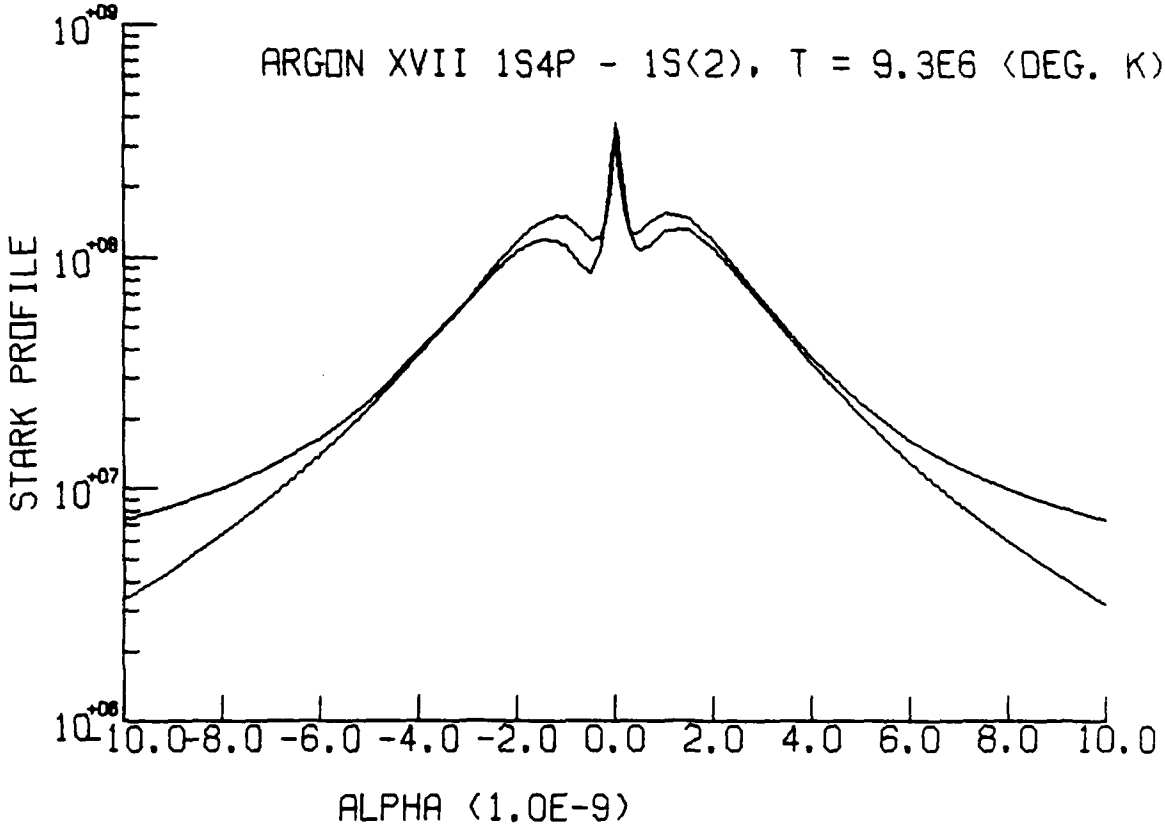

Fig. 40 — Stark profile of Ar XVII 1s4p—1s^2

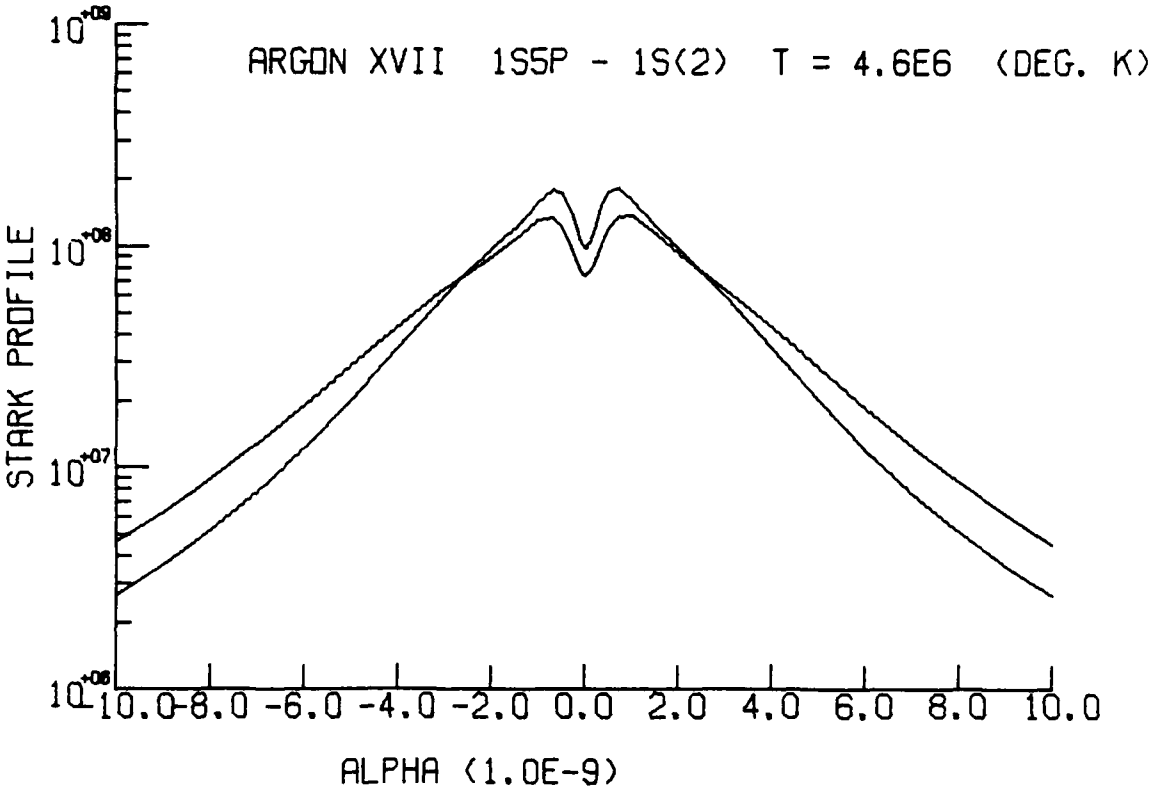

Fig. 41 — Stark profile of Ar XVII $1s5p-1s^2$

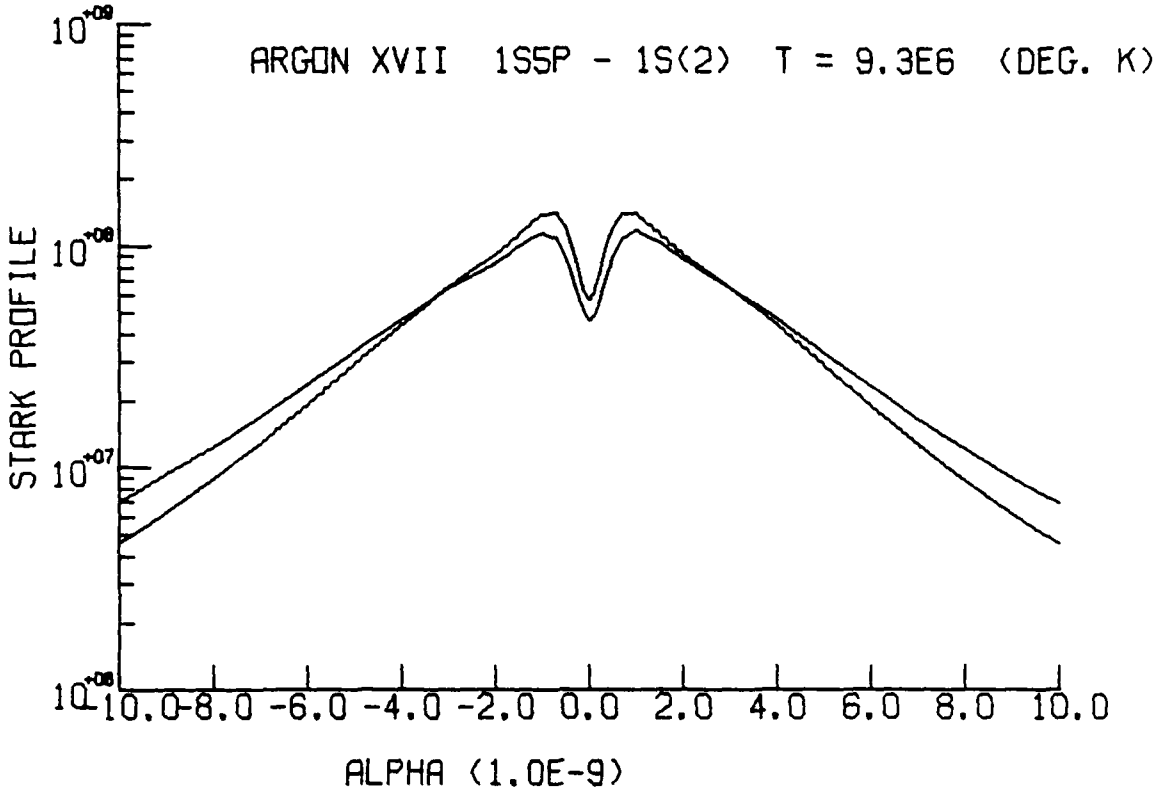

Fig. 42 — Stark profile of Ar XVII 1s5p—1s^2

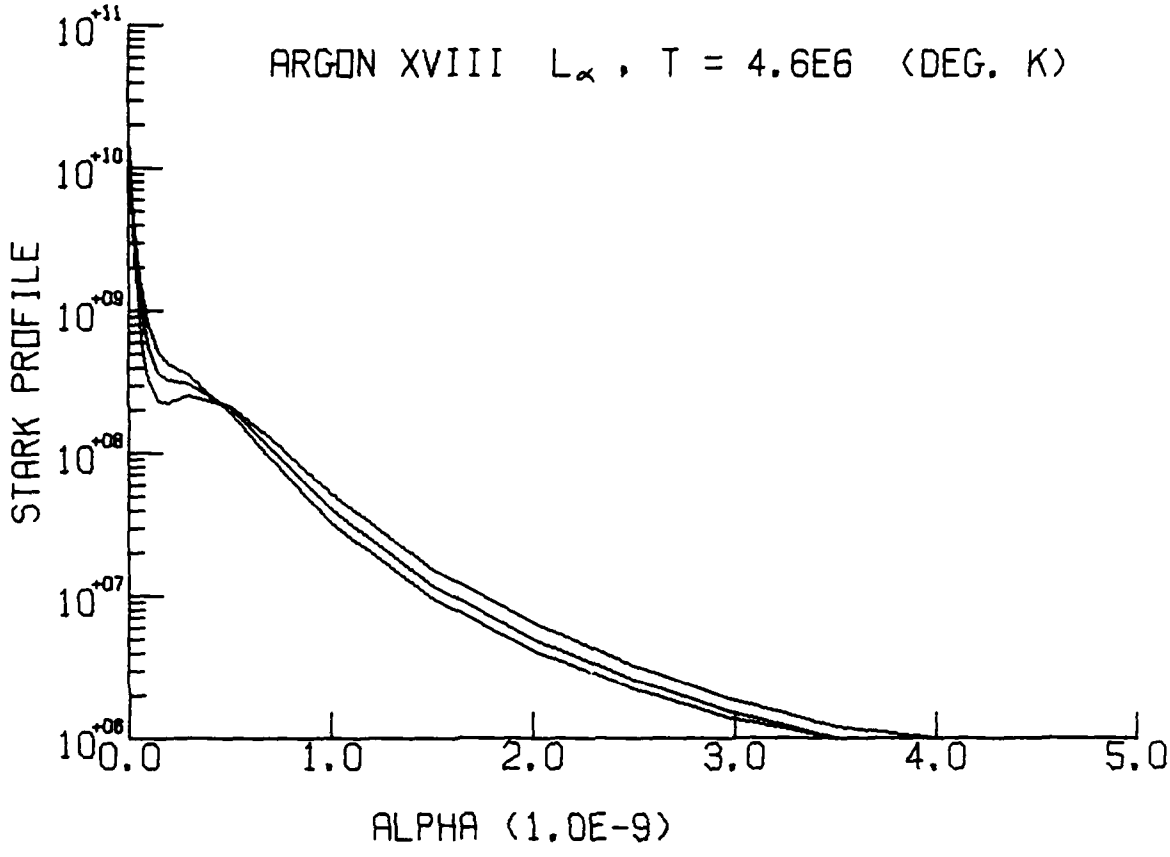

Fig. 43 — Stark profile of Ar XVIII Lα

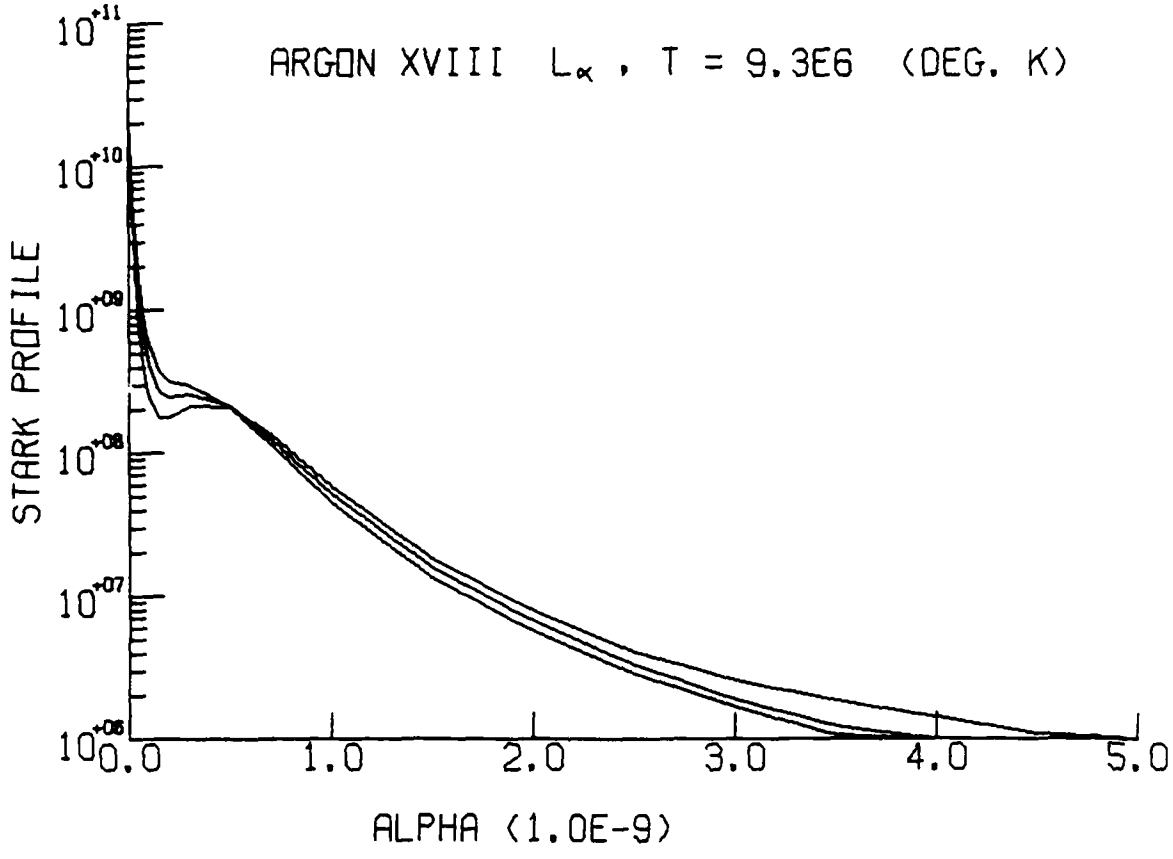

Fig. 44 — Stark profile of Ar XVIII Lα

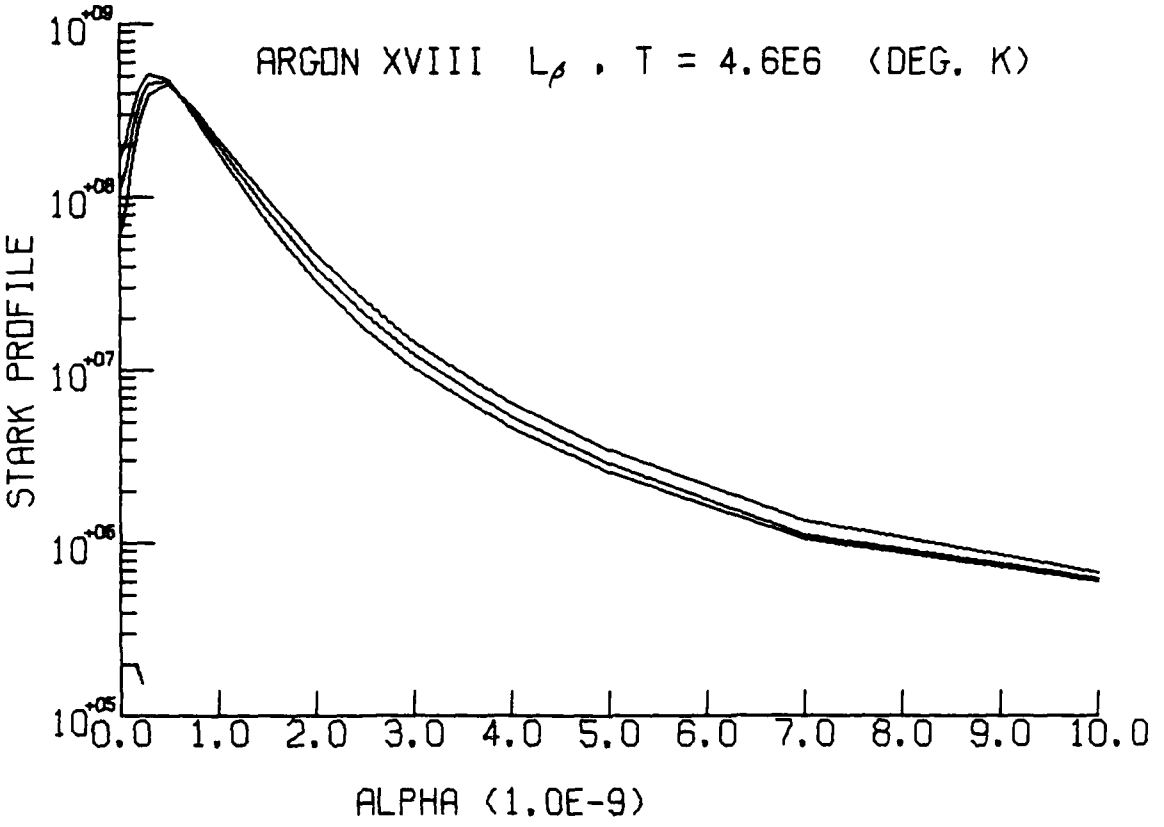

Fig. 45 — Stark profile of Ar XVIII Lβ

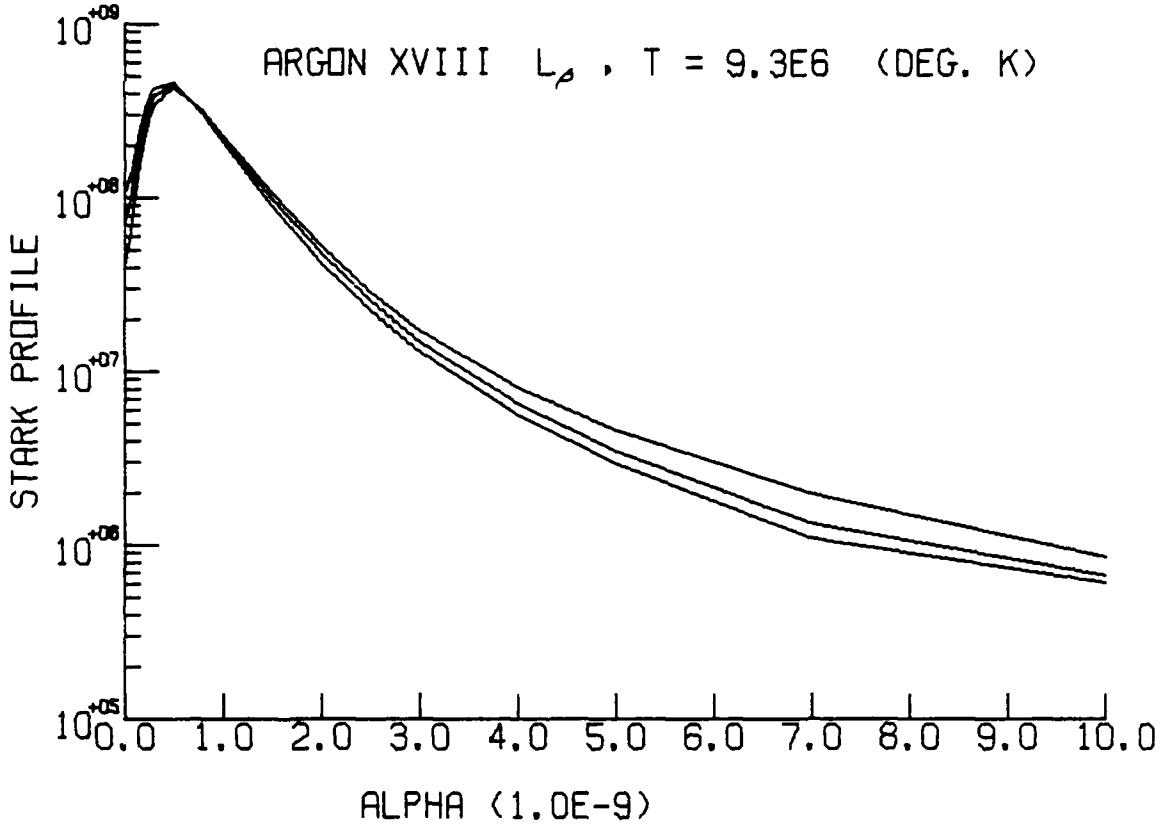

Fig. 46 — Stark profile of Ar XVIII Lβ

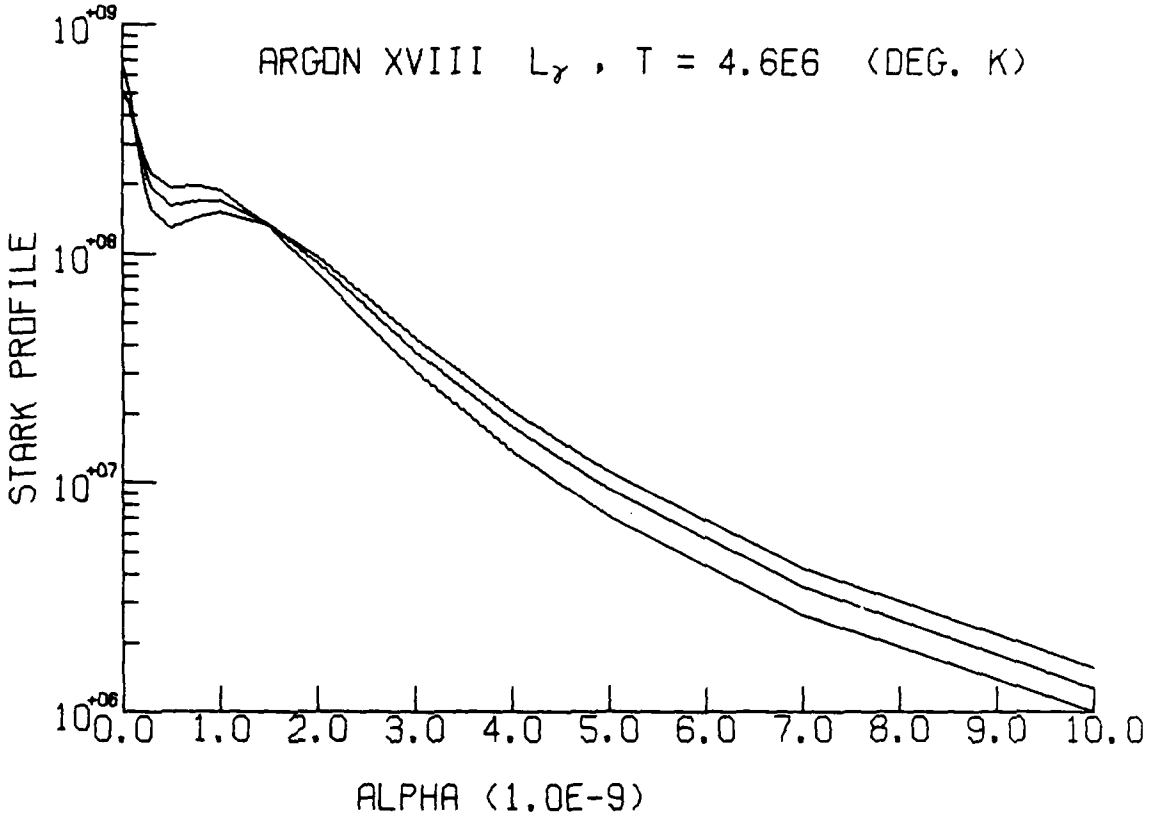

Fig. 47 — Stark profile of Ar XVIII Lγ

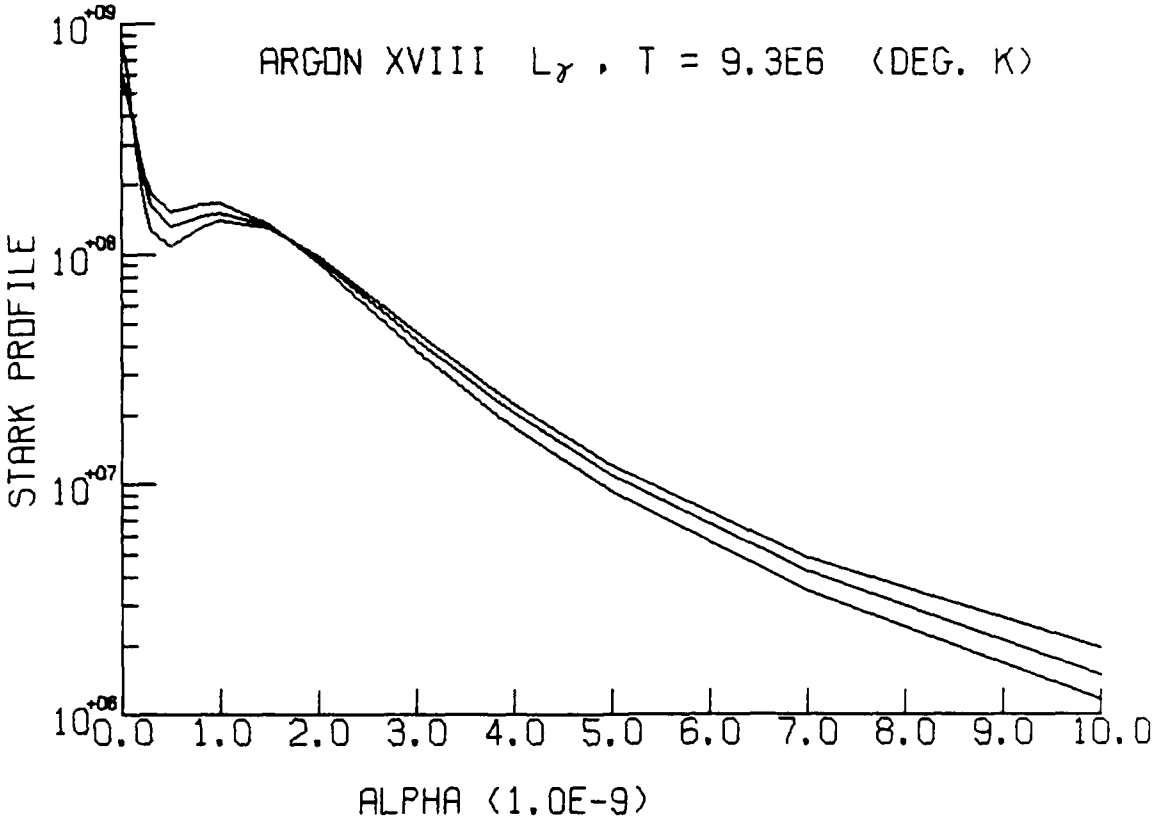

Fig. 48 — Stark profile of Ar XVIII Lγ

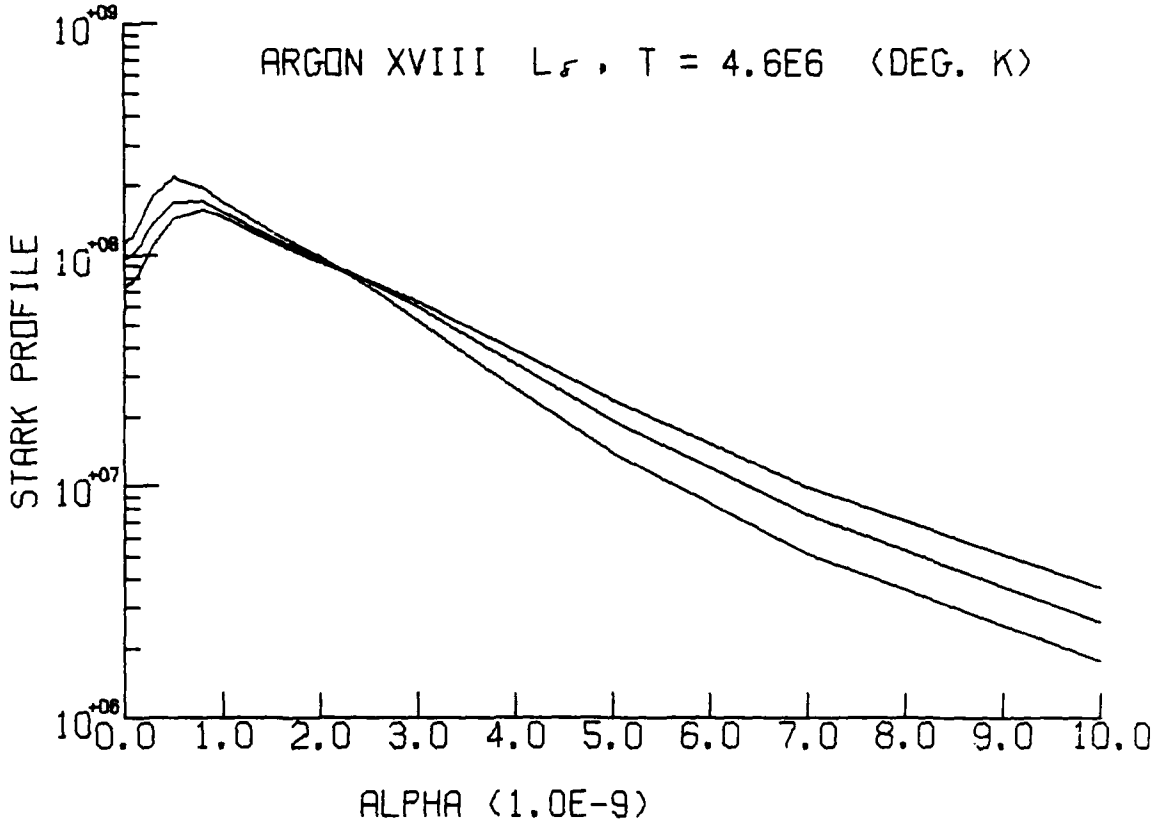

Fig. 49 — Stark profile of Ar XVIII Lδ

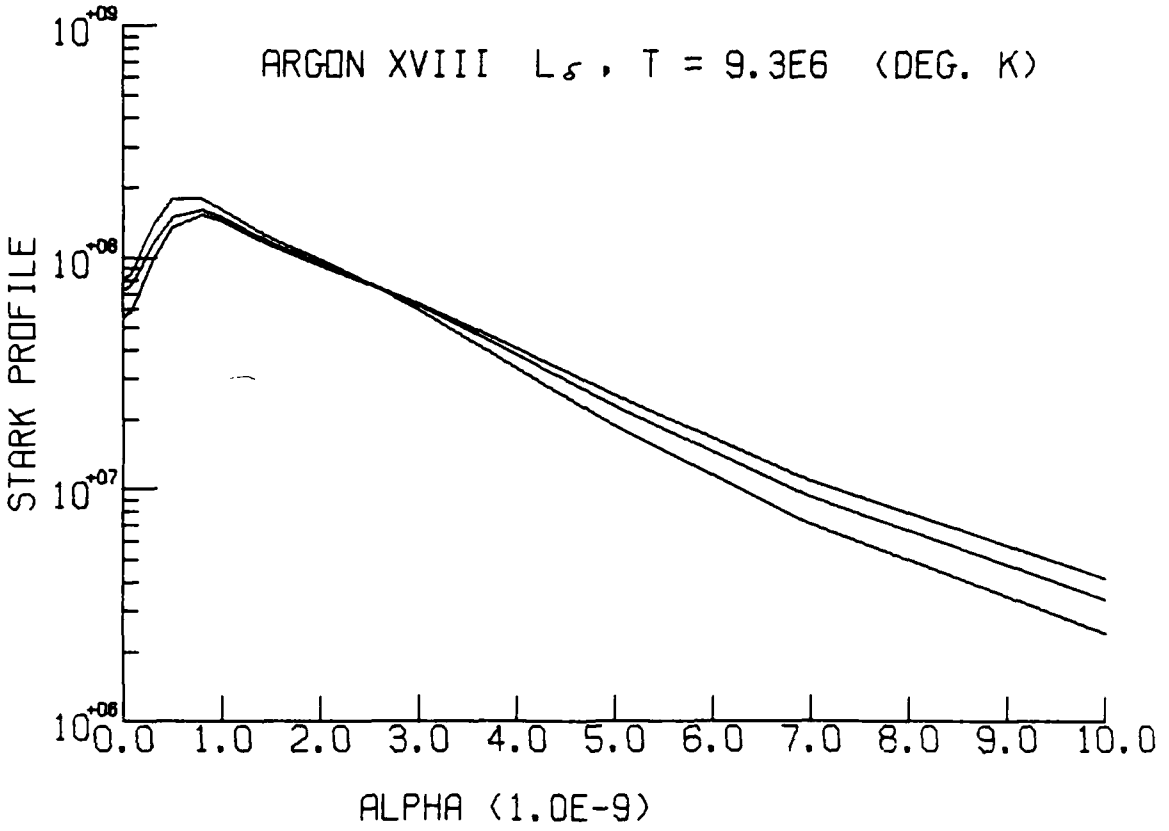

Fig. 50 — Stark profile of Ar XVIII Lδ

Table 1

Ar XVII, n = 3

	^1S	^1P	^1D	^3S	^3P	^3D
^1S 29694422 -4.58 eV		1				
^1P 29731382 0.00 eV	1		.88421			-.46709
^1D 29729378 -0.25 eV		.88421			-.46709	
^3S 29654518 -9.52 eV					1	
^3P 29697464 -4.20 eV			-.46709	1		-.88421
^3D 29725922 -0.68 eV		-.46709			-.88421	

Table 2

Ar XVII, n = 4

	^1S	^1P	^1D	^1F	^3S	^3P	^3D	^3F
^1S 31253221 -1.90 eV		1						
^1P 31273557 0.00 eV	1		-.903				.429	
^1D 31273143 -0.05 eV		-. 903		0.965		.429		0.259
^1F 31274163 0.08 eV			0.965				0.259	
^3S 31241873 -3.92 eV						1		
^3P 31259573 -1.73 eV			.429		1		.903	
^3D 31271579 -0.24 eV		.429		0.259		.903		-0.965
^3F 31273555 0.00 eV			0.259				-0.965	

Table 3

Ar XVII n = 5

	^1S	^1P	^1D	^1F	^1G	^3S	^3P	^3D	^3F	^3G
^1S 319 79 581 −0.970 eV		1								
^1P 319 87 403 0.0 eV	1		-.9097					+.4152		
^1D 319 87 311 −0.01 eV		-.9097		.9630			-.4152		-.2690	
^1F 319 87 906 +0.06 eV			.9630		.9996			.2693		-.0286
^1G 319 88 300 +0.11 eV				.9996					.0286	
^3S 319 71 606 − 1.96							1			
^3P 319 80 726 −0.83			-.4152			1		-.9097		
^3D 319 86 769 −0.08		.4152		.2693			-.9097		.9630	
^3F 319 87 583 +0.02			-.2693		.0286			.9630		.9996
^3G 319 88 279 +0.11				-.0286					.9996	

Table 4

α_c (10^{-9})

T	4.6×10^6		9.3×10^6	
N_e	10^{23}	5×10^{23}	10^{23}	5×10^{23}
Ar XVII				
1s2p	.11	.12	.09	.11
1s3p	.24	.27	.20	.23
1s4p	.43	.49	.36	.41
1s5p	.67	.76	.56	.64
Ar XVIII				
$L\alpha$	.08	.09	.07	.08
$L\beta$	.18	.21	.15	.17
$L\gamma$	.32	.37	.27	.31
$L\delta$	.50	.57	.42	.48

Table 5
Stark Profiles for

ARGON XVII 1S2P - 1S(2), T =4.63E6 (DEG. K)

α \ N_e =	1.00E 23	5.00E 23
-1.00E-09	4.93E 06	7.64E 06
-8.00E-10	7.58E 06	1.07E 07
-5.00E-10	1.86E 07	2.42E 07
-3.00E-10	4.89E 07	6.09E 07
-2.50E-10	6.87E 07	8.45E 07
-2.00E-10	1.04E 08	1.25E 08
-1.50E-10	1.75E 08	2.07E 08
-1.00E-10	3.57E 08	4.07E 08
-7.00E-11	6.53E 08	7.12E 08
-5.00E-11	1.11E 09	1.15E 09
-2.00E-11	3.63E 09	3.14E 09
-1.00E-11	6.27E 09	4.82E 09
0.00E 00	1.08E 10	7.42E 09
1.00E-11	1.33E 10	9.93E 09
2.00E-11	9.88E 09	9.55E 09
5.00E-11	3.57E 09	3.81E 09
7.00E-11	2.37E 09	2.51E 09
1.00E-10	1.46E 09	1.65E 09
1.50E-10	7.73E 08	9.78E 08
2.00E-10	4.56E 08	6.31E 08
2.50E-10	2.95E 08	4.32E 08
3.00E-10	2.01E 08	3.05E 08
5.00E-10	6.35E 07	9.83E 07
8.00E-10	2.07E 07	2.96E 07
1.00E-09	1.19E 07	1.62E 07

Table 6
Stark Profiles for

ARGON XVII 1S2P - 1S(2), T = 9.3E6 (DEG. K)

α \ N_e =	1.00E 23	5.00E 23
-1.00E-09	4.10E 06	6.76E 06
-8.00E-10	6.28E 06	9.32E 06
-5.00E-10	1.54E 07	2.09E 07
-3.00E-10	4.03E 07	5.25E 07
-2.50E-10	5.67E 07	7.30E 07
-2.00E-10	8.58E 07	1.09E 08
-1.50E-10	1.46E 08	1.82E 08
-1.00E-10	3.03E 08	3.67E 08
-7.00E-11	5.66E 08	6.60E 08
-5.00E-11	9.93E 08	1.11E 09
-2.00E-11	3.64E 09	3.36E 09
-1.00E-11	6.86E 09	5.44E 09
0.00E 00	1.28E 10	8.67E 09
1.00E-11	1.39E 10	1.07E 10
2.00E-11	8.38E 09	8.61E 09
5.00E-11	2.86E 09	2.78E 09
7.00E-11	2.01E 09	1.82E 09
1.00E-10	1.35E 09	1.26E 09
1.50E-10	7.92E 08	8.65E 08
2.00E-10	5.04E 08	6.40E 08
2.50E-10	3.51E 08	4.87E 08
3.00E-10	2.53E 08	3.77E 08
5.00E-10	9.55E 07	1.54E 08
8.00E-10	3.66E 07	5.44E 07
1.00E-09	2.19E 07	3.10E 07

Table 7
Stark Profiles for

ARGON XVII 1S3P - 1S(2), T = 4.6E6 (DEG. K)

α \ N_e =	1.00E 23	5.00E 23
-1.00E-08	6.76E 05	7.97E 05
-9.00E-09	8.80E 05	1.00E 06
-8.00E-09	1.19E 06	1.30E 06
-7.00E-09	1.74E 06	1.75E 06
-6.00E-09	2.76E 06	2.51E 06
-5.00E-09	4.93E 06	3.94E 06
-3.00E-09	2.63E 07	1.63E 07
-2.50E-09	4.36E 07	2.78E 07
-2.00E-09	6.38E 07	5.17E 07
-1.70E-09	6.88E 07	7.75E 07
-1.50E-09	7.73E 07	1.02E 08
-1.20E-09	1.19E 08	1.54E 08
-1.00E-09	1.76E 08	2.06E 08
-7.00E-10	2.97E 08	3.14E 08
-5.00E-10	3.89E 08	4.00E 08
-3.00E-10	2.52E 08	3.89E 08
-1.00E-10	8.76E 07	2.07E 08
0.00E 00	1.20E 08	1.76E 08
1.00E-10	2.12E 08	2.56E 08
3.00E-10	4.11E 08	4.58E 08
5.00E-10	4.48E 08	4.72E 08
7.00E-10	3.74E 08	3.65E 08
1.00E-09	2.35E 08	2.16E 08
1.50E-09	1.04E 08	9.05E 07
2.00E-09	5.10E 07	4.32E 07
3.00E-09	1.60E 07	1.41E 07
5.00E-09	3.68E 06	3.73E 06
8.00E-09	1.09E 06	1.27E 06

Table 8
Stark Profiles for

ARGON XVII 1S3P - 1S(2), T = 9.3E6 (DEG. K)

α \ N_e =	1.00E 23	5.00E 23
-1.00E-08	1.05E 06	7.97E 05
-9.00E-09	1.39E 06	1.03E 06
-8.00E-09	1.89E 06	1.40E 06
-7.00E-09	2.94E 06	2.00E 06
-6.00E-09	4.83E 06	3.12E 06
-5.00E-09	8.50E 06	5.35E 06
-3.00E-09	3.60E 07	2.50E 07
-2.50E-09	5.56E 07	4.23E 07
-2.00E-09	7.55E 07	7.42E 07
-1.70E-09	8.02E 07	1.04E 08
-1.50E-09	9.11E 07	1.30E 08
-1.20E-09	1.33E 08	1.80E 08
-1.00E-09	1.87E 08	2.32E 08
-7.00E-10	2.76E 08	3.08E 08
-5.00E-10	3.32E 08	3.27E 08
-3.00E-10	1.58E 08	2.58E 08
-1.00E-10	4.46E 07	1.14E 08
0.00E 00	6.11E 07	9.04E 07
1.00E-10	1.17E 08	1.40E 08
3.00E-10	2.88E 08	3.08E 08
5.00E-10	3.80E 08	3.92E 08
7.00E-10	3.58E 08	3.60E 08
1.00E-09	2.52E 08	2.51E 08
1.50E-09	1.29E 08	1.23E 08
2.00E-09	7.15E 07	6.36E 07
3.00E-09	2.54E 07	2.13E [illegible]
5.00E-09	6.17E 06	4.[illegible]
8.00E-09	1.68E 06	1.[illegible]E 06

Table 9
Stark Profiles for

ARGON XVII 1S4P - 1S(2), T = 4.6E6 (DEG. K)

α \ N_e =	1.00E 23	5.00E 23
-1.00E-08	2.10E 06	1.65E 06
-9.00E-09	2.83E 06	2.13E 06
-8.00E-09	3.97E 06	2.88E 06
-7.00E-09	5.89E 06	4.11E 06
-6.00E-09	9.31E 06	6.31E 06
-5.00E-09	1.58E 07	1.06E 07
-3.00E-09	5.49E 07	4.24E 07
-2.50E-09	7.51E 07	6.30E 07
-2.00E-09	9.88E 07	9.50E 07
-1.70E-09	1.12E 08	1.18E 08
-1.50E-09	1.18E 08	1.34E 08
-1.20E-09	1.22E 08	1.54E 08
-1.00E-09	1.19E 08	1.62E 08
-7.00E-10	1.12E 08	1.60E 08
-5.00E-10	1.18E 08	1.60E 08
-3.00E-10	1.68E 08	2.00E 08
-2.00E-10	2.33E 08	2.60E 08
-1.00E-10	3.34E 08	3.53E 08
0.00E 00	4.08E 08	4.15E 08
1.00E-10	3.61E 08	3.64E 08
2.00E-10	2.66E 08	2.74E 08
3.00E-10	1.99E 08	2.15E 08
4.00E-10	1.64E 08	1.85E 08
5.00E-10	1.46E 08	1.74E 08
7.00E-10	1.37E 08	1.71E 08
1.00E-09	1.39E 08	1.69E 08
1.50E-09	1.29E 08	1.36E 08
2.00E-09	1.02E 08	9.46E 07
3.00E-09	5.29E 07	4.15E 07
4.00E-09	2.70E 07	1.95E 07
5.00E-09	1.48E 07	1.04E 07
6.00E-09	8.76E 06	6.20E 06
7.00E-09	5.60E 06	4.06E 06
8.00E-09	3.81E 06	2.85E 06
9.00E-09	2.73E 06	2.12E 06
1.00E-08	2.04E 06	1.64E 06

Table 10
Stark Profiles for

ARGON XVII 1S4P - 1S(2), T = 9.3E6 (DEG. K)

α \ N_e =	1.00E 23	5.00E 23
-1.00E-08	3.26E 06	2.18E 06
-9.00E-09	4.43E 06	2.95E 06
-8.00E-09	6.19E 06	4.17E 06
-7.00E-09	8.99E 06	6.20E 06
-6.00E-09	1.36E 07	9.77E 06
-5.00E-09	2.15E 07	1.65E 07
-3.00E-09	6.07E 07	5.63E 07
-2.50E-09	7.75E 07	7.68E 07
-2.00E-09	9.40E 07	1.01E 08
-1.70E-09	1.00E 08	1.14E 08
-1.50E-09	1.01E 08	1.21E 08
-1.20E-09	9.64E 07	1.23E 08
-1.00E-09	8.86E 07	1.20E 08
-7.00E-10	7.78E 07	1.10E 08
-5.00E-10	8.52E 07	1.13E 08
-3.00E-10	1.39E 08	1.62E 08
-2.00E-10	2.15E 08	2.34E 08
-1.00E-10	3.54E 08	3.56E 08
0.00E 00	4.76E 08	4.46E 08
1.00E-10	3.88E 08	3.68E 08
2.00E-10	2.47E 08	2.46E 08
3.00E-10	1.67E 08	1.74E 08
4.00E-10	1.28E 08	1.39E 08
5.00E-10	1.11E 08	1.24E 08
7.00E-10	1.01E 08	1.19E 08
1.00E-09	1.08E 08	1.27E 08
1.50E-09	1.13E 08	1.24E 08
2.00E-09	9.91E 07	1.02E 08
3.00E-09	5.96E 07	5.56E 07
4.00E-09	3.41E 07	2.91E 07
5.00E-09	2.04E 07	1.61E 07
6.00E-09	1.29E 07	9.56E 06
7.00E-09	8.57E 06	6.09E 06
8.00E-09	5.92E 06	4.11E 06
9.00E-09	4.25E 06	2.92E 06
1.00E-08	3.15E 06	2.15E 06

Table 11
Stark Profiles for

ARGON XVII 1S5P - 1S(2) T = 4.6E6 (DEG. K)

α \ N_e =	1.00E 23	5.00E 23
-1.00E-08	4.60E 06	2.65E 06
-9.00E-09	6.28E 06	3.63E 06
-8.00E-09	8.83E 06	5.17E 06
-7.00E-09	1.28E 07	7.76E 06
-6.00E-09	1.91E 07	1.22E 07
-5.00E-09	2.90E 07	2.03E 07
-3.00E-09	6.43E 07	6.03E 07
-2.50E-09	7.63E 07	7.77E 07
-2.00E-09	9.02E 07	9.79E 07
-1.70E-09	1.01E 08	1.12E 08
-1.50E-09	1.09E 08	1.22E 08
-1.20E-09	1.23E 08	1.43E 08
-1.00E-09	1.32E 08	1.59E 08
-7.00E-10	1.35E 08	1.80E 08
-5.00E-10	1.23E 08	1.76E 08
-3.00E-10	1.00E 08	1.45E 08
-2.00E-10	8.84E 07	1.24E 08
-1.00E-10	7.89E 07	1.06E 08
0.00E 00	7.43E 07	9.83E 07
1.00E-10	7.64E 07	1.05E 08
2.00E-10	8.47E 07	1.22E 08
3.00E-10	9.69E 07	1.44E 08
4.00E-10	1.10E 08	1.64E 08
5.00E-10	1.23E 08	1.77E 08
7.00E-10	1.38E 08	1.84E 08
1.00E-09	1.39E 08	1.63E 08
1.50E-09	1.15E 08	1.25E 08
2.00E-09	9.36E 07	9.86E 07
3.00E-09	6.48E 07	6.01E 07
4.00E-09	4.35E 07	3.48E 07
5.00E-09	2.85E 07	2.02E 07
6.00E-09	1.87E 07	1.21E 07
7.00E-09	1.25E 07	7.69E 06
8.00E-09	8.66E 06	5.13E 06
9.00E-09	6.17E 06	3.61E 06
1.00E-08	4.53E 06	2.64E 06

Table 12
Stark Profiles for

ARGON XVII 1S5P - 1S(2) T = 9.3E6 (DEG. K)

α \ N_e =	1.00E 23	5.00E 23
-1.00E-08	7.06E 06	4.58E 06
-9.00E-09	9.27E 06	6.28E 06
-8.00E-09	1.24E 07	8.88E 06
-7.00E-09	1.70E 07	1.29E 07
-6.00E-09	2.37E 07	1.93E 07
-5.00E-09	3.37E 07	2.94E 07
-3.00E-09	6.43E 07	6.52E 07
-2.50E-09	7.34E 07	7.74E 07
-2.00E-09	8.39E 07	9.17E 07
-1.70E-09	9.22E 07	1.03E 08
-1.50E-09	9.90E 07	1.12E 08
-1.20E-09	1.10E 08	1.29E 08
-1.00E-09	1.14E 08	1.39E 08
-7.00E-10	1.08E 08	1.40E 08
-5.00E-10	9.03E 07	1.22E 08
-3.00E-10	6.75E 07	8.99E 07
-2.00E-10	5.74E 07	7.40E 07
-1.00E-10	5.00E 07	6.21E 07
0.00E 00	4.65E 07	5.71E 07
1.00E-10	4.79E 07	6.09E 07
2.00E-10	5.41E 07	7.24E 07
3.00E-10	6.39E 07	8.84E 07
4.00E-10	7.59E 07	1.06E 08
5.00E-10	8.83E 07	1.21E 08
7.00E-10	1.09E 08	1.41E 08
1.00E-09	1.19E 08	1.41E 08
1.50E-09	1.04E 08	1.14E 08
2.00E-09	8.77E 07	9.30E 07
3.00E-09	6.54E 07	6.54E 07
4.00E-09	4.75E 07	4.45E 07
5.00E-09	3.34E 07	2.92E 07
6.00E-09	2.34E 07	1.91E 07
7.00E-09	1.67E 07	1.28E 07
8.00E-09	1.22E 07	8.81E 06
9.00E-09	9.13E 06	6.24E 06
1.00E-08	6.96E 06	4.55E 06

Table 13
Stark Profiles for

ARGON XVIII L_α , T = 4.6E6 (DEG. K)

α \ N_e =	1.00E 22	1.00E 23	5.00E 23
0.00E 00	1.69E 10	9.81E 09	7.02E 09
3.00E-12	1.60E 10	9.62E 09	6.95E 09
1.00E-11	1.01E 10	8.05E 09	6.34E 09
3.00E-11	2.42E 09	3.34E 09	3.63E 09
5.00E-11	9.92E 08	1.59E 09	2.01E 09
7.00E-11	5.55E 08	9.31E 08	1.26E 09
1.00E-10	3.27E 08	5.53E 08	7.76E 08
1.50E-10	2.31E 08	3.67E 08	5.06E 08
2.00E-10	2.24E 08	3.24E 08	4.22E 08
3.00E-10	2.50E 08	3.05E 08	3.47E 08
5.00E-10	2.13E 08	2.08E 08	1.94E 08
7.00E-10	1.27E 08	1.09E 08	9.15E 07
1.00E-09	5.14E 07	4.06E 07	3.24E 07
1.50E-09	1.54E 07	1.19E 07	9.55E 06
2.00E-09	6.54E 06	5.01E 06	4.13E 06
2.50E-09	3.21E 06	2.57E 06	2.21E 06
3.00E-09	1.86E 06	1.52E 06	1.37E 06
3.50E-09	1.21E 06	9.73E 05	9.32E 05
4.00E-09	8.39E 05	6.56E 05	6.71E 05
4.50E-09	6.12E 05	4.67E 05	5.04E 05
5.00E-09	4.75E 05	3.50E 05	3.92E 05

Table 14
Stark Profiles for

ARGON XVIII $L\alpha$, T = 9.3E6 (DEG. K)

α \ N_e =	1.00E 22	1.00E 23	5.00E 23
0.00E 00	2.27E 10	1.29E 10	9.00E 09
3.00E-12	2.04E 10	1.24E 10	8.85E 09
1.00E-11	1.02E 10	9.28E 09	7.60E 09
3.00E-11	1.91E 09	2.90E 09	3.41E 09
5.00E-11	7.50E 08	1.25E 09	1.67E 09
7.00E-11	4.15E 08	7.08E 08	9.84E 08
1.00E-10	2.44E 08	4.10E 08	5.78E 08
1.50E-10	1.78E 08	2.71E 08	3.70E 08
2.00E-10	1.79E 08	2.46E 08	3.18E 08
3.00E-10	2.16E 08	2.56E 08	2.95E 08
5.00E-10	2.09E 08	2.12E 08	2.10E 08
7.00E-10	1.36E 08	1.26E 08	1.15E 08
1.00E-09	5.83E 07	5.14E 07	4.44E 07
1.50E-09	1.80E 07	1.56E 07	1.33E 07
2.00E-09	7.84E 06	6.65E 06	5.65E 06
2.50E-09	4.06E 06	3.31E 06	2.88E 06
3.00E-09	2.58E 06	1.91E 06	1.67E 06
3.50E-09	1.87E 06	1.24E 06	1.06E 06
4.00E-09	1.41E 06	8.48E 05	7.07E 05
4.50E-09	1.09E 06	6.15E 05	5.09E 05
5.00E-09	8.61E 05	4.75E 05	3.75E 05

Table 15
Stark Profiles for

ARGON XVIII L_β , T = 4.6E6 (DEG. K)

α \ N_e =	1.00E 22	1.00E 23	5.00E 23
0.00E 00	6.21E 07	1.15E 08	1.73E 08
1.00E-11	6.30E 07	1.16E 08	1.74E 08
3.00E-11	6.93E 07	1.23E 08	1.83E 08
5.00E-11	8.12E 07	1.37E 08	1.98E 08
7.00E-11	9.83E 07	1.57E 08	2.20E 08
1.00E-10	1.29E 08	1.93E 08	2.63E 08
1.20E-10	1.53E 08	2.20E 08	2.94E 08
1.50E-10	1.93E 08	2.64E 08	3.41E 08
1.70E-10	2.21E 08	2.94E 08	3.72E 08
2.00E-10	2.64E 08	3.38E 08	4.16E 08
2.50E-10	3.33E 08	4.04E 08	4.76E 08
3.00E-10	3.90E 08	4.53E 08	5.14E 08
5.00E-10	4.57E 08	4.70E 08	4.76E 08
8.00E-10	3.12E 08	2.95E 08	2.75E 08
1.00E-09	2.20E 08	2.03E 08	1.83E 08
1.50E-09	9.82E 07	8.50E 07	7.23E 07
2.00E-09	4.70E 07	3.94E 07	3.28E 07
2.50E-09	2.50E 07	2.09E 07	1.73E 07
3.00E-09	1.46E 07	1.23E 07	1.03E 07
4.00E-09	6.41E 06	5.36E 06	4.65E 06
5.00E-09	3.45E 06	2.85E 06	2.55E 06
7.00E-09	1.35E 06	1.11E 06	1.05E 06
1.00E-08	6.72E 05	6.24E 05	6.05E 05

Table 16
Stark Profiles for

ARGON XVIII L_β , T = 9.3E6 (DEG. K)

α \ N_e =	1.00E 22	1.00E 23	5.00E 23
0.00E 00	4.15E 07	7.39E 07	1.08E 08
1.00E-11	4.22E 07	7.47E 07	1.09E 08
3.00E-11	4.76E 07	8.06E 07	1.15E 08
5.00E-11	5.35E 07	9.20E 07	1.28E 08
7.00E-11	7.21E 07	1.08E 08	1.46E 08
1.00E-10	9.87E 07	1.38E 08	1.79E 08
1.20E-10	1.20E 08	1.60E 08	2.04E 08
1.50E-10	1.55E 08	1.98E 08	2.45E 08
1.70E-10	1.81E 08	2.24E 08	2.72E 08
2.00E-10	2.20E 08	2.65E 08	3.14E 08
2.50E-10	2.85E 08	3.29E 08	3.79E 08
3.00E-10	3.42E 08	3.83E 08	4.27E 08
5.00E-10	4.35E 08	4.48E 08	4.60E 08
8.00E-10	3.17E 08	3.09E 08	2.99E 08
1.00E-09	2.29E 08	2.20E 08	2.08E 08
1.50E-09	1.06E 08	9.83E 07	8.96E 07
2.00E-09	5.24E 07	4.76E 07	4.21E 07
2.50E-09	2.85E 07	2.55E 07	2.24E 07
3.00E-09	1.72E 07	1.49E 07	1.31E 07
4.00E-09	8.08E 06	6.53E 06	5.64E 06
5.00E-09	4.65E 06	3.49E 06	2.96E 06
7.00E-09	2.01E 06	1.35E 06	1.11E 06
1.00E-08	8.61E 05	6.75E 05	6.06E 05

Table 17
Stark Profiles for

ARGON XVIII L_γ , T = 4.6E6 (DEG. K)

α \ N_e =	1.00E 22	1.00E 23	5.00E 23
0.00E 00	6.51E 08	4.99E 08	4.95E 08
1.00E-11	6.47E 08	4.98E 08	4.93E 08
3.00E-11	6.21E 08	4.87E 08	4.84E 08
5.00E-11	5.73E 08	4.68E 08	4.67E 08
7.00E-11	5.15E 08	4.41E 08	4.44E 08
1.00E-10	4.26E 08	3.96E 08	4.04E 08
1.20E-10	3.73E 08	3.65E 08	3.76E 08
1.50E-10	3.07E 08	3.21E 08	3.36E 08
1.70E-10	2.72E 08	2.96E 08	3.13E 08
2.00E-10	2.30E 08	2.63E 08	2.83E 08
2.50E-10	1.84E 08	2.22E 08	2.46E 08
3.00E-10	1.56E 08	1.95E 08	2.21E 08
5.00E-10	1.29E 08	1.62E 08	1.93E 08
8.00E-10	1.45E 08	1.70E 08	1.97E 08
1.00E-09	1.52E 08	1.60E 08	1.88E 08
1.50E-09	1.34E 08	1.35E 08	1.33E 08
2.00E-09	9.66E 07	9.09E 07	8.18E 07
2.50E-09	6.49E 07	5.84E 07	4.94E 07
3.00E-09	4.32E 07	3.78E 07	3.07E 07
4.00E-09	2.05E 07	1.74E 07	1.36E 07
5.00E-09	1.11E 07	9.27E 06	7.07E 06
7.00E-09	4.23E 06	3.53E 06	2.64E 06
1.00E-08	1.55E 06	1.26E 06	9.49E 05

Table 18
Stark Profiles for

ARGON XVIII L_γ , T = 9.3E6 (DEG. K)

α \ N_e =	1.00E 22	1.00E 23	5.00E 23
0.00E 00	8.26E 08	5.92E 08	5.46E 08
1.00E-11	8.18E 08	5.90E 08	5.44E 08
3.00E-11	7.62E 08	5.70E 08	5.30E 08
5.00E-11	6.69E 08	5.34E 08	5.03E 08
7.00E-11	5.68E 08	4.89E 08	4.68E 08
1.00E-10	4.32E 08	4.16E 08	4.10E 08
1.20E-10	3.61E 08	3.70E 08	3.72E 08
1.50E-10	2.80E 08	3.11E 08	3.21E 08
1.70E-10	2.41E 08	2.78E 08	2.91E 08
2.00E-10	1.97E 08	2.39E 08	2.55E 08
2.50E-10	1.53E 08	1.93E 08	2.12E 08
3.00E-10	1.28E 08	1.64E 08	1.84E 08
5.00E-10	1.09E 08	1.33E 08	1.54E 08
8.00E-10	1.30E 08	1.46E 08	1.65E 08
1.00E-09	1.40E 08	1.52E 08	1.67E 08
1.50E-09	1.31E 08	1.34E 08	1.36E 08
2.00E-09	9.85E 07	9.64E 07	9.23E 07
2.50E-09	6.80E 07	6.48E 07	5.95E 07
3.00E-09	4.62E 07	4.33E 07	3.86E 07
4.00E-09	2.23E 07	2.05E 07	1.77E 07
5.00E-09	1.21E 07	1.10E 07	9.29E 06
7.00E-09	4.79E 06	4.19E 06	3.43E 06
1.00E-08	1.95E 06	1.49E 06	1.16E 06

Table 19
Stark Profiles for

ARGON XVIII $L\zeta$, T = 4.6E6 (DEG. K)

α \ N_e =	1.00E 22	1.00E 23	5.00E 23
0.00E 00	7.35E 07	9.67E 07	1.14E 08
1.00E-11	7.35E 07	9.68E 07	1.14E 08
3.00E-11	7.40E 07	9.73E 07	1.15E 08
5.00E-11	7.49E 07	9.84E 07	1.17E 08
7.00E-11	7.62E 07	9.99E 07	1.19E 08
1.00E-10	7.88E 07	1.03E 08	1.25E 08
1.20E-10	8.11E 07	1.06E 08	1.29E 08
1.50E-10	8.50E 07	1.10E 08	1.37E 08
1.70E-10	8.79E 07	1.13E 08	1.43E 08
2.00E-10	9.28E 07	1.19E 08	1.52E 08
2.50E-10	1.02E 08	1.29E 08	1.67E 08
3.00E-10	1.11E 08	1.39E 08	1.82E 08
5.00E-10	1.45E 08	1.70E 08	2.16E 08
8.00E-10	1.57E 08	1.71E 08	1.96E 08
1.00E-09	1.47E 08	1.56E 08	1.71E 08
1.50E-09	1.15E 08	1.20E 08	1.28E 08
2.00E-09	9.41E 07	9.71E 07	9.87E 07
2.50E-09	7.79E 07	7.72E 07	7.30E 07
3.00E-09	6.31E 07	5.97E 07	5.24E 07
4.00E-09	3.90E 07	3.40E 07	2.65E 07
5.00E-09	2.37E 07	1.94E 07	1.40E 07
7.00E-09	9.88E 06	7.52E 06	5.11E 06
1.00E-08	3.64E 06	2.59E 06	1.76E 06

Table 20
Stark Profiles for

ARGON XVIII L_δ, T = 9.3E6 (DEG. K)

α \ N_e =	1.00E 22	1.00E 23	5.00E 23
0.00E 00	5.60E 07	7.30E 07	8.05E 07
1.00E-11	5.60E 07	7.30E 07	8.06E 07
3.00E-11	5.65E 07	7.35E 07	8.13E 07
5.00E-11	5.74E 07	7.45E 07	8.28E 07
7.00E-11	5.88E 07	7.59E 07	8.49E 07
1.00E-10	6.16E 07	7.88E 07	8.92E 07
1.20E-10	6.40E 07	8.13E 07	9.27E 07
1.50E-10	6.81E 07	8.56E 07	9.89E 07
1.70E-10	7.13E 07	8.88E 07	1.04E 08
2.00E-10	7.64E 07	9.41E 07	1.11E 08
2.50E-10	8.62E 07	1.04E 08	1.25E 08
3.00E-10	9.67E 07	1.14E 08	1.39E 08
5.00E-10	1.35E 08	1.50E 08	1.80E 08
8.00E-10	1.54E 08	1.61E 08	1.80E 08
1.00E-09	1.45E 08	1.50E 08	1.61E 08
1.50E-09	1.12E 08	1.16E 08	1.22E 08
2.00E-09	9.20E 07	9.48E 07	9.81E 07
2.50E-09	7.73E 07	7.82E 07	7.79E 07
3.00E-09	6.39E 07	6.29E 07	6.00E 07
4.00E-09	4.09E 07	3.83E 07	3.37E 07
5.00E-09	2.55E 07	2.30E 07	1.89E 07
7.00E-09	1.10E 07	9.33E 06	7.14E 06
1.00E-08	4.14E 06	3.33E 06	2.40E 06

DISTRIBUTION LIST

1. Naval Research Laboratory — 25 Copies
Plasma Radiation Group
Washington, D.C.

Code 4707

2. Mr. Dennis A. Roybal — 50 Copies
Los Alamos National Laboratory
Department of Supply and Property
Los Alamos, New Mexico 87545

3. Dr. Allen Hauer — 5 Copies
Los Alamos National Laboratory
M/S 554
P. O. Box 1663
Los Alamos, New Mexico 87545

4. Naval Research Laboratory — 25 Copies
Plasma Physics Division
Washington, D.C.

Code 4700